Discrete Stiffness Tailoring of Aerospace Composite Structures: Analysis, Optimisation and Testing

Culliford, Lucie

Award date:
2021

Awarding institution:
University of Bath

Discrete Stiffness Tailoring of Aerospace Composite Structures: Analysis, Optimisation and Testing

Lucie Elizabeth Culliford

A thesis for the degree of Doctor of Philosophy

University of Bath

Department of Mechanical Engineering

May 2021

Acknowledgements

First and foremost, I would like to acknowledge and thank my supervisors, Dr Andy Rhead and Professor Richard Butler, who have guided me through this PhD. They have been incredibly supportive and encouraging, particularly during the coronavirus pandemic this past year.

This PhD was supported jointly by an EPSRC grant, as part of the ADAPT Project, in conjunction with GKN Aerospace, which is gratefully acknowledged. The experimental work contained in this thesis simply could not have been completed without the experience and hard work of the technicians at the University of Bath: Clare Ball, Steve Thomas, Steve Coombes, Mark Wellman and William Bazeley, and I would like to thank them all.

The years I have spent in the Department of Mechanical Engineering have been made immensely better by the friendship of other students and postdocs, in particular Fedra Zaribaf, Tomás Chuaqui, Sophie McNair, Thomas (Little T) Maierhofer, Raj Jagpal, Zo Rymansaib and James Evans. Carl Scarth is also part of the former list, but deserves special acknowledgement as his help and guidance during the last years of my PhD have been invaluable.

I would also like to thank my parents, Paul and Lynda, and the rest of my extended family, who have always supported me despite not quite understanding the lure of a life as an eternal student. I could not be more thankful for their love, family madness and constant encouragement. I cannot wait to see you all post-lockdown.

Contents

Abstract

Variable Stiffness (VS) designs allow variation of the fibre angle within a single ply layer, enabling a significant expansion in the design space available for stiffness tailoring of composite laminates. Tailoring is typically achieved through continuous steering of fibres, which maintains transverse structural continuity, but manufacturing methods capable of fabricating such designs are unable to achieve industrial manufacturing rates, and also impose minimum fibre steering radii constraints, limiting performance improvements. Discrete Stiffness Tailoring (DST) is a novel manufacturing concept where stiffness tailoring is achieved using discrete changes in ply angle to favourably redistribute stresses. Resulting performance increases can be exploited to potentially achieve rapidly manufacturable lightweight structures, uninhibited by the minimum tow-turning radii which limit continuous fibre steering approaches.

In this thesis, the Discrete Stiffness Tailoring concept is initially demonstrated through the simple redistribution of material within a quasi-isotropic laminate, and is shown both analytically and experimentally to improve buckling stress by 16% with no failure observed in regions of discrete angle change. Discrete tailoring introduces discontinuities, ply seams, within a laminate and the reduced tensile strength of these seams is investigated. Although a marked reduction in tensile strength is observed with greater numbers of discontinuous plies, it is found that for uni-axial compressive loading with seams parallel to the load, the decrease in transverse strength is not found to be critical.

An efficient two-stage optimisation routine is implemented to design a DST minimum-mass T-stiffened aircraft wing panel subject to buckling and manufacturing feasibility constraints. The panel is manufactured and compression tested to failure, extending the DST design concept to component level for the first time. A weight reduction of 14% is achieved compared to a constant stiffness optimum, through redistribution of load to the stiffener region. The optimum design removes material from the skin, between stiffeners. Experimentally, the optimised tailored panel achieved a buckling load, without failure, within 4% of that predicted, validating both the methodology and modelling.

The validated optimisation routine is used to perform a parametric study of infinitely wide stiffened panels under varying uni-axial compressive loads, representative of those experienced by commercial aircraft. Amendments to the original optimisation methodology allow for the selection of non-standard angle designs, and a blending constraint is added to maximise the arrangement of continuous plies between regions. Greater mass reductions due to tailoring are obtained with smaller in-plane loads, and the same level of material efficiency is able to be maintained for wider stiffener spacings with the application of stiffness tailoring.

List of Figures

List of Tables

Publications

The following thesis is created in part by publications, either published in international journals or presented at conferences, that are listed here:

Journal Publications:

[1] Culliford, L.E., Choudhry, R.S., Rhead, A.T. & Butler, R. *Buckling and strength analysis of panels with discrete stiffness tailoring.* Composite Structures, 2020, Vol. 234, Article 111672.

[2] Culliford, L.E., Scarth, C., Maierhofer, T., Jagpal, R., Rhead, A.T. & Butler, R. *Discrete Stiffness Tailoring for manufacturable minimum mass stiffened composite panels.* Composites Part B: Engineering, September 2021, Vol. 221, Article 109026.

Conference Papers:

[3] Culliford, L.E., Choudhry, R.S., Rhead, A.T. & Butler, R. *Discrete stiffness tailoring for improved buckling performance.* Proceedings of ICCM21, Xian, 20-25th August, 2017.

Declaration

I declare that the work in this thesis was carried out in accordance with the requirements of the University's Regulations and Code of Practice for Research Degree Programmes and that it has not been submitted for any other academic award. Except where indicated by specific reference in the text, the work is the candidate's own work. Work done in collaboration with, or with the assistance of, others, is indicated as such. Any views expressed in the thesis are those of the author.

Nomenclature and Abbreviations

$\boldsymbol{\epsilon}^0$	Mid-plane strain vector
$\boldsymbol{\kappa}$	Mid-plane plate curvature vector
$\boldsymbol{M}$	Moment vector
$\boldsymbol{N}$	In-plane stress vector
$\boldsymbol{x}$	Design variables vector
δ_{P}	Minimum length for shear transfer
ℓ	Effective buckling length
$\epsilon_{\max}$	Maximum strain allowable
ϵ_x	Buckling strain
η	Transverse wavelength parameter, ranging from 0 to 1
λ	Half-wavelength in x axis in VIPASA
λ_{T}	Transverse (y-axis) half-wavelengths
ν_{12}	Major Poisson's ratio
ρ	Material density
θ	Individual ply angle
$\xi_{1-4}^{A,B,D}$	Lamination parameters
ξ_1^A, ξ_2^A	In-plane lamination parameters
ξ_1^D, ξ_2^D	Out-of-plane lamination parameters
b_{ext}	Extension of 'Outer' width
b_{fl}	Stiffener flange width
b_{seam}	Seam width
b_{sk}	Stiffener bay spacing width
b_{taper}	Taper width
c_1	Cognitive parameter
c_2	Social parameter

d	Levenstein distance
f	General objective function
F_i	Buckling factors
g	General constraint function
h	Laminate thickness (lamination parameter calculation)
h_{st}	Stiffener height
N_x	Design in-plane loading
p^g	Global best
p^i	Local best
p_{mutate}	Mutation percentage
Q_{ij}	Reduced lamina stiffnesses in ij^{th} direction
r_{st}	Outer radius for stiffener
t	Laminate thickness
V_{max}	Maximum velocity vector
w	Inertial vector
$w_i^{A,D}$	Weighting functions
z	Distance of ply mid-plane from laminate mid-plane
$(\text{EA})_{\text{bay}}$	Axial stiffness of a single stiffener bay
$(\text{EA})_{\text{st}}$	Axial stiffness of additional stiffener section
$\mathbf{A}$	In-plane stiffness matrix
$\mathbf{B}$	In-plane/out-of-plane coupled stiffness matrix
$\mathbf{D}$	Out-of-plane stiffness matrix
$\mathbf{U}$	Material invariants vector
AFP	Automated Fibre Placement
ATL	Automated Tape Laying
CLT	Classical Laminate Theory
CO	Constrained Optimisation
CTS	Continuous Tow Shearing
DST	Discrete Stiffness Tailoring

EA	Evolutionary Algorithm
GA	Genetic Algorithm
L	Panel length
MTOW	Maximum Take-Off Weight
N_T	Number of transverse modeshapes
NCF	Non-Crimp Fabric
NSA	Non-Standard Angle
P_x	Overall applied load
PSO	Particle Swarm Optimisation
QI	Quasi-Isotropic
SA	Standard Angle (0°, ±45°, 90°)
SQP	Sequential Quadratic Programming
VAT	Variable Angle Tow
VICON	see VIPASA. VIpasa with CONstraints.
VICONOPT	see VIPASA. VIpasa with CONstraints and OPTimisation
VIPASA	Vibration and Instability of Plate Assemblies including Shear and Anisotropy
VS	Variable Stiffness

Chapter 1

Introduction

Due to their superior stiffness-to-weight material properties and tailoring capability when compared with conventional metallic materials, the use of composite materials in aerospace structures has increased exponentially during the last half-century. Aerospace composite structures are created by depositing specifically orientated layers, created from continuous unidirectional fibres. The mechanical properties of the whole structure are defined by the selected orientations, and their position from the neutral axis within the laminate. The fibre angle and ply stacking sequence can be tailored for specific loading cases, currently cross-ply angles 0° and 90° are typically utilised for strength, aligning fibres parallel to applied loads, and ±45° pairs used for damage tolerance, buckling resistance and shear loading cases. This current industrial practice, however, does not make use of the full potential of stiffness tailoring, as panels typically employ a constant stiffness design, where the ply orientations and laminate thickness are constant throughout a structure. This design conservatism results in excess structural mass, which the aerospace industry is keen to reduce in order to decrease in-flight fuel burn and carbon emissions in the face of unprecedented global temperature increases. In consequence, there has been significant interest in Variable Stiffness (VS) concepts since the nineties, where the stiffness properties are varied spatially across a laminate, tailoring the local stiffness for the specific applied load and achieving greater material efficiency.

Research has demonstrated that compared to constant stiffness laminates, the use of variable stiffness designs results in significant performance improvements for a range of structural properties, such as stiffness [5, 6], strength [7], buckling behaviour [8–11], and post-buckling response [12]. Out of these, the large majority of recent work has focused on designing for increased buckling capacity, as a it is possible to obtain a significant level of increased performance [13]. This is particularly applicable to the design of aerospace wings, as they are thin-walled structures and therefore are vulnerable to buckling induced failure. However, the application of VS tailoring is still generally confined to the analysis of these designs and development of optimisation methodologies to manage variable stiffness concepts, with a paucity of experimental and analytical work conducted on larger, realistic industrial structures. Obstacles to wider implementation are the manufacturability of variable stiffness concepts, and the complexity of optimising these designs, as they require a far greater number of variables to describe the structure when compared to constant-stiffness laminates.

Previous work has implemented variable stiffness tailoring generally either in a discontinuous piecewise manner, dropping or adding plies to create a patchwork design [14, 15], or through the continuous variation of fibre paths [16]. Out of these, the latter, where the fibre path is parametrised as a curvilinear function over the laminate width, is the most researched, as it both ensures the preservation of structural continuity and reduces the number of design variables.

The manufacture of VS laminates is facilitated by manufacturing techniques such as Automated Fibre Placement (AFP) [17] and Continuous Tow Shearing (CTS) [18], although these technologies impose limitations on the design space which are necessary to ensure the creation of defect-free parts. As APF is capable of automatically depositing variable angle paths over complex geometries, this manufacturing method is the most commonly applied to VS problems, however this is a time-consuming process and, as such, unsuitable for use as part of large-scale commercial manufacturing operations [17]. The speed of manufacture and quality of the finished part are critical for the successful industrial implementation of VS designs as accompanying the need for more efficient aircraft design, commercial demand for new aircraft has also increased (pre the 2020 Coronavirus pandemic). At present, even considering automated deposition of only constant-stiffness carbon fibre designs, the manufacturing capacity does not meet demand and this deficiency is estimated to be somewhere in the order of four times the expected demand for short-haul aircraft in the next twenty years [19].

Alternatively, it has been proposed that the possibilities of structural optimisation using continuous fibre steering can be imitated by laying as few as three strips of material of different angle orientations across a flat plate [1]. The major advantage of this strip method, optimising the angle orientation, and hence referred to as Discrete Stiffness Tailoring (DST), is the speed at which a laminate using this technique could theoretically be laid up, especially when using an Automated Tape Laying (ATL) machine, and exploiting the use of Non-Crimp Fabrics (NCF), depositing two unidirectional plies of alternative ply angles simultaneously [20]. The DST laminate design would retain the buckling performance increase but now would be unrestricted by fibre angle turning radii and manufacturing defects associated with steered designs. The caveat, however, is that the plies are no longer completely continuous across the width, and the abutment of the plies creates a stress concentration in that region and subsequently there is a loss of transverse strength, although this is unquantified as of yet.

This thesis therefore aims to investigate the implementation of Discrete Stiffness Tailoring for the improved buckling performance of aerospace composite structures, capitalising on the assumed ease of manufacture that this methodology offers. Initially, a proof-of-concept study where DST is applied to compression panels through a simple redistribution of stiffness is used to validate the use of an efficient analytical model to design VS laminates for buckling. This is coupled with tensile testing to characterise the loss in transverse strength due to the discontinuous ply angles. It is clear that for VS designs to progress closer to

commercial implementation they must be demonstrated on a large-scale representative aircraft structure and, accordingly, DST is then employed to design a T-stiffened panel. In order to exhibit the full potential of the DST technique an optimisation routine, capable of efficiently and robustly returning optimum designs, is developed and then validated experimentally. A numerical study using the aforementioned optimisation methodology is conducted using a variety of compressive loadings and stiffener spacings, indicative of those experienced along a commercial aircraft wing.

Major contributions:

- Implementation and experimental demonstration of the DST manufacturing concept that avoids complex and inefficient tow steering technologies, and has no restrictions on fibre steering radii. This is supplemented with an investigation into the tensile strength of DST designs with varying percentages of seamed plies composing a laminate design.
- Novel application of a two-stage variable stiffness optimisation methodology to a variable stiffness, assembly-level, composite structure. Compared to previous work, the design space is uninhibited by specific VS manufacturing processes, although industrial manufacturing and design rules are implemented to ensure the generation of a realistic design.
- Investigation of the improved performance, and subsequent reduction in mass of VS stiffened wing panels under compressive loading. The buckling behaviour of the optimised DST designs are compared to baseline cases, and the effect of the tailoring technique is qualitatively, as well as quantitatively, assessed. This is the first time that fully optimised DST T-stiffened panel designs have been experimentally critically evaluated.

The thesis is structured as follows:

Chapter 2: Literature Review

A comprehensive literature review is presented, covering variable stiffness design concepts in depth, highlighting the advantages and disadvantages of each, and the current state of VS research. This review serves to highlight the need of a simple tailoring technique suitable for commercial application, compatible with high-speed automated manufacturing methods. A critical appraisal of optimisation methodologies used for the design of composite laminate structures is also undertaken, in anticipation of selecting an appropriate methodology for the optimisation of DST laminates.

Chapter 3: Discrete Stiffness Tailoring

This chapter contains a preliminary analytical and experimental feasibility study of the application of Discrete Stiffness Tailoring for increased buckling performance. This proof-

of-concept research also evaluates the criticality of 'seamed' regions, where the ply angle changes instantly, introducing a weakness within the structure. In this chapter, the concept of DST is used to redistribute material within a standard ply quasi-isotropic baseline laminate without loss of in-plane stiffness. Improvements in buckling performance are assessed using numerical and experimental methods. Two different ways of staggering seams are explored and experimental and numerical tensile testing is used to evaluate their impact on transverse tensile strength.

Chapter 4: Optimisation Methodology

A two-stage optimisation methodology is implemented for the optimisation of tailored laminate structures, specifically focused on the design of a T-stiffened panel. The first stage optimises continuous lamination parameters, structural widths and laminate thicknesses to return a minimum mass design able to withstand a given compressive load without buckling. Two approaches, a gradient-based method and Particle Swarm Optimisation (PSO) are implemented and compared for functionality and efficiency for the first optimisation stage. The second stage uses a Genetic Algorithm (GA) to return a discrete stacking sequence, optimised to best replicate the lamination parameters selected by the first stage. Manufacturing constraints are applied in both stages to ensure the realistic feasibility of the design.

Chapter 5: Stiffened Panel: Analysis

The previously developed optimisation methodology is used to optimise several different configurations of a T-stiffened panel for minimum mass, including a fully discretely stiffness tailored case with thickness variation, and these panel designs are compared to a baseline case. Comparisons are made between the critical buckling modes and final stiffened panel designs and geometries.

Chapter 6: Stiffened Panel: Experimental Validation

The DST case from Chapter 5 is manufactured and tested to failure to provide validation of the optimisation routine established in Chapter 4. The manufacturing and test procedure is described, the experimental results are presented and compared to Strip Model and FE analyses. The failure mode is discussed with significance to the transverse discontinuities introduced using discrete stiffness tailoring.

Chapter 7: Study - Infinitely Wide Panels

In this Chapter, the optimisation methodology implemented in Chapter 4 is adapted to consider the use of non-standard angles in DST design, and to maximise the number of continuous plies present in adjacent laminate regions, preserving transverse strength. A numerical study of infinitely wide T-stiffened panels under varying levels of compressive load, alternative stiffener spacings, and panel lengths is undertaken using this expanded methodology. The load cases are representative of commercial aircraft upper wing skin panels, and the benefit of using DST is discussed with reference to industrial application.

Chapter 8: Conclusion

Final conclusions are drawn, considering all the work contained in this thesis. Future work is suggested.

Chapter 2

Literature Review

This chapter presents a review of relevant academic literature for the work conducted within this thesis, the main topics being Variable Stiffness (VS) composites and the optimisation of VS structures. A focus is placed on the current state-of-the-art applications of stiffness tailoring, particularly those designing for buckling performance. The review highlights the disadvantages of current variable stiffness concepts in regards to fabrication, and presents an argument for an alternative method that would be more efficient to manufacture, such as the one presented in this thesis. Alongside this, a general brief review of methodologies for laminate optimisation are mentioned and the major optimisation techniques employed when considering variable stiffness structures are discussed.

The topics covered are divided as follows:

2.1 Variable stiffness concepts

2.2 Manufacturing processes for VS laminates

2.3 Experimental testing of VS laminates

2.4 Optimisation techniques for VS composite design

2.5 Industrial design rules

The topics listed above are interrelated so, for clarity, the scope of each section is as follows: the variable stiffness concepts section lists the methods implemented for the theoretical and experimental design of variable stiffness laminates, and quantifies the performance improvements achieved, depending on problem formulation and applied constraints. The manufacturing section details the techniques used for fabricating the designs, manufacturing issues, defects and VS process constraints. Experimental testing covers VS experimental work, particularly comparing theoretical and experimental results. The optimisation section lists and critiques methodologies for comparative efficiency and functionality, but does not comment on the optimisation results.

2.1 Variable Stiffness Concepts

Fibre-reinforced composite materials are employed widely in the aerospace industry due to superior specific stiffness and strength properties. In addition, the material anisotropy of unidirectional fibre composites allows the designer to tailor fibre orientations through

a stacking sequence of plies to suit a given design requirement. Accordingly, the traditional design of a composite part is made through the selection of ply angle combinations that provide certain desired mechanical properties, where the stacking sequence is uniform across the part: the fibre direction is kept constant and ply thickness is unvaried. Greater material efficiency and improved structural performance can, however, be achieved if tailoring is advanced to allow variation of stiffness with location in the structure, expanding the available design space compared to constant stiffness designs.

Variable Stiffness (VS) designs redistribute the in-plane loads and stresses within a structure benefiting the laminate performance; previous theoretical work has shown improvements in stiffness-based design problems [5, 6, 21], increased strength in laminates with cutouts [22–24], buckling and post-buckling behaviour of flat panels [1, 9, 11, 12, 14, 16, 25–56] and buckling resistance in plates with circular holes [8, 57–59] compared to constant stiffness designs. Additional work has also applied variable stiffness techniques for increased buckling capacity of cylinders and cylindrical shells [60–62], and for improved laminate aero-elastic response [63–65].

In the maturity assessment of VS design process conducted by Sabido et al. [13] in 2016, 39 out of 90 evaluated papers either focused solely on designing for buckling performance or included buckling constraints. Preliminary research into VS applications for buckling optimisation indicated that significant improvements, on the order of doubling the buckling load [14], were possible compared to other applications. The increase in buckling load for VS flat panels is accredited to the redistribution in axial stiffness (0° plies) to the regions that are supported by a boundary, which are physically restricted from deforming out-of-plane [25]. Whilst the load is supported at the boundary, placing buckling resistant 'softer' material such as ±45° plies, the optimum constant angle for buckling resistance [66], is permitted away from the constrained boundary, ultimately increasing the load at which buckling occurs. As VS designs allow for greater material efficiency, Ijsselmuiden et al. noticed that the additional design flexibility caused the first two buckling modes for optimised variable stiffness panels to coincide, showing the importance of assessing multiple modes within an optimisation routine [11]. A focus on buckling research also exists as a significant number of aerospace structures, such as wing covers, fuselage and empennage panels, are thin-walled plate-like structures, stiffened with ribs or stringers, that carry compressive loads and, naturally, buckling is assessed as the critical mode of failure [67]. However, the vast majority of work is limited to simple flat panel buckling, and only a small number of papers have extended the variable stiffness concept to realistic structures, such as the optimisation of stiffened panels [68] or wing-boxes, where the top and bottom covers are variable stiffness, stiffened panels [69, 70].

Spatial variation of in-plane stiffness can be achieved through the application of three main concepts: variable fibre volume, a curvilinear fibre format and discrete stiffness variation, as illustrated in Figure 2.1. Preliminary variable stiffness designs were achieved through the variation of the fibre volume fraction within a ply, where a single layer is described as

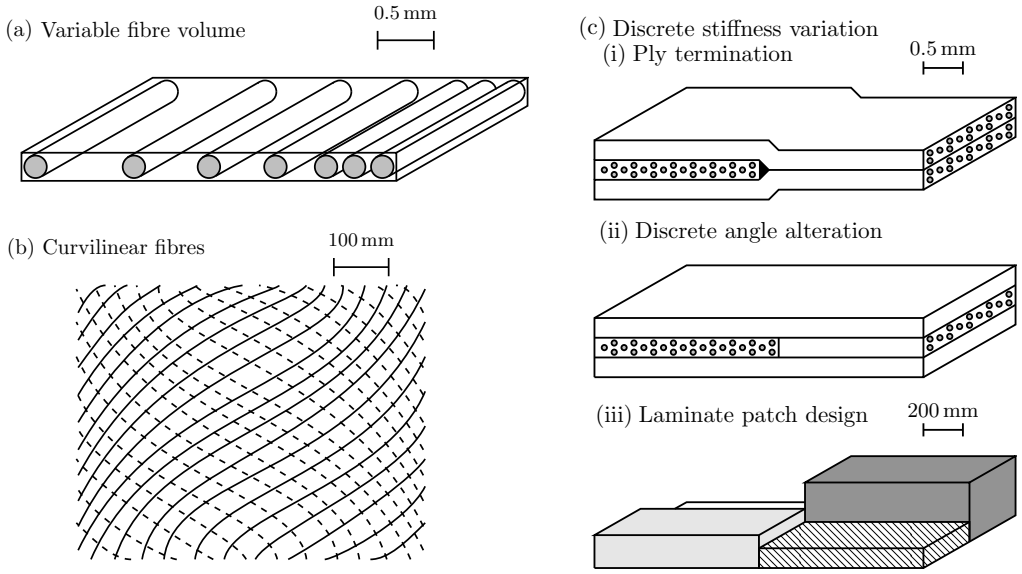

Figure 2.1: Variable stiffness formulations (a) variable fibre volume, (b) curvilinear fibre paths, and (c) Discrete tailoring concepts. Scales provided are approximate to show relative sizes.

'*macroscopically orthotropic, but nonhomogenous*' [71, 72]. In this work, the Ritz method was applied successfully to determine the stress distribution in a single ply plate, and subsequently to calculate buckling loads and fundamental frequencies, which showed performance increases of up to 40% compared to constant stiffness designs. Concurrent with this work, Hyer and Charette introduced a curvilinear fibre format, where the fibre angle is a function of location [8, 22], and this was applied to design plates containing central holes for increased tensile strength and buckling resistance. Improvements in performance were achieved but, as was necessary for the application of a finite-element model, the discretisation of the laminate geometry into separate, unconstrained regions did not guarantee realistic smooth fibre paths, only approximating continuous fibres. Nevertheless, when compared to the variable fibre volume concept, the curvilinear parametrisation of the fibre path allows for tailoring greater possibilities and an expanded design space allowing for local optimisation of fibre orientations.

2.1.1 Curved Fibre Design

The curvilinear concept was reinterpreted by Gürdal and Olmedo into its contemporary format which assumes that fibres are continuously curved, and hence the fibre path variation can be parametrised by shape functions, which, depending on the function order, reduces the number of variables describing the path to a handful [16]. A consequence of modelling the fibre path with regards to laminate geometry allows for manufacturing constraints, such as the fibre steering radius, to be easily enforced. In addition, as fibres can only be deposited in parallel courses due to practical manufacturing limitations, the fibre orientation across a single ply is restricted to only vary in one fibre reference axis i.e., either the x or y-axis. Exploratory studies have found that stiffness variation in the axis

perpendicular to the direction of the applied load is most beneficial for buckling improvements [15, 16]. Variation in the direction parallel to the load produced some buckling improvement, but this was not as significant and was found to be due to more favourable induced transverse stresses, rather than redistribution of the applied load. A 80% improvement in buckling load was obtained for an example Variable Angle Tow (VAT) plate, with angle variation perpendicular to the load, compared to a baseline plate of the same thickness. Equations again based on the Ritz method were derived for the response in terms of stress and strain developed in a variable stiffness panel under axial loading for a linear variation in the fibre angle.

The use of variable angle designs can decouple the relationship between buckling response and overall axial stiffness of a compression panel [25]. Work suggests, however, that the increase in buckling performance can come at the expense of decreased laminate strength, if this is not implemented as a constraint [73]. Subsequent research optimising VS flat panels, maximising a combined buckling-stiffness (implemented as a surrogate for strength) objective function, indicates an upper bound of double the buckling load of a comparable quasi-isotropic panel, whilst the same in-plane stiffness is maintained, [11]. Subsequent work using topology optimisation suggests that if the ply angle variation was combined with variable laminate thickness, that this can mitigate the effect of the stiffness constraint inhibiting the maximum achievable buckling load [46]. Irisarri et al. [74] also investigated optimising the thickness distribution alongside fibre steering, indicating that combining the two produces a 100% increase in panel buckling load when compared to the best constant thickness steered fibre panel. This indicates that both the thickness and the fibre angle variation, as commented on in [1], ought to be combined to produce the greatest increase in buckling efficiency.

2.1.2 Discrete Tailoring Design

The stiffness can also be varied in a piecewise manner, where the structure is discretised into regions with alternative stacking sequences, and plies are terminated or added, as depicted in Fig 2.1c. Techniques utilising a discrete variation in stiffness include the piecewise redistribution and thickness variation of 0° plies [14, 15] and discontinuous ply angle alterations without thickness variation [7, 75]. DiNardo and Lagace experimentally investigated the buckling and post-buckling behaviour of panels with ply-drop offs and discrete angle changes, concluding that tapering compression panels has a marked effect on their response under load [76]. Biggers and Srinivasan [14] found that simply redistributing material within laminates with conventional ply angles can increase the compressive buckling load by approximately 200% from a baseline flat panel. The same volume of stiff material was maintained between the baseline and tailored cases, preserving the overall axial stiffness of the plate. The parametric study included altering the flexural stiffnesses in the central and edge regions through stacking sequence permutations, varying the ratio of the inner and outer strip widths, and applying different boundary conditions. An

ABAQUS finite element model was used to model the response. Using discrete ply steps and strips is a highly simplistic way of achieving tailoring, and theoretically this can be highly effective as large changes in stiffness can be altered abruptly.

Discrete tailoring solutions, however, introduce material discontinuities within a structure, and differing angle plies laid side-by-side attract high stress concentrations due to stiffness mismatching, as the load is redistributed around the abutment. Vizzini [7] developed a finite element model to analyse the stress at ply junctions and then used failure criteria to predict the seam transverse strength. Experimental testing of rotor-craft blades with altered edge stacking sequences, where two plies of different fibre orientations are laid down in the same ply plane, showed the failure of the specimens resulted from damage emanating from the material discontinuity [75]. The zones at the tip of a ply drop or in-between discrete ply changes are resin-rich which makes them inherently weak, and delamination can easily initiate and subsequently propagate from these areas. Hence, a minimum distance between subsequent ply drops or angle joints, as small as three times the ply thickness, should be maintained in order to avoid local damage accumulating in one region [77].

It is important to note that there is a significant subsection of work in focused on optimally designing large composite structures that experience varying loads across the length and width, in which the structure is discretised into regions and each region is optimised for the local load, i.e a 'patch' design as illustrated in Fig 2.1c. This is essentially a 'variable stiffness' structure, with the exception that no load redistribution occurs as a consequence of the design. However, to ensure the design is manufacturable and structural integrity is not critically reduced, it is necessary to apply 'blending' constraints that limit the stacking sequence variation between adjacent regions [78]. The problem of matching regions to ensure manufacturability also occurs in discrete stiffness tailoring, similar to continuity constraints for curvilinear fibres, as maintaining an adequate level of transverse continuity is necessary for strength and structural integrity. Applying this constraint is likely to lead to a loss in buckling performance [79], or excess mass. Techniques for implementing blended designs are detailed in Section 2.4.

2.1.3 Concept Comparison

The curvilinear fibre tailoring concept, when represented with low-order polynomial expressions, provides an analytically simple way to model structures with variable fibre orientations, and this guarantees structural continuity across the part. However, the radius of curvature that can be obtained realistically is a limiting factor to the achievable designs. Besides this, other manufacturing considerations, such as the width of the deposited fibre tows, and tow overlaps and gaps, must also be built into predictive models used for optimisation and design, as they affect the response of the laminate, this is discussed in detail in Sections 2.2 and 2.3. In addition, despite the advantage of a gradual stiffness transition, all other mechanical properties vary with the fibre angle change, including the

Poisson's ratio which peaks at a value of 1.5 at approximately 25°, creating a more highly strained region compared to those adjacent.

Discrete tailoring techniques, where plies are terminated or added at discrete locations within the laminate, have to maintain a level of transverse continuity in the form of constant angle plies that are shared between adjoining regions, whereas curvilinear fibre paths innately maintain integrity of the part. The optimisation of curvilinear fibre paths are constrained by minimum fibre steering radius, but discrete stiffness transitions are able to effect abrupt changes in stiffness and thickness. The ability to simultaneously tailor the laminate thickness and fibre angle across a width of a compression panel has been shown to analytically achieve a 40% weight reduction, attaining the same critical buckling load, provided that the fibre steering radius can be precisely controlled [1]. However, the same mass reduction can theoretically be achieved using four discrete prismatic strips of material with constant angles, with the added advantage of being easy to manufacture with already developed methods. This review therefore concludes that discrete stiffness tailoring is a promising candidate technique, as it is able to theoretically attain the same performance increase as curvilinear fibres, but is superior in terms of manufacturing complexity and speed of material deposition.

2.2 Manufacturing Processes for VS Laminates

Aerospace composite structures are fabricated using automated manufacturing methods in order to achieve a high-rate of fibre deposition and to regulate the variation in finished components compared to the uncertainties with hand lay-up. The manufacturing tolerance and uncertainty associated with automated fibre placement systems is in the order of ±3°. Automated processes also reduce time that would be lost visually inspecting each component in full for defects and reworking of defected parts [80]. Fibre rolls, pre-impregnated with resin (pre-pregs) are generally used instead of processing dry fibre, as they are easily handled during the manufacturing process and provide consistent quality laminates [81]. There are two significant technologies employed in the aerospace industry today for the precision manufacture of composite parts using pre-preg material: Automated Fibre Placement (AFP) and Automated Tape Laying (ATL).

The AFP process uses an automated placement head, controlled by a robotic arm, which places short pre-preg tows with widths of under 15 mm onto a mandrel or mould, and is capable of laying down 8-32 strips in one movement. The flexibility of the process allows for the fabrication of complex curved structural geometries and the creation of variable stiffness panels, as the deposition paths are precisely controlled and able to follow predefined curvilinear paths to create the fibre angles desired [82]. Automated Tape Laying is similar in principle to Advanced Fibre Placement, but is able to deposit strips of material that are significantly wider, approximately 75-300 mm, in comparison to AFP, which uses 3.2-12.7 mm wide tows [17]. Therefore, ATL technology is more suitable for achieving the high rates of material deposition required by the aerospace industry, although it is

generally restricted to forming flat surface parts as the larger tow widths are unable to achieve the precision required for VS laminate fibre curvatures. For the formation of more complex curved geometries, the tapes can be laid flat and then created using hot-drape forming processes [83]. Accordingly, AFP is the primary method for the construction of variable angle laminates, as identified in the review of the automated techniques for creating Variable Angle Tow (VAT) structures produced by Lozano et al. [84].

A historical study of automated technologies conducted by Lukaszewicz et al. [17] highlights the interdependency of the design and manufacture of composite components. Achieving optimised variable stiffness designs requires manufacturing methods with the ability to create such structures, and the design process must account for the limitations of manufacturing feasibility [84]. Manufacturing constraints for the design of curvilinear fibre paths identified in the literature can be ordered into four categories: continuity constraints, to maintain a smooth fibre trajectory across a part; steering constraints, which limit the rate of change in fibre angle with location; the tow width, determining the 'coarseness' of the design achieved as the deposition of discrete tows approximates a smooth curve; and the presence of ply gaps and overlaps in the final design, which affect both the final performance and material efficiency of the manufactured part.

Continuity constraints are generally easily incorporated through parametrisation of the fibre path [16] and are commonly applied in optimisation studies to achieve a smooth distribution of the fibre angles [16, 25, 73, 85, 86]. However, the achievable steering radius of these fibre paths using AFP is a significant limitation when designing VAT laminates. The limits on the turning radius are between 12 and 25 inches (300 mm and 635 mm respectively) depending the tow width [10, 26, 87]. Radii smaller than these theoretically could be achieved, but not without inducing local fibre buckling and distortion. Imposition of a minimum steering radii is commonly applied as a constraint for optimisation, particularly when designing for buckling to guarantee manufacturability [6, 26, 31, 46, 74]. A study conducted by Campen et al. [85] focused on generating realistic fibre angle distributions from lamination parameters, which found that imposing a $4.878\,\mathrm{m}^{-1}$ maximum curvature constraint (approximately equivalent to a 210 mm minimum steering radius) on a square 0.5 by 0.5 m panel reduced the maximum achievable buckling load by 8% compared to the unconstrained case, similar to markdown found in [88]. A similar study in [56], using a minimum fibre turning radius of 333 mm, found that the imposition of a minimum manufacturable turning radius produced a 17.5% decrease in optimal buckling load after retrieving fibre courses from lamination parameters.

Besides the restriction on fibre steering, AFP also creates unavoidable process induced defects, as most methods assume that the fibres are shifted with respect to each other, and this forces the designer to choose between including gaps and/or overlaps [27, 89]. Figure 2.2 illustrates variable-angle designs manufactured with tow overlaps and gaps, compared to a constant-angle ply, and these defects create local discrete thickness variations that introduce fibre waviness in surrounding material. In the two major studies on

the effects of gaps and overlaps conducted by Croft et al. [90] and Marouene et al. [53], the compressive behaviour of variable stiffness laminates are affected by the presence of the defects, where compression panels with complete overlaps produce higher pre-buckling stiffness and buckling loads than those with gaps. The gaps and overlaps can also induce in-plane extension shear coupling (A_{16}, A_{26}) due to laminate asymmetry, although the experimentally measured effect on structural response was found to be negligible [53]. Traditional constant stiffness plies are commonly added as outer layers to laminates that are formed using these processes, to mitigate any risks associated with impact damage, which can decrease overall material efficiency [89]. Out-of-plane wrinkling of the tows can also occur during the variable angle manufacturing process [55]. The process parameters, the speed of deposition, temperature control etc., were found to have a significant impact on the quality of the laminates created, where process efficiency is generally traded for higher laminate quality.

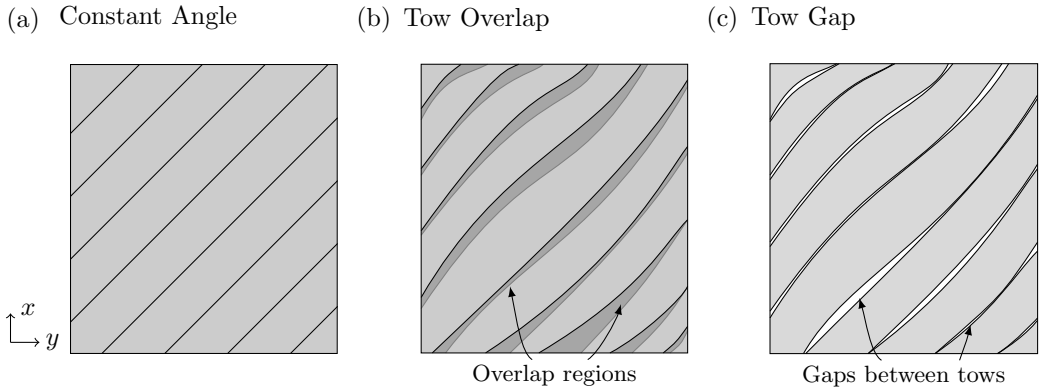

Figure 2.2: Ply courses for (a) constant-angle traditional laminate, and variable-stiffness laminae created using (b) tow overlaps and (c) tow gaps.

To overcome the fibre wrinkling associated with tighter radii of curvature, the Continuous Tow Shearing (CTS) process was developed, which utilises the deformable characteristics of dry fibre tows in shear to produce continuous curvature [91]. This shearing process alters the cross-sectional area of the tow across the width of a structure, creating a gradual thickness variation across the width which could be exploited for further structural optimisation. The fibre deformation means a smaller (<30 mm) radii of curvature can be achieved without fibre wrinkling, proven experimentally in [18], and also avoids the production of tow-drop defects as found inherently in AFP laminates and described above. The difference in the fibre courses between each process is illustrated in Fig. 2.3. The increased flexibility of CTS allows for a theoretical 23% mass reduction when optimising a panel with buckling constraints, over a AFP design with no thickness variation [92]. A similar study in [1] found that the freedom of CTS to tailor local thickness and the smaller steering restrictions allowed for the panel to buckle into a higher energy modeshape than a constant thickness AFP design, procuring a 32% weight saving. However, the CTS procedure is inefficient in terms of the time required to create a tailored structure, usually a flat panel. A recent conference paper has shown that this technique can now also be

applied for manufacturing a variable angle component using wide pre-preg tows as used in ATL. The rate of deposition, however, is still far lower than commercially acceptable, between 2 and 8 mm/s, dependant on the steering radius [93]. For comparison, deposition speeds of 1 m/s are typical for AFP and ATL systems, corresponding to productivity rates of 8.6 kg/h and 29.2 kg/h respectively [17]. The CTS process, in this instance, can achieve a 50 mm radius of curvature with 100 mm wide pre-preg tapes. The fibre steering radius achievable using this technique is significantly smaller than possible with AFP (300-635 mm) or ATL (11000 mm with 100 mm wide tapes) [93]. An alternative manufacturing technique uses an embroidery based process to achieve the flexibility of CTS, allowing for greater variation of fibre angles across a given distance, without the associated undulation in thickness or fibre volume fraction across a part [10].

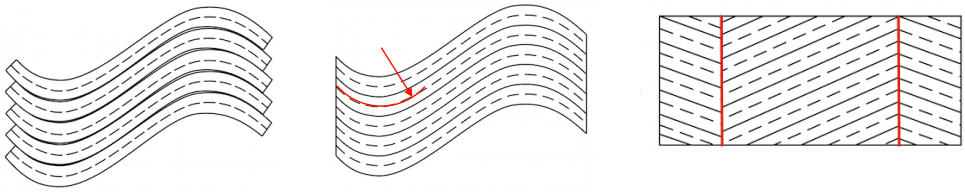

Figure 2.3: Comparison of (a) AFP, (b) CTS, and (c) DST fibre path variations. The radius of curvature of the fibre path is marked in (b).

Alternatively, variable stiffness laminates can be manufactured using discrete ply variations, creating laminates with ply drops, additions or discrete angle alternations across the width, creating a joint [1, 14, 74, 94]. Sliseris and Rocens [94] use a discrete variable stiffness concept to optimise the core of sandwich structure, which is composed of a wooden internal ribs. Fig 2.3c depicts a discrete change in fibre angle within a single ply layer, where the red line indicates the joint. Discrete methods benefit from being compatible with high-deposition automated manufacturing techniques such as ATL, which is able to accomplish both a high rate and precise deposition of unidirectional pre-preg suitable for these designs [95]. Sharp changes in stiffness can be effected over comparatively smaller distances, allowing for greater flexibility in the design of variable stiffness structures. Continuity constraints, however, must be applied to remove significant discontinuities between adjacent regions that are either impossible to manufacture or critically reduce structural integrity [78]. The effect of these constraints on the performance of variable-stiffness discrete designs are, as of yet, unquantified.

The advent of multi-material additive manufacturing methods allows the fabrication of spatially varying micro-scale fibre structures, blurring the line between material and structure. Boddeti et al. [96] demonstrated the optimal design and manufacture of variable stiffness laminate plates, with and without holes, using this methodology. The resulting optimised designs are a combination of varying fibre volume and curvilinear fibres. The manufactured parts, however, contained large numbers of defects due to the discontinuous deposition of material, typical of additive manufacturing processes, and the rate of

deposition is low.

2.3 Experimental Variable Stiffness Research

Experimental studies of variable stiffness laminates in general are limited, with approximately twenty papers covering all applications for performance and manufacturing process defect investigations. Proof-of-concept exercises, demonstrating both the capability of manufacturing technologies in creating variable stiffness panels and validating of the magnitude of the predicted buckling performance increase with flat panels have been presented in a small number of papers [10, 27, 28, 52, 53, 57, 58, 76]. The weight-normalised, experimentally obtained, buckling performance increases for optimised variable stiffness designs, when compared to quasi-isotropic laminates, are in the region of 22% for panels with gaps, 45% for those with overlaps [52], and approximately 30% for a panel containing neither [10].

Tatting and Gürdal [27] were the first to integrate manufacturing considerations in an optimisation routine for buckling panels with holes, and the first to directly transfer designs to manufacturing instructions. The work in [28] and [57] investigates the effect of tow gaps and overlaps within buckling panels with and without holes. The specimens with overlaps significantly out-performed those with ply gaps in comparison those containing tow gaps. Buckling behaviour was poorly predicted by FEA for both sets of VS panels, with discrepancies as high as 15-20%. As the experimental behaviour of the constant fibre baseline cases were accurately assessed, the errors can be assumed to come from the modelling of the tow steered designs. Similar modelling errors were also found in [10], where FEA was also used to predict the buckling load increase of tow placed, embroidered VS simple flat panels. In this study, a quasi-isotropic stacking sequence is used as a base for the tailored designs, and the 0° and 90° layers are tailored longitudinally or transversely respectively, creating flat panels with central variable-angle regions whilst the cross-ply design is maintained in the outer frame. The conclusion from these studies suggest that in order to accurately predict the buckling performance of VAT laminates, a high fidelity, detailed finite element mesh is required, accounting for any thickness variation. Marouene et al. [53] confirms this by obtaining excellent correlation between numerical and experimental buckling results, using a MATLAB routine to identify the defect locations, which was used to assign material properties and geometric features in the FE model. The gaps were modelled using resin material properties, and the overlaps as double thickness plies.

A maturity assessment of the variable stiffness design methods conducted by Sabido et al. [13] found that although the performance improvements of simple flat panels with stiffness tailoring can be well-predicted and are validated with the limited experimental tests as discussed above, there is a lack of work quantifying the benefit of applying tailoring to complex structural components. The first structural level variable stiffness aerospace parts have been fabricated: both Wang et al. [69] and Oliveri et al. [70] have designed, manufactured and tested wingboxes with fully steered skins. However, neither of these

designs is optimised, and so the design of variable angle panel is based on achieving the orientation of $\pm 45^{\circ}$ plies in the unsupported skin region between the stiffeners for maximum buckling resistance. Specifying the ply angle in the free skin region limits the variation that can be obtained either side, as the steered tows are subject to minimum radii manufacturing restrictions, so the final steered fibre orientations vary between $\pm 35 - 55^{\circ}$. A third-scale minimum-mass wingbox was optimised for both aerodynamic and structural constraints, then manufactured and tested [65], however, the fibre stacking sequence is restricted to be locally orthotropic with respect to the global tow path, and these stacks are created of plies with predefined curved fibre architectures. The pre-set curved fibre geometry and stacking sequence reduces the number of variables but overly constrains the design space.

2.4 Optimisation Techniques for Composite Design

A full review of optimisation techniques applied for the design of traditional constant stiffness laminates can be found in [97], and a companion paper, reviewing strategies for the optimum design of Variable Stiffness Laminate is found in [98].

2.4.1 Overview of Constant Stiffness Laminate Optimisation Techniques

The target of any composite structure optimisation is the identification of the most optimal laminate formulation. This is composed of a discrete number of plies, a selection of ply angles (generally from a restricted set of orientations), and their order within the stack. The optimum design of composites is intrinsically challenging owing to the non-linearity and non-convexity of the design space due to the trigonometric relationship between ply angles and laminate stiffness, as well as the existence of large numbers of both discrete ply stacking and continuous fibre orientation and geometric variables. In reality, the angle variation may be restricted to discrete steps of $\pm 5^{\circ}$ due to manufacturing constraints, but even with a limited set of allowable angles, a significant number of design variables still remain. The design of minimum-mass structures is particularly complicated as the number of plies, and hence number of design variables, can change with each iteration, and thick laminates can require significant numbers of variables which can become unwieldy. Schmit and Farshi [99] optimised the ply thicknesses of a fixed set of standard angle plies in a predefined stacking sequence for buckling, using linearised approximations of the objective and constraint functions, which allowed for the use of an efficient Linear Programming (LP) method. However, this method does not return discrete ply variables or allow for the optimisation of through-thickness ply positions.

Gradient-based methods, where the gradient information of the objective and constraint functions influences the direction and step size of the search, are commonly applied optimisation techniques to composite design, as the objective function or constraints are usually are non-linear [97]. Use of a gradient method is generally dependant on being able to express the objective and constraint functions as differentiable expressions, although

approximations can be used if not available, though this tends to be computationally expensive. This optimisation algorithm tends to converge rapidly, requiring few iterations, but if response of the structure is evaluated using an expensive model then this efficiency is markedly reduced. To overcome this, Blom et al. [35] used a surrogate model, which approximated the results of the FE model with much smaller computational expense, to reduce the number of finite element analyses in the optimisation of VS cylindrical shells. The surrogate model was also used to determine objective function derivatives, avoiding excess computation associated with calculating derivatives using finite differences. Analytical models are often used in optimisation studies, and in conjugation with gradient based methods, as these can be solved more efficiently than Finite Element (FE) analyses, and for the ease of obtaining function derivatives. The derivation of closed-form equations based upon a Rayleigh-Ritz approach is particularly common for buckling analysis [100–102] and the results from these show excellent correlation with FE models with far less computational expense.

Stroud and Anderson [103] developed the computer code PASCO for the minimum mass optimisation of stiffened composite structures subject to buckling, stiffness and strength constraints, where ply angles, ply thickness and structural widths are continuous variables. The buckling problem is solved using an efficient finite strip model, which solves the governing equations exactly for prismatic structures discretised into lengthwise strips, producing results comparable with FE models with far smaller computational expense [104, 105]. The optimisation algorithm uses a non-linear programming approach requiring evaluation of the derivatives with each iteration, using Taylor series for approximate analysis of the constraint functions to improve computational efficiency. However, using ply angles as primary variables gives rise to a highly non-convex design space, potentially trapping the optimiser in local optima. The position of the final converged solution is also dependent on the initial starting point, so the likelihood of returning a global optimum can be increased by re-running the optimisation from random start points, providing this is not computationally too expensive. Besides this, a requisite of gradient-based approaches is continuous formulation of the design variables. Hirano [106] solved the unconstrained buckling maximisation problem of plates under axial compression using a conjugate direction technique (Powell's method), eliminating dependence on derivative calculations. Laminate symmetry and equal number of the optimum angle $\pm\alpha^\circ$ plies are assumed, but otherwise complete continuous freedom in the choice of ply angles is allowed, leading to unmanufacturable non-standard angle designs.

Optimising solely and directly using discrete variables has been achieved using integer programming formulations, using ply identity design variables to formulate a linear problem that is easily solved by commercially available software [107], or direct search methods, e.g. Particle Swarm Optimisation (PSO) [108] or Genetic Algorithm (GA), an evolutionary algorithm based on the Darwinian principle of 'survival of the fittest' [109, 110]. In a genetic algorithm, design variables are simply encoded in bit strings, mimicking genetic

sequencing. A population of solutions is randomly created, assessed using the objective function and then are ranked. With each iteration the algorithm preserves some of the best solutions, known as elitism; mates a percentage of high ranked solutions, crossover, to push the designs towards the best known solutions; and randomly mutates a number of genes in some solutions, mutation, to promote exploration and avoid premature convergence to a local optima. Applications of GAs are common for stacking sequence optimisation [111, 112], as they are not dependent on gradient assessment, and the discrete formulation means that laminate design rules, such as symmetry and ply contiguity, can easily be enforced with penalty functions. However, GAs (as with all direct search methods) are computationally expensive as convergence is slow and each iteration requires the evaluation of the objective function and constraints for the whole population, and more efficient methods can be used allowing for continuous variation of the parameters. In order to implement a gradient-based approach for the design of composite structures, it therefore becomes necessary to express the design variables in an alternative way that reshapes the relationship between the ply angles and stiffnesses.

2.4.2 Lamination Parameters

The relationship between ply angle and ply stiffness as defined by Classical Laminate Theory (CLT) [113] is trigonometric, which leads to the creation of a non-convex response surface if used directly in optimisation techniques. The lack of convexity creates the presence of local optima, which masks the search for the global optimum. This therefore creates an optimisation problem best not solved with a gradient-based approach, which is most desired for its rapid rate of convergence. Optimising with lamination parameters can, however, overcome the limitations associated with ply angles. These continuous, non-dimensional variables, first introduced by Tsai and Pagano [113, 114], enable the stiffness of any laminate to be characterised using a maximum of thirteen variables - one thickness variable and twelve interrelated lamination parameters, which reduces to four for specially orthotropic laminate designs. This is particularly useful for minimum mass problems, as the number of parameters does not change with thickness variation.

Laminate stiffness has linear dependence upon lamination parameters which has been shown to give rise to convex optimisation problems when these are used as design variables [115, 116]. As the space is proved convex, gradient-based optimisation methodologies can be applied. Optimising using lamination parameters is complicated by the fact that all parameters are interrelated to each other, and to maintain solution feasibility, the relationship between parameters must be understood and applied as constraints. Grenestedt and Gudmundson used a variational approach to numerically determine the feasible LP space for orthotropic symmetric laminates. Alongside proving the region to be convex, they derived explicit expressions for the relationships between in and out of plane lamination parameters, work which was extended by Diaconu et al. [117] to cover the standard angle design space for all 12 lamination parameters. Equations expressing the feasible re-

gion for larger sets of ply angles, i.e. including ±30° and ±60° alongside standard angles, have been determined using convex hulls by Bloomfield et al. [118], and a similar approach by Setoodeh et al. [119] created approximate expressions describing the full region of lamination parameters with no restrictions placed on the ply orientations. However, the number of linear equations required to constrain all 12 parameters increases rapidly when including more ply orientations within the predefined range, equalling over 30,000 for the approach in [119], requiring significantly greater computational effort when applied in an optimisation strategy. Based on the approach taken by Bloomfield et al., Wu et al. [86] derived a new, more accurate, set of explicit non-linear inequality constraints that define the interdependent feasible parameter space for the in-plane ($\xi^A_{1,2}$) and out-of-plane ($\xi^D_{1,2}$) lamination parameters with no ply angle restriction, reducing the number of equations required to a maximum of 21.

Fukunaga and Vanderplaats [120] and Miki and Sugiyama [121] first implemented lamination parameters as fundamental design variables in stiffness and buckling optimisation problems for laminates with fixed thicknesses. Lamination parameters can easily be substituted in any problem where the homogenised laminate stiffness obtained from Classical Laminate Theory (CLT) is used. However, this precludes their direct use in the analysis of performance or design criteria, e.g. strength or laminate design rules, that depend explicitly on ply angles and stacking sequences. As a result, global stiffness or strain constraints are often used as a proxy for strength [122–124], but depending on the problem these are not always analogous. Ijsselmuiden et al. [125] incorporated a conservative failure envelope based on Tsai-Wu failure criteria in the lamination parameter design space, and found that optimising directly for strength instead of stiffness resulted in an increase of 48% in the factor of safety. Laminate design rules, as detailed in Section 2.5, must also be derived with respect to lamination parameters, ensuring that the returned designs are manufacturable and realistic. Laminate robustness against secondary unexpected loading is traditionally imposed by limiting the stack to contain a minimum (10%) of each standard angle ply. Abdalla et al. derived expressions that bound the 10% rule feasible region, which was formulated by constraining the ratio of minimum to maximum stiffness of a laminate [126]. The design rules concerning laminate symmetry and balance, which remove extension-bending ($\mathbf{B} = 0$) and extension-shear coupling (A_{16}, $A_{26} = 0$) are more simply applied by setting certain lamination parameters, $\xi^A_{3,4}$ and ξ^B_{1-4}, to zero. Bend-twist coupling can be minimised (D_{16}, $D_{26} \approx 0$) by setting $\xi^D_{3,4} = 0$, as this is always present in symmetric and balanced laminates.

Another difficulty associated with the use of lamination parameters is ensuring that any set of optimal parameters correspond to a physical laminate solution. Retrieving a discrete stacking sequence from continuous lamination parameters is not trivial, as no one-to-one mapping exists for the inverse transformation, and cannot be solved with closed-form equations. Therefore, the problem has been addressed with the use of precomputed laminate databases, which spans the entire lamination parameter space [127], or has been

solved as a separate optimisation problem, where the euclidean distance between the optimal and the discrete trial solution lamination parameters is minimised [85, 118, 128]. The return of discrete stacking sequences using a Genetic Algorithm (GA) was first implemented by Yamazaki [129]. As the combinatorial stacking sequence matching problem is quick to solve, the relative inefficiency of the GA is unimportant, but this algorithm can handle discrete variables, and penalty functions are easily employed to enforce manufacturing constraints [128]. A number of authors have adopted this multi-level approach that initially uses lamination parameters to represent laminate stiffness, and a genetic algorithm [101, 124, 129–131] to retrieve a discrete stack. It is worth noting that the 'best discrete fit' stacking sequence may not be most optimal design for the original problem, as the ideal discrete stacking sequence may not be the that which is best approximated from ideal continuous lamination parameters.

2.4.3 Variable Stiffness Laminate Optimisation

The optimisation of variable stiffness laminates presents with greater complications when compared to straight fibre designs, as additional numbers of variables are required to describe the variability of ply angles and laminate thicknesses across the structure, and supplementary constraints must be enforced to ensure blending between adjacent regions or to limit the permissible steering radius [98]. Parametrising the fibre angle path to vary curvilinearly crucially reduces the number of design variables and maintains continuity across the width of a structure [16, 26, 132, 133]. These path functions, however, must be redefined for alternative geometries and so do not provide a general optimisation framework. Formulating the problem using a coarse discrete patch methodology provides greater design flexibility but more constraints are necessary to enforce compatibility and ply continuity between regions [78, 134]. An additional challenge to discrete design of VS composites is that the use of ply angles as primary design variables results in a highly non-convex design space, but discrete ply angle formulations are necessary to enforce stack blending constraints.

An approach using topology optimisation, called Discrete Material Optimisation (DMO), has been developed for optimisation of VS laminates [135, 136]. This uses a gradient-based technique to maximise the local stiffness of a component by selecting the best material of choice and the optimum fibre orientation, and the authors have achieved agreement with other known optimisation methods. However, the optimisation routine is still considered computationally inefficient, due to the high number of design variables, as each element is a design variable. A patch design, where regions of elements and layers are merged into a single patch section, which, as demonstrated in [8], reduces the run time of a problem, but these regions will need to be specified by a user *a priori*, and the final result may be dependant on this geometric discretisation. Using an approach developed by Abdalla et al. [137], lamination parameters are used to represent local laminate stiffnesses in a constant stiffness VS panel optimised for a combined maximum buckling load and maxi-

mum stiffness objective function [11]. In order to obtain a smooth lamination parameter distribution, the parameters are subscribed to nodes in the FEA model, and the element stiffness properties are obtained by averaging nodal values.

Generating fibre angle distributions from a optimal spatial variation of lamination parameters was accomplished by decomposing the problem into local/global subproblems, where the local stacking sequence is obtained from the local lamination parameters, and then these are all coupled together to produce fibre steering paths, although this requires large numbers of design variables to describe the structure [85]. Wu et al. [86] extended the two stage lamination parameter approach, such as in [129], to the optimisation of Variable Angle Tow (VAT) composite plates with curvilinear fibres, ensuring strict enforcement of feasibility constraints at all spatial coordinates during optimisation by parametrising lamination parameters using Non-Uniform Rational B-Splines (NURBS). Comparatively few design variables are therefore needed to describe the problem. The gradient-based optimisation routine employs the Globally Convergent Method of Moving Asymptotes (GCMMA) [138] where the objective function and non-linear constraints are replaced by a succession of convex approximations based on gradient information, ensuring return of a global optimum. This optimisation methodology has been shown to be computationally efficient and robust, and can be used as a generic solution for a variety of problems. NURBS parametrisation of the fibre angle can also be easily coupled with accurate yet efficient isogeometric analysis for the buckling load optimisation of variable-stiffness panels [139]. The lamination parameter B-spline approximation method developed in [86] and isogeometric analysis method in [139] are combined in [140], creating a highly computationally efficient, multi-level optimisation routine that is able to locate the global optimum. An interpolation method [141] that controls the magnitude and direction of change of lamination parameters across a VS structure can also be employed to generate smooth manufacturable fibre paths, whilst retaining the benefits of lamination parameter based optimisation. A full review of the efficient optimisation of variable stiffness laminates using lamination parameters can be found in [142].

The complexity of the model used for the evaluation of the objective function and/or the constraints also can impede optimisation efficiency, as closed-form solutions for VS laminate performance are rarely available. Finite Element Analysis (FEA) provides highly accurate analysis of particular loading scenarios and therefore is the ideal tool for characterising the response of structures. However, for iterative design work and for quick analysis, high-fidelity FEA is not suitable for optimisation routines due to the necessary mesh refinement, therefore resulting in vast computational expense. In particular, variable stiffness problems often require additional model refinement to capture the response of steered fibres [60]. When FE analysis is used for optimisation, the computational expense can be reduced by using a multi-level approach, such as that described by Peeters et al. [46]. First the problem is optimised using an approximation of the FE response, optimising the stiffness in terms of lamination parameters. The optimised stiffness design

is then used to return an optimal fibre angle distribution using a second-level approximation, which is then assessed using a FE analysis. This two-step process is iterated until the FE analyses converge, minimising the overall number of FE evaluations required.

In addition, many authors have developed efficient analytical methods predicting the buckling response of variable stiffness laminates based on a Rayleigh-Ritz approach, where the varying fibre path can be defined linearly [16] or non-linearly using Bezier surfaces and curves [132], B-splines [26] or polynomial expressions, the coefficients of which can relate directly to the fibre angles [133]. Coburn et al. extended the analytical method based on a generalised Rayleigh-Ritz approach in [133] for the pre-buckling and buckling analysis of a stiffness VAT laminate panel, where the skin has the variable fibre orientation [68]. This was implemented for beam and plate stiffener model geometries, and the results were found to be accurate to within 10% for the global and local buckling analysis. This work not only shows the possibilities of applying variable angle tailoring to an aerospace component but the potential for studying the optimisation in an efficient manner.

Considering discrete stiffness tailoring approaches, Kristinsdottir et al. [78] introduced a methodology referred to as 'blending', ensuring continuity between adjacent regions with different discrete stacking sequences in an optimised 'patch' structure. Key regions, the regions undergoing the most stress and therefore the thickest areas of the structure, are identified by the designer, and all plies present in the total structure emanate from this region. Plies are allowed to be dropped between regions but not reintroduced if not present in adjacent regions leading away from the key region. Similar to this approach, a laminate 'guide' stacking sequence is first specified in the work of Adams et al. [143] from which plies are deleted to create all subsequent regions, depending on the local loading, which is optimised using a genetic algorithm. Blending is enforced by minimising the number of edits between encoded strings that represent the stacking sequences. These methods preserve the through-thickness position of plies, guaranteeing continuity and manufacturability, and reduce the problem complexity. The reduced complexity is necessary as the performance of the structure is re-assessed at each design iteration, but at the expense of limiting the design space. Based on [143], a stacking sequence table based optimisation methodology was used to design the transition between one thick guide laminate and thinner surrounding regions, subject to blending and laminate design rules. Explicit enforcement of the constraints ensured feasibility in every iteration of the GA, as infeasible SST are either dismissed or repaired using a bespoke operator [144].

Stacking sequence continuity equations, measuring the number of ply layers shared between two adjacent laminates were implemented by Liu [134] allowing greater design freedom, as not all layers are contiguous and ply additions are allowed. A supplementary study found that significant improvements in continuity are achievable with little additional structural weight, but penalties increase sharply with increasingly greater blending requirements.

Multi-step optimisation strategies, as per [129] and [101], can reduce computational expense, and to that end Macquart et al. [131] have applied this to a patch-based design, using lamination parameters in the first stage, and returning a discrete stack in the second. As it is well known that some loss in performance is associated with converting continuous lamination parameters to discrete designs, the same authors derived physically relevant blending constraints to be applied in the first stage, limiting the change between lamination parameters in adjacent regions which ultimately created more realistic designs [145].

2.5 Industrial Design Rules

The selection of stacking sequences and ply angle ratios within aerospace components are provisionally constrained by laminate design guidelines which are fully detailed by Niu [67]. Despite this literature dating back to the late 80's, the design rules are still applied to present-day structural designs as they guarantee laminate robustness, and that the laminate design can be manufactured without warping. These are as follows:

(i) Limited set of available ply angles, known as the standard angles: 0°, 90°, and ±45°.

(ii) Placing ±45° plies in the outermost regions of the stack for damage resistance and tolerance.

(iii) Symmetric and balanced stacking sequences. This removes extension-shear coupling and in-plane/ out-of-plane coupling, creating an orthotropic laminate: $A_{16} = A_{26} = \mathbf{B} = 0$.

(iv) Angle ply pairs are placed together in the stack to minimise bend-twist coupling, D_{16} and $D_{26} \approx 0$.

(v) Constraints on the number of contiguous plies, restricting the number of same angle plies placed in sequence together to four. This prevents high inter-laminar stresses from developing within the structure.

(vi) A minimum 10% of each ply angle as a percentage of the total stack thickness, so that the design can be tolerant of uncertain loading.

Tsai has campaigned for challenging these conservative design regulations [146], in order to fully realise the potential of composite materials. Non-conventional laminate designs, such as variable stiffness laminates and the use of non-standard ply angles, show promise in terms of the extended design space and manufacturing benefit [147]. Fukunaga et al. [120] have shown that for any particular feasible point within the boundaries of the in-plane, out-of-plane lamination parameter space, a corresponding stacking sequence can be determined composed of two, or four, non-standard angles ply pairs in a specific ratio, whereas standard angle designs are more limited. Use of non-standard or non-conventional angles in laminate design opens up further possibilities in terms of design space, as illustrated by the comparison of non-standard and standard (0°, ±45° and 90°) lamination parameter space in Fig. 2.4. Bloomfield et al. have shown that theoretically, for a panel constrained

by buckling and minimum strength requirements, a mass saving of over 7% was achievable through expanding the design envelope to include ±30° and ±60° plies, as well as the traditional four angles [148].

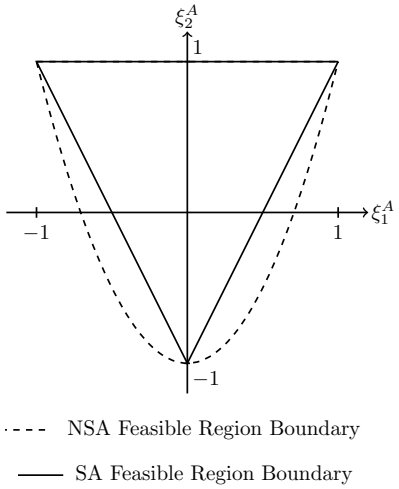

Figure 2.4: Comparison of the standard angle (0°, ±45° and 90°), and non-standard angle in-plane lamination parameter space.

However, the traditional standard angle design rules must be adapted for non-standard angle designs, to ensure the manufacture of warp-free laminates and for laminate robustness. The 10% rule was adapted for non-conventional laminate design, by maintaining a minimum degree of laminate isotropy [149]. However, when this stiffness constraint was applied to the design of buckling panels, the increase in buckling efficiency obtained from using angles other than the conventional set and allowing for fibre steering was half that of the unconstrained design. This shows the importance of applying constraints within the optimisation routine, as the consideration of practical feasibility and physical relevance of the designs will restrict the degree of benefit achieved.

2.6 Conclusions

A literature review has been conducted into concepts for variable stiffness tailoring of composite structures, manufacturing methods to achieve such designs and VS experimental studies, and methods for the optimisation of composite materials, the use of lamination parameters in laminate design and the additional requirements for optimising VS laminates. The findings can be summarised as follows:

- Buckling performance improvements using variable stiffness laminates are well-understood to be associated with the redistribution of stiffer material to boundaries restrained from out-of-plane displacement, and buckling resistant, more pliant, material to unsupported central regions that are prone to buckling.
- The majority of VS research has been conducted into the buckling performance of flat panels, using the curvilinear fibre parametrisation to vary the fibre angle,

and consequently the stiffness, across the panel width. Optimisation of the fibre path perpendicular to the direction of compressive load returns significant buckling load improvement, so work commonly isolates variation of stiffness in the transverse direction. Tailoring both the stiffness and thickness across the width produce the largest increases in buckling performance.

- Variable angle designs created with curvilinear fibres are subject to four main manufacturing constraints: fibre angle continuity, tow steering radius, tow width and tow gaps and overlaps. These constraints impose restrictions on the laminate design space that limit the achievable optimised designs.

- Discrete tailoring methods can achieve abrupt changes in stiffness across a structure, albeit by introducing material discontinuities that could weaken the structure. Blending of discrete regions, maintaining some continuous plies across the width, is important to preserve transverse strength and manufacturing feasibility.

- The manufacture of curved fibre architecture is made possible through Automated Fibre Placement and Continuous Tow Shearing techniques, but neither achieve the rapid rate of deposition as required by aerospace industrial targets. Continuously curved fibre paths can be approximated using discrete strips, producing the same increase in performance whilst being compatible with high-rate deposition manufacturing methods, but little research has been conducted into the feasibility of this approach.

- The design of complex aerospace structures with variable stiffness tailoring is just starting to be explored. Few papers have already applied the VS concept to stiffened panels, but as of yet, this problem has not been fully optimised.

- The optimisation of composite laminates is a complicated design problem, involving large numbers of discrete and continuous variables, and the trigonometric relationship between fibre angle and stiffness creates a non-convex design space if ply angles are used as design variables.

- Gradient-based approaches rapidly converge to an optimum design, but are prone to becoming trapped in local optima in non-convex design spaces. Direct-search methods, such as genetic algorithms, are not reliant on the calculation of derivatives and therefore are more likely to return a global optimum. However, genetic algorithms are slow to converge and are computationally expensive, requiring significant numbers of objective and constraint function evaluations.

- To reduce computational expense, efficient analytical (Ritz methods) or numerical models (Strip Models) are used to predict the buckling behaviour of composite laminates. These generally show good correlation between theoretical and experimental results, except for curvilinear designs with defects, where a detailed FE mesh is required to account for local thickness and stiffness variations.

- Lamination parameters can represent the stiffness of a full stacking sequence with just 12 variables. The parameters have a linear relationship to laminate stiffness, removing the complications associated with directly optimising with ply angles, and the design space is shown to be convex with respect to buckling.
- A two-stage optimisation methodology, the first stage employing lamination parameters and using a gradient-based optimiser, and the second converting the continuous lamination parameter optimum to a discrete stack using a genetic algorithm, is commonly used for composite laminate design, including the optimisation of variable stiffness composites.
- The optimisation of variable stiffness laminates requires greater number of variables and extra constraints to model each region and ensure continuity of either the curved fibre angles or maintain a proportion of continuous plies between adjacent stacks. Defining a curvilinear fibre path to vary using a shape function reduces the number of variables needed to describe the structure, implicitly maintains continuity and allows manufacturing constraints to easily be applied.
- Discrete 'blending' of plies in adjacent regions in a structure is generally optimised using an inefficient and computationally expensive genetic algorithm, although constraints can be applied in the lamination parameter space to limit the change in stiffness between regions.

A gap in the literature has been identified for variable stiffness laminates that can be manufactured with high deposition rates, whilst retaining the structural benefits associated with this increased design space. It is also noted that unconstrained optimisation, where the stiffness is allowed to vary without consideration of minimum fibre steering radius, results in the most optimal designs.

Discrete Stiffness Tailoring (DST) has been identified as a technique that would be appropriate for increased manufacturing rates, as the material will be laid in strips, and is suited to ATL techniques. A discrete method of fibre steering would also be beneficial, as the design would no longer have to account for fibre angle transition. The fibre discontinuities, however, force the redistribution of load across the strip seams, generating high interlaminar stresses, and this could promote delamination and failure in these regions. The transverse strength of the resultant structure will be reduced compared to constant fibre laminates, and this reduction will need to be investigated.

The efficient strip model, VIPASA/VICONOPT, used in [105] is available for use at the University of Bath. At present, this has the ability to model and analyse complex prismatic structures, i.e. stiffened panels, cylinders and wing box sections, in approximately 0.1% of the time of Finite Element Model computational time [150]. Hence, this strip model is incorporated in a two-stage lamination parameter-based optimisation methodology, in order to achieve optimum design of structures comprised of discretely tailored strips. The developed method is demonstrated upon minimum-mass optimisation of a stiffened

panel under compressive load, subject to buckling and longitudinal strain constraints. The resulting design is manufactured and experimentally tested in order to validate this novel tailoring framework. This thesis includes the demonstration of this design and manufacturing philosophy at an assembly level for the first time, to achieve large-scale variable stiffness panels uninhibited by restrictions on fibre radii.

Chapter 3

Discrete Stiffness Tailoring: Proof of Concept

3.1 Introduction

In this chapter, the concept of Discrete Stiffness Tailoring is introduced, as it is conceived within this thesis. A simple redistribution of stiffness within a compression panel, where the overall axial stiffness and relative volumes of material remain constant, is used to prove an increase in buckling performance is obtained due to this technique. As such, these designs do not represent optimised variable stiffness laminates, but this exploratory experimental study allows for the potential of this technique to be shown, and will demonstrate the predictive capability of the analysis methods used. Two types of tailored panel, one maintaining 50% continuous plies and one with 100% altered plies, are designed and compared to a quasi-isotropic baseline. A comprehensive experimental regime is conducted which supports and validates the analytical modelling, performed using the infinite Strip Model VICONOPT. The reduction in strength due to discontinuous transverse plies is also investigated using experiments and complementary FE analysis.

The FE analysis included in this Chapter, for assessing both buckling and tensile strength, is the work of R. Choudhry, as this Chapter is based on the collaborative work presented in [151].

3.2 Background

Buckling optimisation of panels via spatial variation of stiffness has predominantly focused on the application of continuous curvilinear fibre concepts which are subsequently manufactured using tow steering methods such as Automated Fibre Placement (AFP) and Continuous Tow Shearing (CTS) [16, 18, 22]. However, a review of variable stiffness laminate designs for buckling [13] reports that the achievable buckling load capacity of a tow steered flat plate may be limited by the manufacturable steering radius of the fibres. Dodwell et al. [1] have shown that if angle and ply thickness are simultaneously varied across the width of a compression panel, a weight saving of up to 40% can be achieved compared to a baseline design, but only provided that the fibre steering radius can be precisely controlled ($< 30\,\text{mm}$). Radii size on this scale can only be manufactured using CTS, which is unsuitable for high rate manufacture of composite parts and creates an

unavoidable variation in ply thickness.

However, results in [1] theoretically demonstrated that equal weight savings and buckling performance obtained using steered fibre CTS panels can be achieved with as few as three discrete strips of straight fibres, each with a different fibre orientation. Figure 3.1 presents the two concepts, which illustrates how the curved fibre path can be approximated by constant angles laid in strips. By discretely altering the fibre angle using strips of material, the issues related to fibre steering radii with continuous steering methods can be circumvented. Furthermore, discrete tailoring provides greater design freedom as laminate thickness and angle can be altered independently across the geometry of a structure, whereas the two are linked in CTS designs. Such discrete designs are also compatible with high rate deposition methods such as Automated Tape Laying (ATL), which can theoretically achieve productivity rates three times greater than AFP, where CTS is several orders of magnitude slower than both industrial systems [17, 93].

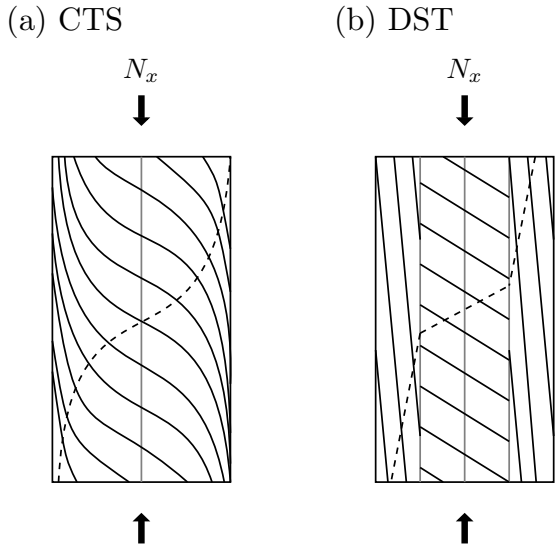

Figure 3.1: Comparison of (a) a continuously steered fibre panel, manufactured with CTS, with (b) a discretely tailored structure, composed of three adjacent strips of constant angle material, as suggested in [1].

The experimental work conducted in this chapter draws directly from this theoretical study, and from the work of Biggers and Srinivasan [14], who identified that the redistribution of very stiff (e.g. 0° plies) to the boundary regions of a compressive panel results in an increase in the buckling load for uni-axial compression. The numerical studies allowed for thickness variation across the structure, but in this case the thickness remains constant, isolating the effect of angle change on the buckling performance from that resulting from a change in thickness. It was shown that the distribution of alternative ply orientations within a flat panel has greater impact on delaying the onset of buckling than altering the thickness along the width [1] and so tailoring is constrained to angle variation only. To the best of the authors knowledge, no work has explicitly tested buckling panels with discrete variations in the fibre angle, laid as adjacent strips.

Despite the manufacturing and design advantages of using discrete fibre tailoring, the point at which one orientation terminates and another commences, called a ply seam, creates a vulnerable region at which high levels of stress concentrate. This makes the seam susceptible to failure through delamination, or through failure of the resin surrounding the discontinuous ply edges. The corresponding reduction in transverse strength, with respect to the number of shared plies between two regions, is therefore experimentally tested and used to validate finite element analyses, which investigate failure progression.

3.3 Methodology

Discrete Stiffness Tailoring uses discrete angle variation to enable component manufacture where stiffness is tailored in different zones to enhance the buckling performance of the structure, as depicted in Figure 3.2. The literature review highlighted that Gürdal et al. [16] studied two types of tow path design, one that linearly varied along the longitudinal x direction and the other varying in the transverse y direction. Results indicated that due to redistribution of the longitudinal compressive load, N_x, fibre angle variation in the y direction is more efficient than variation in the x direction in the case of initial buckling. Therefore, in order to achieve the best structural efficiency whilst retaining prismatic conditions required for VICONOPT analysis (see Section 3.4.1), stiffness variation is only considered in the direction transverse to load.

The stacking sequences and panel design are based on the simple premise of redistributing 0°, ±45° and 90° material without altering the relative volume or angle of 0°, ±45° and 90° material, in a balanced symmetric quasi-isotropic laminate to bring about buckling performance improvements. Such a design experiment offers a simple way to demonstrate the potential for DST buckling improvements, whilst offering a suitable example against which analysis methods can be validated. However, it must be reiterated that these designs **are not** optimised for performance.

Two methods for DST are considered, where each offers different degrees of continuity to the seams: 'Full seam', where all plies have discrete junctions between material with different fibre angles, and 'Half seam' where 50% of plies contain junctions or 'seams'. The tailored panels are divided into three strips, corresponding to two regional (A and B) stacking sequence designs as shown in Figure 3.2. As this experiment is a simple demonstration of the DST technique, the widths of Regions A and B are selected to be, respectively, a quarter and a half of the total width of the panel between the vertical simple supports and are not optimised. Cross-section representation of each panel type are illustrated in detail in Figure 3.3, and the stacking sequences for each panel, and for each panel region, are presented in Table 3.1. Regions A and B in Fig. 3.2 are partitioned by transitional widths over which discrete changes in ply orientation occur.

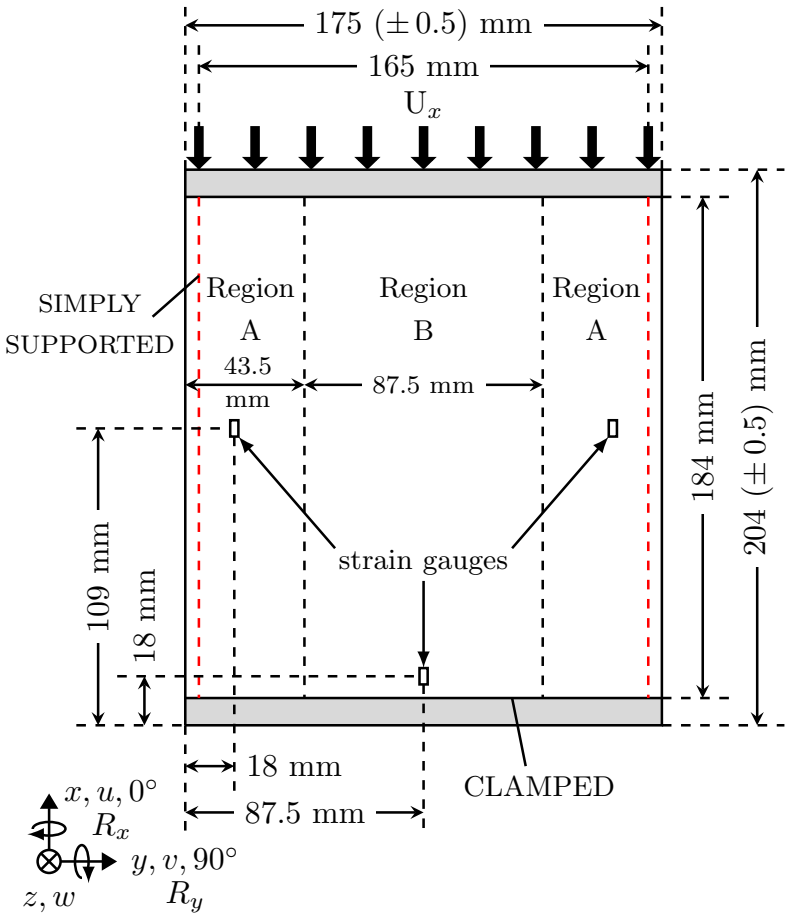

Figure 3.2: Plan view of a DST compression coupon showing idealised boundary conditions, panel dimensions and loading regime for buckling tests. Red dashed lines indicate simply-supported boundary conditions.

The in-plane stress is transferred through shear between discontinuous plies. By adapting shear lag theory, the ply overlap length required for full stress redistribution can be estimated. Assuming homogeneous strength properties for the ply, and a ply thickness, t_P of 0.25 mm, the minimum length, δ_{P}, required for full shear transfer can be calculated using the analytical approach developed in [152]:

$$\delta_{\mathrm{P}} = 1.15 \left(\frac{E_{11T}}{G_{12}} \right)^{1/2} (t_{\mathrm{P}} + 2t_{\mathrm{MX}})^{1/2} (2t_{\mathrm{MX}})^{1/2} \tag{3.1}$$

where E_{11T} is the longitudinal tensile modulus, G_{12} the shear modulus, t_{MX} is the thickness of the resin interface. Using the material properties in Table 3.2, and a resin interface thickness of 0.02 mm, the effective minimum length is 0.6511 mm, which is roughly equivalent to three times the ply thickness, agreeing with the study by Mukherjee et el. cited in the literature review [77]. The resin interface thickness is estimated from the average thickness of the experimental laminates (4.31 mm) and the known thickness of the plies (0.25 mm), which is in line with reported values. However, ply angle alterations, transitioning from one Region to the other, are all achieved over a width of 30 mm, with 10 mm

minimum length local staggering of neighbouring intra-laminar seams to avoid large stress concentrations interacting. The transition width is deliberately selected to be conservative, and much larger than would be necessary for shear stress transfer and redistribution of load between Regions.

Table 3.1: Table of stacking sequences for each panel and, for the tailored cases, the stacking sequences in each region.

Panel	Region A	Region B
QI	$[\pm 45/90/0]_{2S}$	
Half seam	$[\pm 45/(90/0)_3]_S$	$[\pm 45_2/(90/0)/\pm 45]_S$
Full seam	$[\pm 45]_{4S}$	$[90/0]_{4S}$

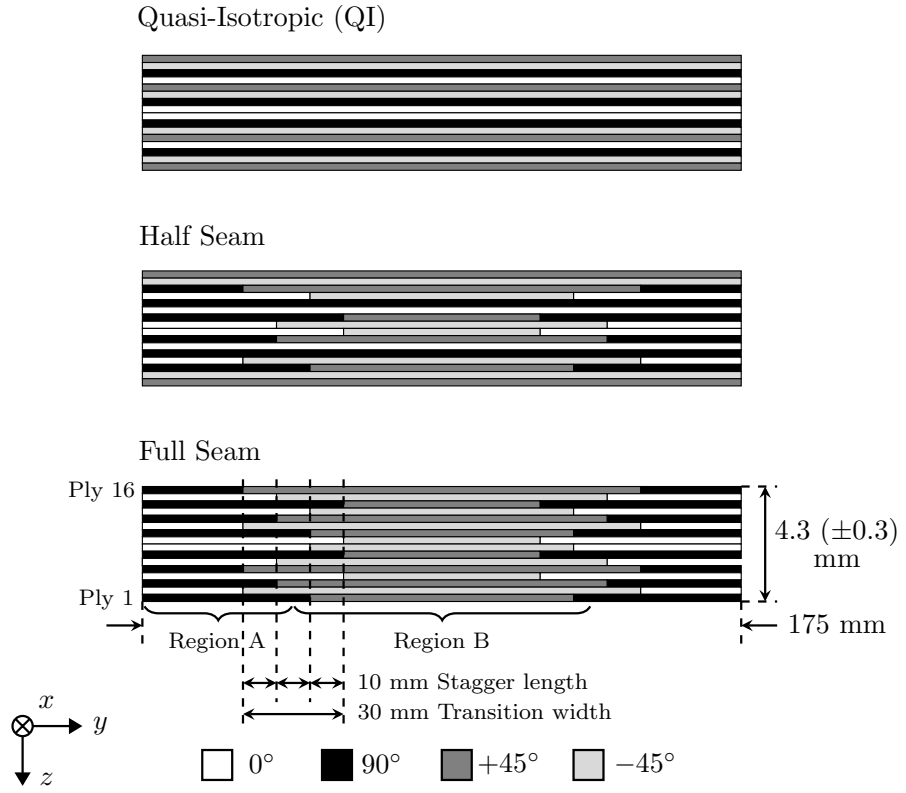

Figure 3.3: Cross-section representations of the QI, Half seam and Full seam compression panels, detailing the design of the staggered seams through the stacking sequence.

As the seam region is expected to reduce the transverse strength of the panels [7], three types of tensile coupons based on the buckling coupon designs were created. The design of the tensile coupons is presented in Figure 3.4, where a single seam, as per those dividing Regions A and B in the compressive panels, is isolated and tensile load is applied perpendicularly. The orientation of the plies with respect to the x-y axes is maintained between the compression panels and tensile coupons.

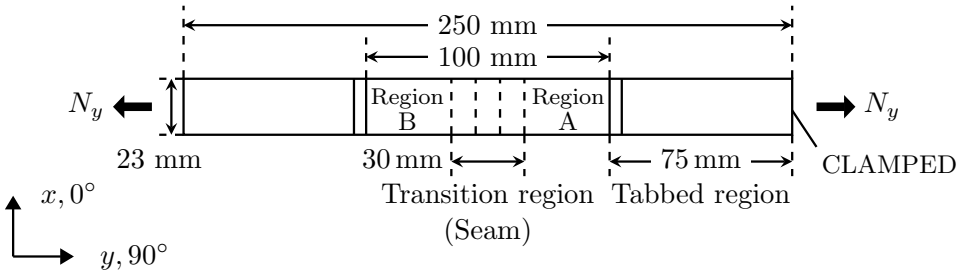

Figure 3.4: Plan view of DST tensile coupon.

In order to design and optimise DST panels efficiently in future, the use of computationally efficient methods for assessing buckling performance and seam strength must be validated. As such, the methods for analysing buckling performance outlined below have deliberately been constrained to those that are in standard use and are computationally efficient. The predictive capabilities of these models and thus their use in future design studies will form part of the discussion of this chapter.

3.4 Numerical analyses for buckling and strength

Two methods are employed for determining buckling performance of the QI, Half seam and Full seam panels: the finite strip program VICONOPT [2] and Finite Element Analysis. The compressive panels and tensile coupons are manufactured, as per the stacking sequences and seam regions given in Fig. 3.2, using HTS40/977-2 material with material properties listed in Table 3.2, and hence these properties are used in the numerical analyses.

Table 3.2: Material properties for HTS 40/997-2, and properties for the isolated epoxy 977-2 [3, 4].

Material Properties			
HTS 40/977-2 Elastic		977-2 Epoxy	
E_{11T}, E_{11C} (GPa)	135.405, 112	E (GPa)	3.5
E_{22} (GPa)	10.3	ν	0.38
G_{12}, G_{13} (GPa)	4.9	Strength (MPa)	81
G_{23} (GPa)	5.2		
ν_{12}, ν_{13}	0.3		
HTS 40/977-2 Strength		Cohesive Zone	
X_T (MPa)	2450	K_n, K_t (N/mm^3)	1e^5
X_C (MPa)	1500	Y_T^{CZ} (MPa)	60
Y_T, Z_T (MPa)	82	S_{XY}^{CZ} (MPa)	80
Y_C, Z_C (MPa)	236	G_{IC} (N/mm)	0.352
S_L (MPa)	101	G_{IIC} (N/mm)	1.45

3.4.1 VICONOPT Model

As the majority of aerospace structures, such as wing and fuselage panels, are prismatic structures, the computationally efficient and accurate finite strip method VIPASA [153], which uses prismatic assumptions, can be applied. VIPASA models the structure as connected plates, a singular example of which is given in Fig. 3.5. The deflection of the assembly is assumed to vary sinusoidally in the longitudinal direction with half-wavelength, λ, and the buckling solutions are obtained through exact plate analysis. VIPASA is discussed in greater detail in Chapter 4. In this Chapter, VICONOPT [154], an extension to VIPASA that allows for the application of clamped transverse boundary conditions and accounts accurately for shear loading or presence of material anisotropy, is used to return the critical buckling loads of the compression panels. VICONOPT has previously been used to predict buckling performance of DST laminates [1].

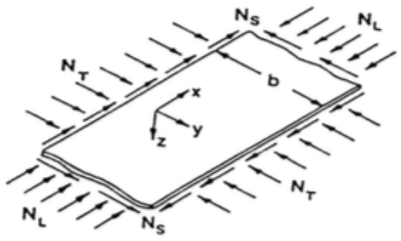

Figure 3.5: Single plate component example, annotated with the applied forces and the co-ordinate system used by VIPASA/VICONOPT [2]. Note that the force labelled N_L is equivalent to the longitudinal compressive load N_x used in this thesis.

For panels and loadings that are prismatic in the x direction and under the assumption that there is no coupling between in-plane and out-of-plane deformation (i.e. the B matrix of classical lamination theory is null), VICONOPT, as with VIPASA, provides infinite periodic solutions to the equilibrium equation that governs buckling:

$$D_{11}\frac{\partial^4 w}{\partial x^4} + 2(D_{12}+2D_{66})\frac{\partial^4 w}{\partial x^2 \partial y^2} + D_{22}\frac{\partial^4 w}{\partial y^4} + 4D_{16}\frac{\partial^4 w}{\partial x^3 \partial y} + 4D_{26}\frac{\partial^4 w}{\partial x \partial y^3} + \left(N_x\frac{\partial^2 w}{\partial x^2} + 2N_{xy}\frac{\partial^2 w}{\partial x \partial y} + N_y\frac{\partial^2 w}{\partial y^2}\right) = 0 \quad (3.2)$$

where N_x, N_y and N_{xy} are in-plane forces, and D_{11}, D_{12}, D_{22}, D_{16} and D_{66} are the bending stiffness terms of classical lamination theory. A single plate component, labelled with the in-plane forces and width b is shown in Fig. 3.5. The solution of Eq. 3.2 is found via exact, periodic formulations of the form:

$$w = f_1(y)\, cos\frac{\pi x}{\lambda} - f_2(y)\, sin\frac{\pi x}{\lambda} \quad (3.3)$$

where the functions $f_1(y)$ and $f_2(y)$ allow various boundary conditions to be applied on

the longitudinal edges of the panels, including free, simple, clamped and elastic supports. The half-wavelengths λ in Eq. 3.3 are defined by the length of the plate L divided by the number of half-wavelengths assumed along the length of the plate. In VICONOPT, the different wavelength responses of the VIPASA stiffness matrices are coupled using Lagrangian multipliers, which are used to minimise the total potential energy of the plate, subject to the prescribed boundary conditions. The compression plate is modelled using a series of strips, necessary as the clamped boundary conditions are applied at the nodal points connecting the strips. Convergence for the QI panel is achieved with fewer than five strips, but more are required to define the stacking sequence variation across the seamed regions. In the DST panels, each strip has a different set of bending stiffnesses and, in the results that follow, 13 to 18 strips are used depending on the presence of transition regions. The number of strips used is based on both the minimum number of strips needed to define the different regional panel stacking sequences, and the minimum number of strips spread evenly across the panel width required to apply the clamped boundary condition accurately. A minimum of nine strips are necessary to define each different stacking sequence present in the tailored panels.

Buckling load factors are derived through an eigenvalue analysis which is executed on the transcendental stiffness matrix derived from the solution of the governing differential equations of the constituent strips. The transcendental eigenproblem requires an iterative solution that is performed using the Wittrick-Williams algorithm [155]. The lowest buckling load found for a range of values of λ is taken as the critical buckling for the panel.

3.4.2 Finite Element Buckling Analysis Method

Finite element buckling and strength analyses were carried out using commercially available software package ABAQUS^{TM} Standard [156] in order to (i) confirm the predictive capacity of VICONOPT simulations, (ii) investigate alternative boundary conditions, (iii) explore non-linear buckling behaviour of the panels, and (iv) model the strength of the seams. Eigenvalue buckling analysis (perturbation method) [157] was used to estimate buckling stress and strain. Non-linear FEA continuation analysis [157] was used, for capturing the post-buckling path. Since the QI panel has a trivial fundamental path, an imperfection in the form of bifurcation mode having the lowest bifurcation load was applied to the mesh. An imperfection magnitude of $\delta_o = t_h/100$, where t_h is the thickness of the laminate, was used. The imperfection size in this case was selected to be large enough to trigger the correct buckling mode (as illustrated in Fig. 3.11d) but small enough that it did not increase structural instability to the point of reducing the buckling load. Solutions used the Riks (Arc length) [158] method based solver in ABAQUS. In the case of the Half seam and Full seam panels, due to the material asymmetry in the seam transition zone, it is not necessary to force an artificial imperfection. Thus, for these cases it was sufficient to use the geometrically non-linear solver (employing a Newton method) in ABAQUS with incrementally increasing loads to capture the bifurcation point and post-buckling path.

Each panel was modelled with a mesh consisting of 30,360 S8R doubly curved thick shell elements each having 8-nodes, quadratic reduced integration and an edge length of around 1 mm. A mesh convergence study was carried out. The complete panel was modelled as a single part with uniform mesh density. A lamina type [156] material definition was used for each layer and the orthotropic material constants for the unidirectional HTS40/977-2 CFRP material are summarised in Table 3.2 [3, 4]. The layup sequence corresponding to each part for each region (as described in Table 3.1) was specified as part of the section definition in ABAQUS using the composite layup tool and by creating appropriate partitions for each zone.

3.4.3 Finite Element Method for Tensile Strength

In this study, finite element analysis of DST panels under tension was undertaken with a view to understanding the failure process. This was accomplished by studying the evolving stress state, resulting from the progressive damage growth from the seams that connect regions of dissimilar stiffness. Finite element simulations were carried out using ABAQUS^{TM} Standard. Geometrically non-linear (large displacement) analysis was carried out for modelling damage growth. Cohesive Zone Modelling (CZM) [159] was used to simulate both the inter-laminar and intra-ply crack growth at the seams. Other ply damage mechanisms were not modelled directly, instead the failure indices for these modes were evaluated during post processing at various load steps to understand the evolving nature of damage within the test panels. The model assumed a plane strain (in the y-z plane) representation of the tensile panel in Fig. 3.4, thereby ignoring free edge effects. Each ply, its associated polymeric inter-laminar interface region as well as polymeric seams that define the transition between sections of different fibre orientation were modelled discretely and separate material models were defined for each zone. The material behaviour for each ply was assumed to be linear orthotropic. Although previous studies by Atas et al. [4] suggest that $\pm 45^{\circ}$ plies in tension can display highly non-linear shear behaviour it was decided not to include this description in the material model for the tensile simulations. Instead, the intention here is to establish an indication of stress and damage in the seams whereas accounting for non-linear shear of plies, whilst not accounting for ply failure as noted above, would only complicate the model with little change in accuracy in the seamed region.

Figure 3.6 illustrates the converged finite element mesh where the following element dimensions were used for each of the zones: plies 62.5 µm x 50 µm, inter-laminar regions 4 µm x 5 µm and intra-ply seams 18 µm x 2.5 µm. As shown, a refined mesh (1.629 million and 1.630 million elements for the Half and Full seam cases respectively) was used to capture stress gradients between zones of different stiffness accurately and to enable stable propagation of damage within the cohesive zones. In order to simplify the modelling of seam failure, it was assumed that crack propagation would take place purely within the inter-ply resin region (polymeric seam) as opposed to being an interface crack (de-

cohesion failure). Hence, seams were modelled as a solid layer with embedded cohesive zone (red elements in Fig. 3.6) along the mid-plane of the seam. An isotropic material definition based on the material properties of Epoxy 997-2 was used for the solid region while the embedded cohesive zone was defined using a traction-separation law and mixed-mode failure governed through the BK-criteria [160]. Material properties for all regions are given in Table 3.2. Following Dizy et al. [161] and the ABAQUS Manual [162], regions in Fig. 3.6 were connected using node-based tie-constraints applied at mating surfaces (edges). Tie-constraints were used to connect the non-matching meshes of the ply regions (fewer elements) and the interface and seam regions (more elements) allowing overall for a computationally tractable model with higher fidelity in the interface and seam regions. It was possible to use fewer elements in the ply region as the resolution of the stress field here would see minimal benefit from a high fidelity mesh especially as the use of solid elements to connect ply and interface regions allowed for a smooth transition of strain field between the two zones. All simulations were convergent beyond the maximum loads observed in the experiments but eventually became non-convergent at higher loads following numerical instabilities relating to fast fracture in inter-laminar seam regions.

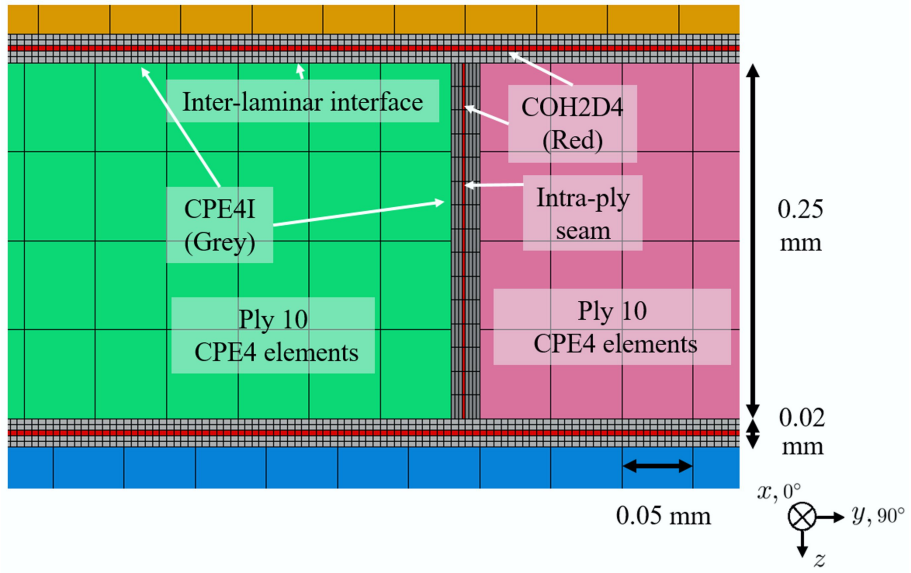

Figure 3.6: Illustrative FEA cross-section details for the tensile damage model indicating element types used in various regions.

3.5 Experimental Methodology

Compression and tensile tests were carried out to assess buckling capacity and tensile strength as described in Fig. 3.2 and Fig. 3.4 respectively. Tensile tests were designed to assess the transverse load carrying capability of the compression panels, using the same seam designs as in the compression panels. Hence, the relative orientation of fibre directions and loads in Figs. 3.2 and 3.4 should be noted.

3.5.1 Compression

Fifteen buckling panels were manufactured with dimensions as labelled in Fig. 3.2a: five quasi-isotropic (QI) baseline panels without seams and five of each seam type. Panels were tested under compression using an Instron 5585H machine, at a displacement rate of 0.1 mm/min applied in the 0° direction of the coupons. Specimens were supported in a modified version (increased gauge width and height) of the test fixture described by ASTM D7137 [163] with the exception that loading edges were clamped to prevent 'brooming' type end failures. A diagram of the test rig is given in Fig. 3.7. The knife edge simple supports were applied with fingertip tightness, in order to restrain out-of-plane displacement but allowing for rotation. The spacing between the support and the panel was tested by running a thin steel shim between the two. All coupons were monitored with 6 strain gauges with positions given on Fig. 3.2. A Spider 8 data acquisition system and Catman software [164] were used to capture strain and load data. A Limess Digital Image Correlation (DIC) system employing a stereo pair of 1MP high speed Photron SA3 Cameras was used to track coupon strain and displacement in three dimensions. Post-processing was undertaken using Correlated Solutions' VIC3D software [165].

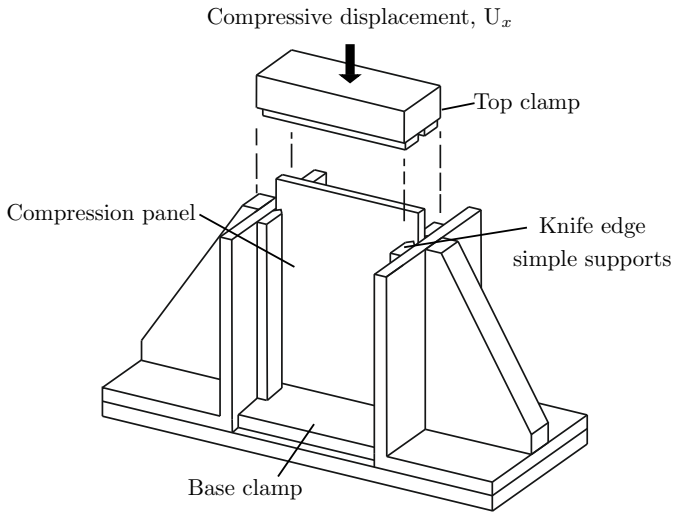

Figure 3.7: Diagram of the compressive test rig.

3.5.2 Tensile

Fifteen tensile coupons were manufactured as with the compression panels, five quasi-isotropic laminate stacks containing no seams as a baseline case, and five of each seam design. All coupons were tested under tension in an Instron 5585H uni-axial test machine with loading applied in the 90° ply direction (relative to the compression panel loading direction). Load was applied via gripping of sections of the coupons that had been tabbed with 2 mm aluminium sheet, as indicated in Fig. 3.2. The initial Full and Half seam coupons were loaded at a fixed displacement rate of 0.2 mm/min, which was then increased to 0.6 mm/min in all subsequent tests. An extensometer, placed either side of the seam region, and DIC system (as described above) were used to monitor strains and

displacement.

3.6 Results

3.6.1 Compressive Results

Experimental buckling results are plotted alongside VICONOPT and FEA analyses in Fig. 3.8. As experimental boundary conditions are indeterminate and never fully equivalent to numerical clamped boundary conditions, numerical results for both clamped and simply supported boundary conditions are presented. The non-loading edges are consistently modelled as simply-supported. Triangular and circular markers indicate clamped and simply-supported loading edges in the numerical models respectively. VICONOPT and FEA use the width between the knife-edge longitudinal supports (165 mm) for the calculation of stress, whereas the experimental results use the full manufactured panel width (175 mm). With the minor exception of the lowest experimental Half seam buckling stress result, these numerical results fully bound those experimentally obtained in Fig. 3.8a. For easier comparison, the averaged experimental results and the numerical results (as per Figure 3.8) are complied in Table 3.3.

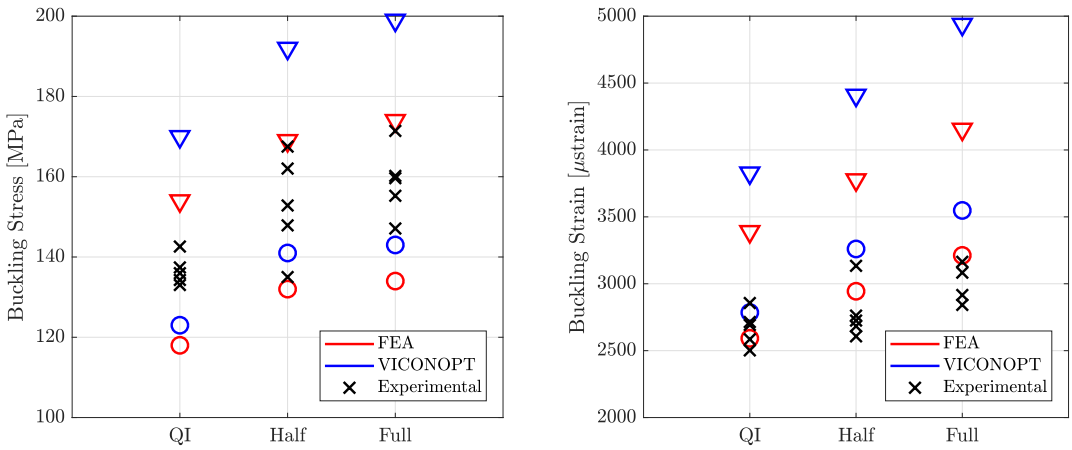

Figure 3.8: (a) Comparison of buckling results obtained from VICONOPT, FEA and all experimental compression tests. Triangular and circular markers denote simply-supported and clamped transverse boundaries respectively. (b) Buckling strain comparison, presented as in (a).

Table 3.3: Critical buckling stresses from experimental data and numerical analyses, where the results from the latter are produced using simply-supported and clamped transverse boundary conditions.

	Exp. (MPa)	VICON (MPa)		FEA (MPa)	
Panel	Avg. (±SD)	Simply Supported	Clamped	SS	CL.
QI	136.7 (±3.2)	123	170	118	154
Half	153.1 (±13.5)	141	192	132	161
Full	158.7 (±10.1)	143	199	134	174

(a) Baseline QI

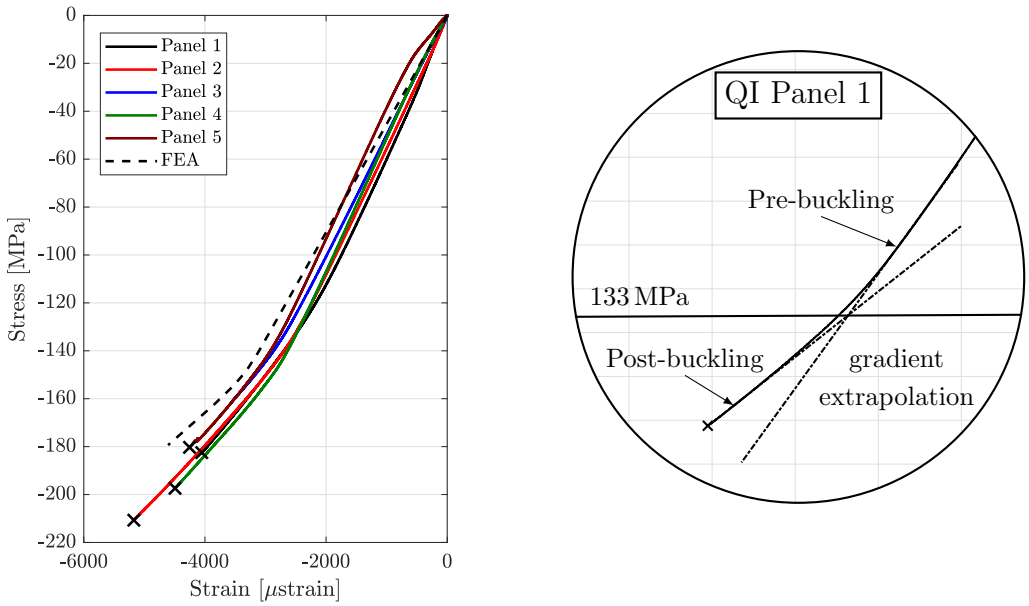

(b) Half seam

(c) Full seam

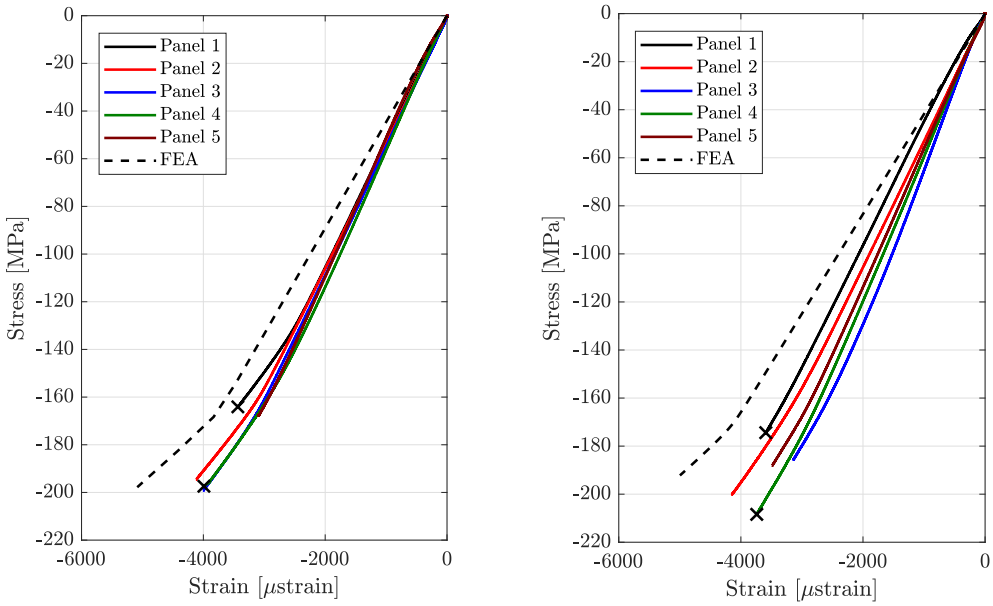

Figure 3.9: Experimental stress vs strain, based on averaged strain gauge readings for (a) QI baseline, (b) Half seam, and (c) Full seam. Black crosses indicate catastrophic failure of the panel for some tests. Results from the numerical simulation, with loading edges simply-supported, are presented for each panel type.

Plots of compressive stress against strain from the compression tests are presented in Fig. 3.9, and results are grouped by panel type. An annotated inset, Fig. 3.9a details the process of determining the critical buckling stress for QI Panel 1. The bifurcation point for each experimental test was determined by using the average strain data of all six gauges to locate the point at which a significant stiffness change was observed. At this point, the

two linear regions either side of that kink were extrapolated until they crossed each other. The stress at which they met, calculated from the experimental loads and cross-sectional area for each panel, was taken as the buckling stress of the panel.

(a) Baseline QI

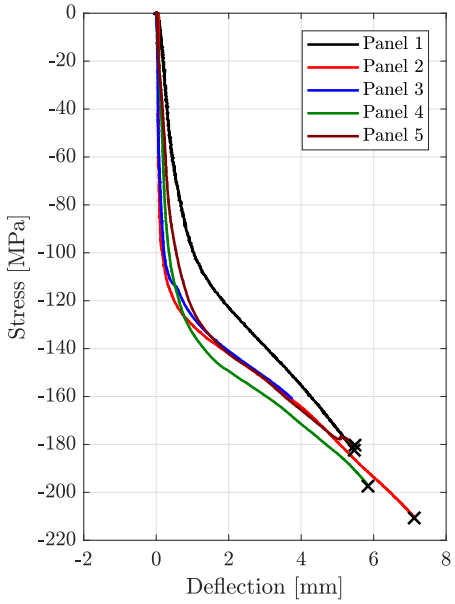

(b) Half seam

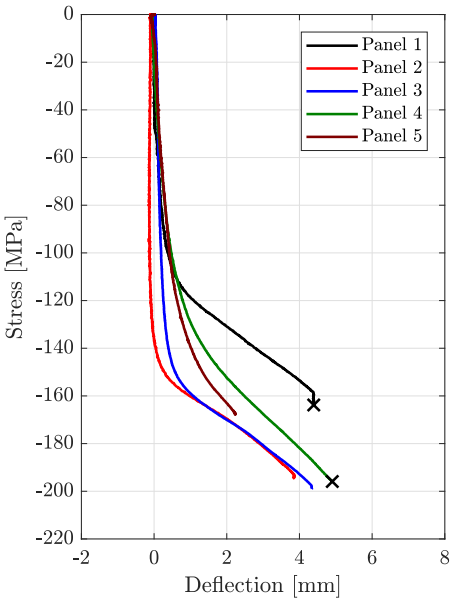

(c) Full seam

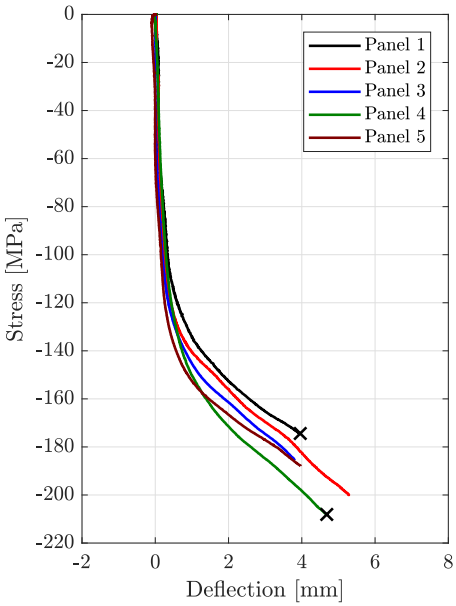

Figure 3.10: Stress vs absolute value of out-of-plane (z) deflection, taken from the DIC analysis at the centre of the panel buckle.

At the experimentally determined critical buckling stress, the average strain for all six gauges was taken as the buckling strain result, plotted in Fig. 3.8b. The experimentally recorded strains are consistently below the numerical predictions. The stiffness pre and post buckling was also determined from the average strain data 3.9, and the averaged

value from each panel type is presented in Table 3.4. Critical buckling stress results were confirmed by tracking the central deformation of buckling mode shapes using DIC, see Fig. 3.10. Comparative buckling mode shapes from experimental results for all panels are given in Fig. 3.11, where (i) shows the initial emergence of the buckle, and (ii) shows the fully developed buckling mode shape at the experimentally determined critical buckling load. FEA for the QI panel, under both pinned and clamped boundary conditions, are shown in Fig. 3.11d. The Half and Full seam numerical FEA mode shapes are indistinct to those produced for the QI panel.

Table 3.4: Experimentally determined panel stiffness, pre and post buckling. The percentage difference for the two tailored panels, when compared to the equivalent QI stiffness, is presented in brackets.

	Exp. (MPa)	
Panel	Avg. Pre	Avg. Post
QI	53.7	29.1
Half	56.5 (+5.2%)	36.9 (26.8%)
Full	58.0 (+8.0%)	41.8 (43.6%)

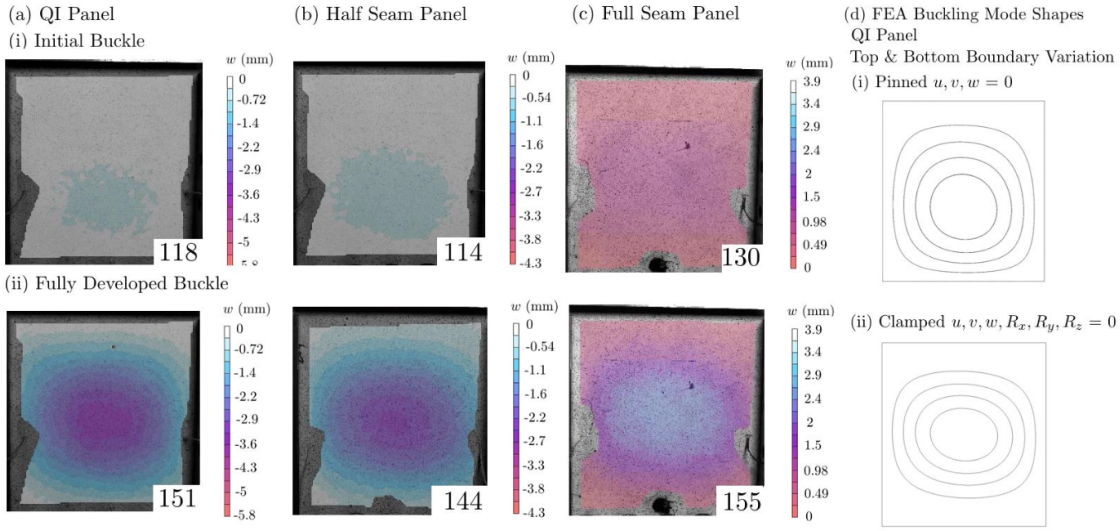

Figure 3.11: Example DIC images, taken from Panel 1 tests, of out-of-plane deflection indicating (i) the emergence of buckling mode shapes, and (ii) the fully developed buckling mode at the critical buckling stress for (a) QI (b) Half Seam and (c) Full Seam. The stresses in MPa at which these images were recorded are given in the bottom right corner. Critical buckling mode shapes for the QI panel, obtained in FEA are shown in (d).

3.6.2 Tensile Results

Figure 3.12a and b present example experimental and FEA stress versus strain curves for Half and Full seams respectively. Experimental strains are derived from DIC data from the first coupon test (No. 1) for all configurations. For each case, the seam coupons strains were extracted from both Regions A and B (25mm and 75mm along the gauge length

respectively) at the mid-width of the coupons. The QI coupon stress vs. strain results were linear, with sudden failure as expected at an average stress of 691 MPa. Average experimental failure stresses for the Half and Full seam tensile tests were 369 MPa and 179 MPa respectively. FEA strains were extracted at corresponding locations in Ply 1 (lower most ply – see Fig 3.3)), for both the Half seam and Full seam cases. The inset FEA diagrams in Fig. 3.12 describe the evolution of seam damage (both inter-laminar and intra-laminar) with increasing load (nominal stress). Only the largest seam damage zone within the specimen is shown. For both the Half and Full seam case, the three insets correspond to (i) the initiation of damage within the seam, (ii) the full degradation of the seam and the onset of damage propagation to the interlaminar region, and (iii) the maximum damage state at the end of the converged simulation.

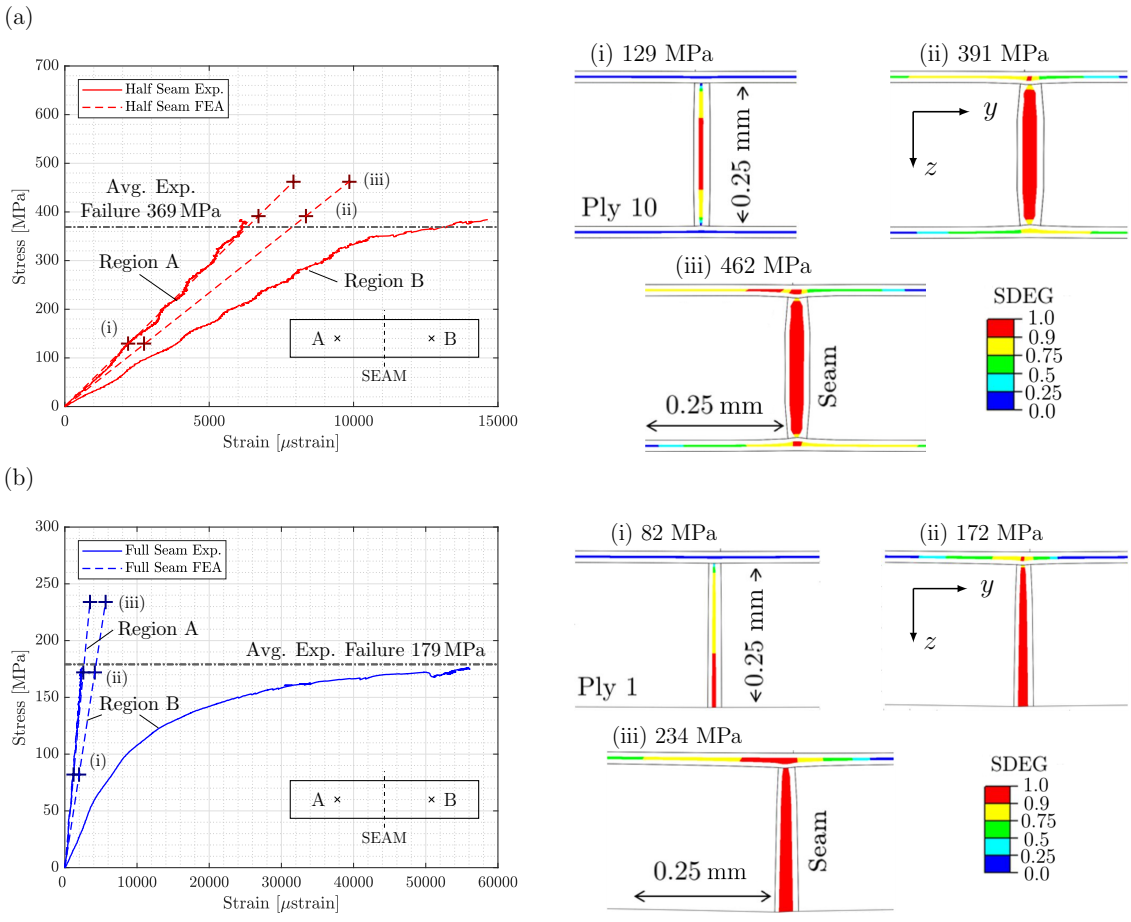

Figure 3.12: FEA and experimental strain vs. stress results for the tensile tests on set of coupons 1 (a) Half Seam and (b) Full Seam. Regions A and B are described in Fig. 3.4. The crosses denote points at which the growth of seam damage in the seam and interlaminar region was evaluated using FEA; (i) initiation of damage, (ii) full development of seam failure and damage propagation from the seam into the interlaminar region and (iii) fully developed damage in the seamed region.

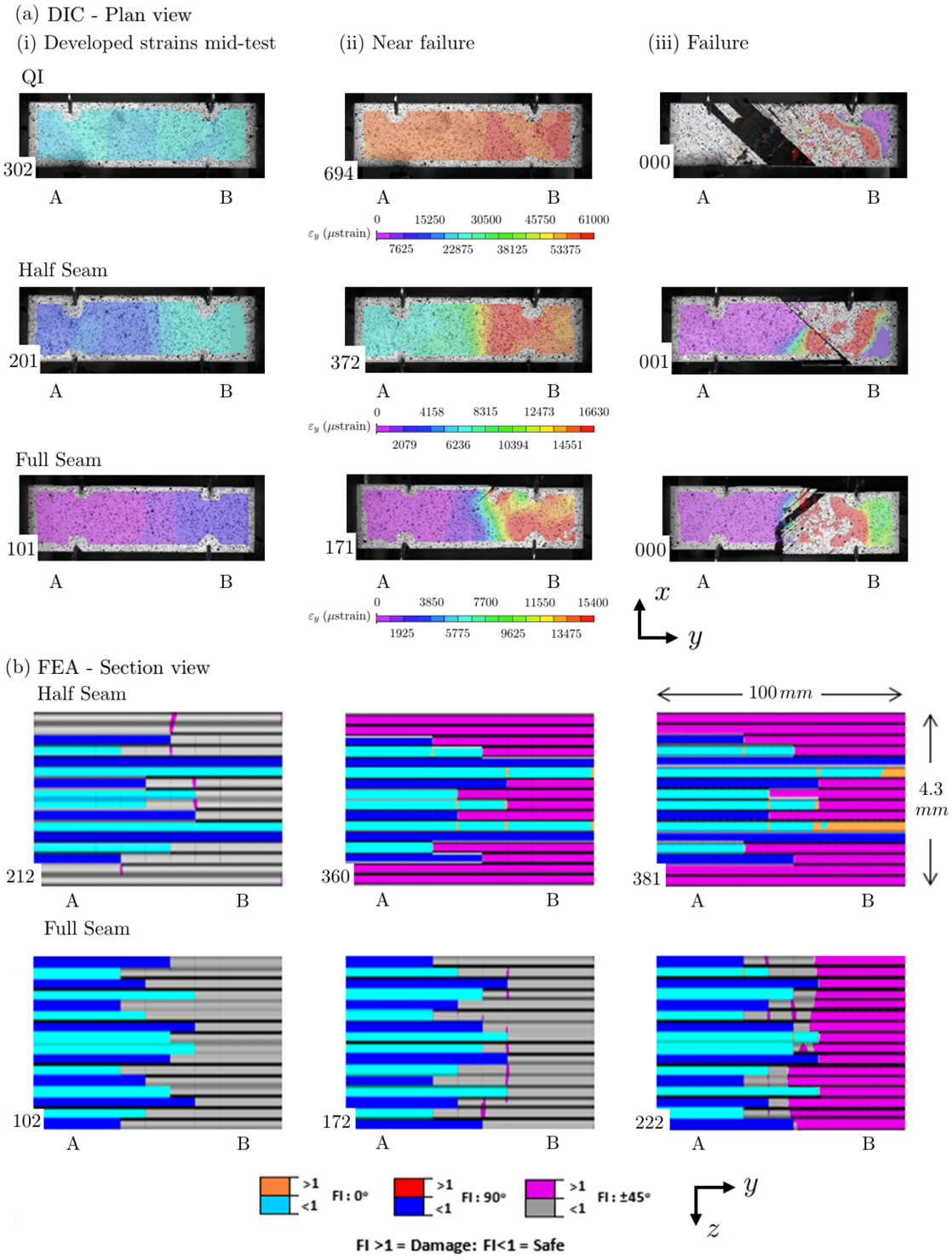

Figure 3.13: DIC planar images of tensile strains developed during the Half Seam and Full Seam tests. The images show the discrete stiffness tailoring in terms of different strains developed in different halves of the coupons. The stresses (in MPa) are given in the bottom right of each image. (b) Cross-section images from the FEA analysis showing failure of the plies.

An example of surface ply strain for key points during the tensile tests are shown in Figure 3.13a using a set of DIC images. In Figure 3.13b the through-thickness failure

index (FI) for each ply has been plotted using FEA results. The failure index is based on max longitudinal stress criteria FI = σ_{yy}/ S^{θ} where σ_{yy} is the longitudinal stress at each integration point within a ply and S^{θ} is the longitudinal strength of the ply at a particular orientation. Thus, for a ply of ±45°, S^{θ} = 202 MPa, for a 90° ply, S^{θ} = 82 MPa, and for a 0° ply, S^{θ} = 2540 MPa (see Table 3.2). A value greater than one indicates onset of damage within the ply and hence less than one indicates that the ply is undamaged.

3.7 Discussion

3.7.1 Buckling Performance

VICONOPT results predict an increase in buckling stress of 12.9-14.6% for the Half seam panel, and 16.3-17% for the Full seam panel with respect to the QI baseline, dependent on the transverse boundary condition, as presented in Table 3.3. Correspondingly, FE analysis predicts an increase of 9.7-11.8% and 13.0-13.6% for the Half and Full seam panels respectively. The FE results are lower both in terms of the absolute magnitude of buckling stress and the relative performance increase obtained using stiffness tailoring. The discrepancy between the numerical analyses can be ascribed to the different model boundary conditions, as in the FE method the longitudinal simple-supports induce a secondary stress in the panel due to the Poisson's ratio, thereby causing buckling to occur at a lower load. Conversely, in VICONOPT the stress is applied within the panel and therefore no transverse stress is assumed or induced. However, the dissimilarity between the two methods is not more than 14% between the same buckling example.

The improvement in DST buckling stress seen in theoretical results is matched by experimental buckling results which show an increase in buckling stress of 12% using a Half seam design, and 16.1% using a Full seam design. The VICONOPT and FE results with the alternative boundary conditions are seen to bound the experimentally obtained results, bar one Half seam result, when all are presented together for comparison in Fig. 3.8. Considering buckling strain instead, a comparison of results in Fig. 3.8b shows on average no noticeable difference between the experimental QI and Half seamed panels, but the Full seam panel produces small increase in average panel buckling strain, approximately 7%.

However, there is an inherent difficulty in determining the precise bifurcation point for each test, and normal manufacturing errors in ply orientation and seam positioning must apply. Hence, a Mann-Whitney U statistical test, which is detailed in Appendix 8.2, was used to determine whether the difference in buckling stress between the Half and Full seamed panel experimental results and those of the QI panels were statistically significant. Using $\alpha < 0.01$, (the lowest limit of acceptable level of significance (magnitude of difference) is $\alpha = 0.05$) the U-test shows that the Full seam buckling stress results are significantly different when compared to the QI baseline. Similarly, a two sided t-test for the Half and Full seamed panels provides sufficient evidence ($\alpha = 0.05$) to accept the original VICONOPT model hypothesis for buckling stress improvements of at least 14.6% with

a simply-supported boundary condition. The relative increase in experimental buckling stress obtained due to stiffness tailoring, 12-16.1%, is closely matched by the increase obtained the VICONOPT analysis, 12.9-16.3%, which validates the use of the efficient Strip model in further analysis of DST composites. Both VICONOPT and FE results are found to agree with experimental values to within 10% when simply-supported boundaries conditions are applied along the loading edges.

The experimentally obtained panel stiffnesses, calculated from the stress-strain data as per Figure 3.10 and presented in Table 3.4, show that the redistribution of the stiffer material to the longitudinal simply-supported boundaries incrementally increases the effective panel stiffness, despite all three panel types being fabricated of the same volume of stiff material. This increase is as much as 8% for the fully seamed panel. More importantly, however, the tailoring is shown to maintain a significantly larger amount of axial stiffness post-buckling, 27% and 41% greater than the QI baseline for Half and Full seam concepts respectively. This increase is as a result of restraining the stiffer plies at the longitudinal boundaries, as post-buckling these regions remain un-deformed out-of-plane and are still capable of bearing significant amounts of stress.

The aim of the compression test was not to investigate damage or failure of the panels, and this was not modelled. However, failure was recorded in several of the tests for each panel type. The mode of failure for these compressive panels, irrespective of panel design and therefore independent of the seams, was twisting of the top clamped fixture, which initiated failure in the 'free' region of the panel, between the knife-edge supports and top clamp. The failed Half and Full panels were examined for damage in the seamed regions, which were found to be intact and undamaged. The reduction in transverse strength as a result of the material discontinuities is therefore not seen to be critical in applications where the load is applied parallel to the seam.

Considering that the size of seam regions on production aircraft structures are likely to be larger than the seam width used here, and the likely ratio of primary and secondary loadings on aerospace components, the results indicate that DST should be a suitable manufacturing process for improving laminate structural efficiency.

3.7.2 Tensile Strength

The development of strain across the experimental tensile coupons, taken from the DIC analyses, is presented in Fig. 3.13a. Failure of the QI coupons was recorded at an average of 690 MPa with sudden failure in the middle of the gauge length. The average final failure stress of the Half and Full seam coupons were 47% and 74% lower respectively. For both seam cases, failure images in Fig. 3.13 show significant cracking in ±45° surface plies, with the majority of damage and considerably higher strains observed in Region B. The ±45° ply surface cracks are seen to develop from the free edges of coupon for both the Half and Full seam coupons. Free edge effects, which are known to develop at ±45° ply interfaces [166], contribute to matrix cracking developing in this region and propagating

across the width of the coupon. Post-test visual inspection also indicates that overall failure was likely not a result of seam failure, although some interaction of damage within the seam is seen for the Full seam test in Fig. 3.13a. This corresponds both with Fig. 3.12, which shows non-linear behaviour in the ±45° ply dominated Region B, and the failure index analysis in Fig. 3.13b, which shows the onset of ply failure, mainly in the ±45° plies in Region B, at loads considerably below the experimental failure load. As Fig. 3.12 shows that Region A has a linear stress-strain response (predicted by the FEA for both seam cases) it is apparent that the discrepancy in failure stress between QI and seamed tests is a principally a result of failure in Region B. In future work, the non-linear shear behaviour of the ±45° should be included in order to accuracy capture the experimentally observed behaviour.

As the aim of the tensile FEA model was to understand seam failure, progressive damage was only considered for the seam interfaces and not within the plies themselves. This meant the non-linear stress-strain relationship, resulting from non-linear ply deformation and fracture in Region B was not captured by cohesive failure of the resin regions around seams, see Fig. 3.13. However, the first onset of interlaminar damage following resin failure at the end of terminated plies coincides well with ultimate failure loads, see Figs. 3.12a(ii) and 3.12b(ii). Similarly, contrasting ply failure indices in Fig. 3.13b with experimental failure loads shows ply failure is broadly indicative of ultimate coupon failure; FEA stresses for the Half seam, that correspond to initiation and widespread failure of ±45° and 90° plies (perpendicular to the tensile load), bound the average experimental result for failure. Similarly, FEA stresses relating to initiation and extensive failure of ±45° plies in Region B bound the average experimental failure stress for the Full seam case.

FEA predicts that the failure of the resin regions at the end of plies within seams initiates without loss of stiffness at the coupon length scale. By noting the linearity of experimental stress vs. strain data in Fig. 3.13, near the stresses suggested by FEA in Fig. 3.12b, it is apparent this is consistent with the experimental results for Region A. Buckling tests that ended in failure of the panel are marked in Figs. 3.9 and 3.10. However, as previously discussed, these failures were not seam related and post-test visual analysis of the panels shows no damage to the seamed regions. Thus with the caveat that optimisation for buckling may further increase stress in seamed regions, it can be concluded that for uni-axial compressive load with seams parallel to the load, reduction in strength due to DST does not seem to be critical. This work also shows that uni-axial buckling loads and tensile strength of seamed coupons can be predicted by readily available numerical methods. The simple FE model introduced in this paper could form a basis for seam design, as the stress at which the interlaminar damage initiates appears to provide a good approximation of seam strength. Additionally, Czel et al. [167] have previously noted the benefits for damage detection and load redistribution for structures containing ply discontinuities that may assist with aircraft certification.

3.8 Conclusions

- Use of Discrete Stiffness Tailoring (DST) to affect simple redistribution of 0°, ±45° and 90° material in a baseline quasi-isotropic panel has been shown, in a statistically significant manner, to improve buckling performance of Half and Full seamed panels, both experimentally and numerically, by up to 12% and 16% respectively in comparison to a $[45/\text{-}45/90/0]_{2S}$ laminate. Note that these results are not examples of optimised DST laminates, so greater gains in material efficiency are possible and should be investigated.
- The strip Model, VICONOPT, is shown to accurately capture relative performance differences between the baseline, Half and Full seam DST panels. The computational efficiency of VICONOPT is appropriate for use in initial design studies and optimisation routines for DST laminates.
- The seams, the points at which the ply orientation alters abruptly, were not found to cause premature failure of the plates even in the most extreme case where no continuous plies are preserved across the width. The presence of the seams was not seen to affect the critical buckling stress the panel was able to achieve.
- Tensile testing of seamed coupons shows significant reductions in strength for Half and Full seam concepts, 47% and 74% when compared to a QI baseline. However, the experimental results suggest that failure is as a result of free-edge effects, which developed in the regions dominated by ±45° plies.
- Assuming an exaggerated seam width which is several orders of magnitude greater than shear lag models calculate would be necessary for the transfer of load through shear, and maintaining some number of continuous plies insures a critical level of transverse strength is retained. Although the seams did not have a detrimental effect on buckling, the preserving continuous plies should be prioritised.

Chapter 4

DST Optimisation Methodology

4.1 Introduction

In Chapter 3, a set of non-optimised flat plates were designed and experimentally tested to demonstrate the capability of DST for improved buckling performance. Leading on from this, the current Chapter focuses on implementation of a robust and efficient optimisation routine that can be used for the minimum mass design of discretely stiffness tailored structures, and hence is suitable for use as a preliminary design tool for aircraft design. This approach generates the optimum stacking sequences and panel geometries required to withstand a particular compressive load without buckling, incorporating laminate design rules and manufacturing limitations alongside maximum strain constraints for damage tolerance.

A two-level optimisation methodology is implemented for the minimum mass design of a stiffened DST panel. The problem is formulated using a stiffened panel model simulating an experimental set-up, with the aim of designing an optimised DST panel for experimental analysis. Lamination parameters are used to describe the stiffnesses of the separate structural regions in terms of continuous design variables so that a highly efficient gradient-based optimisation method can be applied in the first stage. The laminate thicknesses and geometry are optimised simultaneously with stiffness, to produce the minimum mass optimum. Results from the gradient-based approach are compared to solutions obtained using particle swarm optimisation for the same case studies, to ensure the gradient-based algorithm is not adversely affected by discontinuous or non-convex feasible design space. The buckling analysis is performed using a variant of the efficient strip model used in Chapter 3, capable of accurately assessing a list of specified buckling wavelengths with very low computational expense. The second stage then uses a Genetic Algorithm (GA) to convert the lamination parameters and laminate thicknesses into discrete stacking sequences composed of standard ply angles (0°, ±45°, 90°) and constrained by stacking sequence rules.

4.2 Problem Formulation

In the literature review presented in Chapter 2, it was found that research on the optimisation of stiffness tailored structures is limited, and that experimental work validating opti-

mised VS designs, for simple compression panels as well as larger structures, is also scarce. The previous experimental proof-of-concept demonstrated that the ply discontinuities did not adversely affect the gains in buckling performance of a simple DST panel. Therefore, this work now focuses on the analysis and optimised design of a tailored aerospace structure, leading to an experimental test. A T-stiffened panel of length L, illustrated in Figure 4.1, is selected as a suitable representative aircraft structure for the demonstration of DST. The panel is assumed to be an upper wing cover carrying a compressive uni-axial load N_x; the loading edges are assumed clamped, whilst the longitudinal edges are free of restraint. This arrangement with two stiffeners was selected for experimental feasibility, such that sufficient skin-width is present for optimisation while ensuring the panel can be manufactured and tested within the available test machine. While free edges are not typical of aerospace structures, this boundary condition was selected to reflect that of the experimental set up. The panel is composed of a single skin and two T-shaped stiffeners that are attached at either longitudinal edge, separated by a stiffener spacing width, this model simulates an experimental set-up. The critical buckling load is assessed as the main design constraint and a maximum strain allowable is also enforced for damage tolerant design, as this imposes a minimum value on overall panel stiffness.

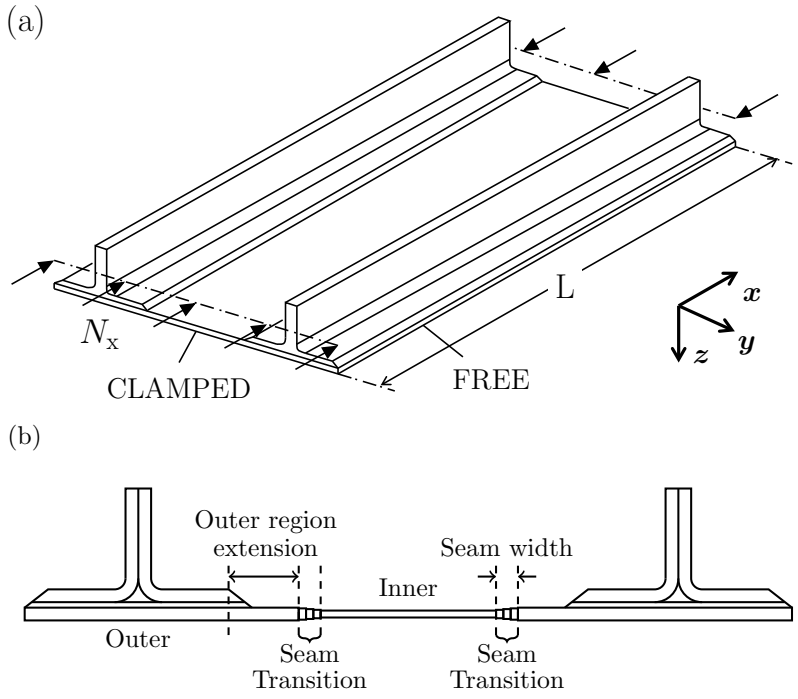

Figure 4.1: a) Isometric view of the panel, length L, indicating boundary conditions and loading N_x applied as uniform end-shortening. b) Cross-section of the Discrete Stiffness Tailored panel, the 'Outer' and 'Inner' skin regions are linked by 3 segment stepped seam transition width. The seam location is measured as the length of the 'Outer' region extension from the stiffener foot.

Tailoring is applied across the skin by division into two regions: underneath the stiffener bond-line - the 'Outer' region, and the length of skin between the stiffeners - the 'Inner' region as labelled on the panel cross-section in Fig. 4.1b. Transition between the two

skin regions is established by way of three piecewise steps (the seam region) which each have constant thickness and stiffness, but over which the thickness and stacking sequence is varied in gradual, discrete steps in order to avoid large stress concentrations and formation of damage in the weaker resin rich region due to discrete ply drops. The 'Outer' region width extends beyond the stiffener foot and the model is able to optimise the location of the transition. With curvilinear variable angle designs the size and site of the transition region is generally dictated by the minimum manufacturable radii, whereas transition can occur as rapidly as needed with the new DST design methodology presented here. The aim of the DST design is to redistribute the load by providing reinforcement where required in the structure, leading to a more efficient use of material which in turn results in a reduction in mass.

4.3 Methodology Overview

A two stage optimisation routine is employed to minimise the mass of the DST stiffened panel, as per those developed in [101, 129], which is illustrated in Figure 4.2. The problem is decomposed into the optimisation of continuous variables in the first stage, returning optimal lamination parameters, structural thicknesses and relative widths for a composite structure, and a second stage returns a discrete stacking sequence solution from the optimised continuous variables. From the literature review presented in Chapter 2, representing laminate stiffness using lamination parameters is seen to be advantageous as the number of parameters required to describe any stack is reduced to a maximum of twelve, and this number is independent of the laminate thickness. The use of lamination parameters also circumvents the trigonometric relationship between ply angle and stiffness, hence creating a convex design space for the buckling optimisation of flat plates, which can be paired with an efficient gradient-based approach without being trapped in local optima.

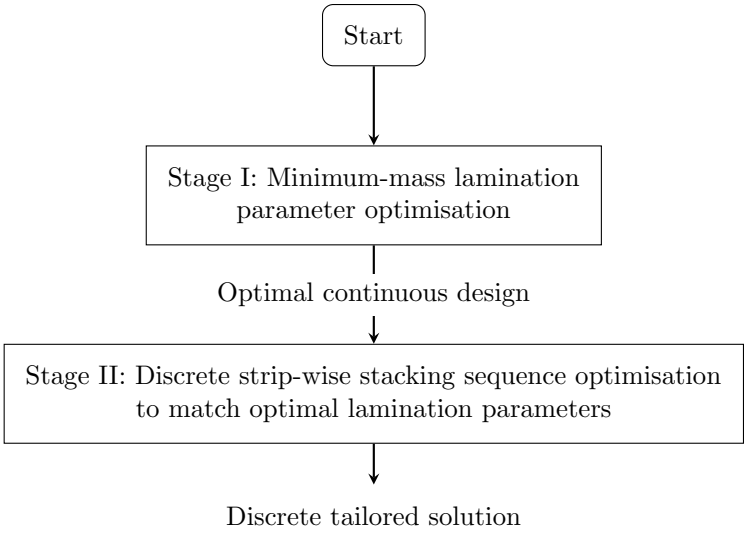

Figure 4.2: Flowchart of optimisation process stages.

The success of the gradient-based solver in finding the global optimum is dependent on the convexity of the design space, in terms of both the objective and constraint functions. The convexity of the lamination parameter feasible region, and the linear relationship between the lamination parameters and laminate stiffness, proven in [115], bypasses the existence of local optima that would otherwise arise when directly optimising ply angles. Although the buckling load of a flat plate has also been shown to be a convex function of the lamination parameters, it is, however, possible that the optimisation of a stiffened panel may not have a convex and continuous feasible design space due to the switching of the critical buckling mode between local skin, stiffener and Euler modes, introduced by the additional geometric variables. Figure 4.3 illustrates how a non-convex and discontinuous feasible design space affects the return of the global optimum when using a gradient-based approach. Therefore, in order to verify that the gradient-based method is returning the best global optimum, a Particle Swarm Optimisation (PSO) is applied to run the same minimum mass optimisation problem to compare the solution quality and algorithm efficiency. PSO is a meta-heuristic, stochastic search method which is not reliant on derivative information and as such, is in theory able to return a global optimum even if the design space is non-convex [168]. The two optimisation algorithms are applied using the same problem formulation, continuous variables and constraints.

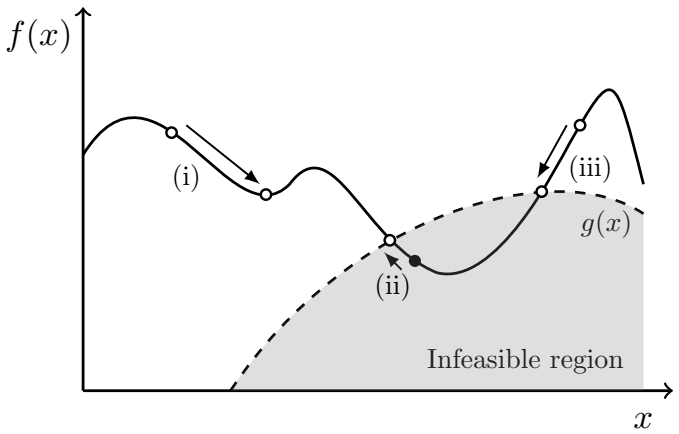

Figure 4.3: Example graph illustrating the result of a non-convex and discontinuous feasible design space on gradient-based optimisation: (i) local optima due to non-convex design space, (ii) global optimum, and (iii) local optima due to constraint.

The second stage then utilises a genetic algorithm to minimise the difference between the optimal continuous lamination parameter design and a candidate discrete stack, as no one-to-one mapping exists for the inverse transformation. Genetic algorithms are commonly used to convert lamination parameters into discrete stacking sequence designs, as they easily handle discrete variables and stacking sequence design constraints can be simply applied. Stage II is discussed in detail in Section 4.8.

4.4 Lamination Parameters

Classical Laminate Theory (CLT) is widely used to define the elastic properties of a laminate stack [113]. The in-plane, coupled response and out-of-plane (**ABD**) stiffness matrices are related to the applied moments and stresses, and the resultant mid-plane strains and curvatures, as follows:

$$\begin{Bmatrix} \boldsymbol{N} \\ \boldsymbol{M} \end{Bmatrix} = \begin{Bmatrix} \mathbf{A} & \mathbf{B} \\ \mathbf{B} & \mathbf{D} \end{Bmatrix} \begin{Bmatrix} \boldsymbol{\epsilon}^0 \\ \boldsymbol{\kappa} \end{Bmatrix} \tag{4.1}$$

where $\boldsymbol{M}$ and $\boldsymbol{N}$ are the moment and in-plane stress vectors, and $\boldsymbol{\epsilon}^0$ and $\boldsymbol{\kappa}$ are the mid-plane strain and curvature vectors respectively. Using lamination parameters, any full laminate stack may be described using a single thickness variable, h, five material invariants, $\boldsymbol{U}$ and twelve lamination parameters, regardless of the number of plies [114]. The twelve lamination parameters can be further reduced to eight for symmetric laminates, as the coupled response matrix **B** becomes zero. As the laminates in this work are restricted to balanced and symmetric designs, and as flexural-twist coupling terms for laminates composed of increasing numbers of plies become small compared to the other out-of-plane terms (D_{11}, D_{12}, D_{22}, D_{66}), the number of variables required further decreases to just four, as the other variables $\xi_{3,4}^{A,D}$ approximate zero. This type of laminate does not have extension-shear (A_{16}, $A_{26} = 0$) or flexural-twist coupling (D_{16}, $D_{26} = 0$). The expressions that relate the **A** and **D** matrices to these lamination parameters are then simplified to the following:

$$\begin{pmatrix} A_{11} \\ A_{22} \\ A_{12} \\ A_{66} \end{pmatrix} = t \begin{bmatrix} 1 & \xi_1^A & \xi_2^A & 0 & 0 \\ 1 & -\xi_1^A & \xi_2^A & 0 & 0 \\ 0 & 0 & -\xi_2^A & 1 & 0 \\ 0 & 0 & -\xi_2^A & 0 & 1 \end{bmatrix} \begin{pmatrix} U_1 \\ U_2 \\ U_3 \\ U_4 \\ U_5 \end{pmatrix} \tag{4.2}$$

$$\begin{pmatrix} D_{11} \\ D_{22} \\ D_{12} \\ D_{66} \end{pmatrix} = \frac{t^3}{12} \begin{bmatrix} 1 & \xi_1^D & \xi_2^D & 0 & 0 \\ 1 & -\xi_1^D & \xi_2^D & 0 & 0 \\ 0 & 0 & -\xi_2^D & 1 & 0 \\ 0 & 0 & -\xi_2^D & 0 & 1 \end{bmatrix} \begin{pmatrix} U_1 \\ U_2 \\ U_3 \\ U_4 \\ U_5 \end{pmatrix} \tag{4.3}$$

where the four lamination parameters are given by:

$$\xi_{1,2}^A = \frac{1}{t} \int_{-h/2}^{h/2} [\ cos(2\theta),\ cos(4\theta)\ ] dz \tag{4.4}$$

$$\xi_{1,2}^D = \frac{12}{t^3} \int_{-h/2}^{h/2} [\ cos(2\theta),\ cos(4\theta)\ ] z^2\ dz \tag{4.5}$$

where z is the distance of mid-plane of the ply from the mid-plane of the laminate which has an overall thickness t, θ is an individual ply angle, and the material invariants $\boldsymbol{U}$ are defined as:

$$\begin{aligned} U_1 &= (3Q_{11} + 3Q_{22} + 2Q_{12} + 4Q_{66})/8 \\ U_2 &= (Q_{11} - Q_{12})/2 \\ U_3 &= (Q_{11} + Q_{22} - 2Q_{12} - 4Q_{66})/8 \\ U_4 &= (Q_{11} + Q_{22} + 6Q_{12} - 4Q_{66})/8 \\ U_5 &= (Q_{11} + Q_{22} - 2Q_{12} + 4Q_{66})/8 \end{aligned} \tag{4.6}$$

where Q_{ij} are the reduced lamina stiffnesses, defined as:

$$\begin{aligned} Q_{11} &= \frac{E_{11}^2}{(E_{11} - E_{22}\,\nu_{12}^2)} \\ Q_{22} &= \frac{E_{11}\,E_{22}}{(E_{11} - E_{22}\,\nu_{12}^2)} \\ Q_{12} &= \nu_{12}\,Q_{22} \\ Q_{66} &= G_{12} \end{aligned} \tag{4.7}$$

where E_{11} is the longitudinal modulus, E_{22} the transverse modulus and G_{12} the shear modulus and ν_{12} the Poisson's ratio for a unidirectional composite material.

4.5 Stage I: Problem Formulation

In Stage I, the objective function is the minimum mass of the stiffened panel, subject to buckling, strain and design constraints. The constrained non-linear optimisation problem, where $\boldsymbol{x}$ is the vector of design variables, is formulated as follows:

$$\begin{gathered} \text{minimise } f(\boldsymbol{x}) \\ \text{subject to } g(\boldsymbol{x}) \leq 0 \\ \text{and } \boldsymbol{x}_{lb} \leq \boldsymbol{x} \leq \boldsymbol{x}_{ub} \end{gathered} \tag{4.8}$$

where $f(\boldsymbol{x})$ is the objective function, $g(\boldsymbol{x})$ the constraints, and $\boldsymbol{x}_{lb}$ and $\boldsymbol{x}_{ub}$ are the lower and upper bounds respectively for the corresponding design variables. A summary of the objective, constraints and decision variables associated with each optimisation stage is provided in the subsequent sections. Each separate laminate region is represented by four lamination parameters, as defined in Section 4.4.

4.5.1 Variables

All variables are normalised to lie on the unit interval for improved solver performance. Lamination parameters ($\xi_{1,2}^{A,D}$) are employed as Stage I variables, describing the stiffness properties of each discrete region of the panel. Lamination parameters and thicknesses in the seam region are taken as discrete values from a linear trend varying between their corresponding values in the 'Outer' and 'Inner' regions, evaluated at each seam mid-line The geometric variables to be optimised for each panel type are listed in Table 4.1 and are indicated on the cross-section of the DST panel in Fig. 4.4. Other labelled variables in Fig. 4.4 are submitted to the optimiser as fixed values; including the outer stiffener radius r_{st}, the seam length b_{seam}. Two plies of $\pm 45°$ degrees, spanning the width of both stiffener flanges and referred to as 'capping plies', are included to contain the noodle within the deltoid region of the stiffener, as is standard industrial practice. The material within the stiffener deltoid region, indicated in Fig. 4.4, is not modelled to contribute structurally to the buckling behaviour of the panels in the optimisation routine. The stiffener flanges have 45 degree chamfer, which are also not modelled, but an extra skin width is accounted for at either longitudinal edge.

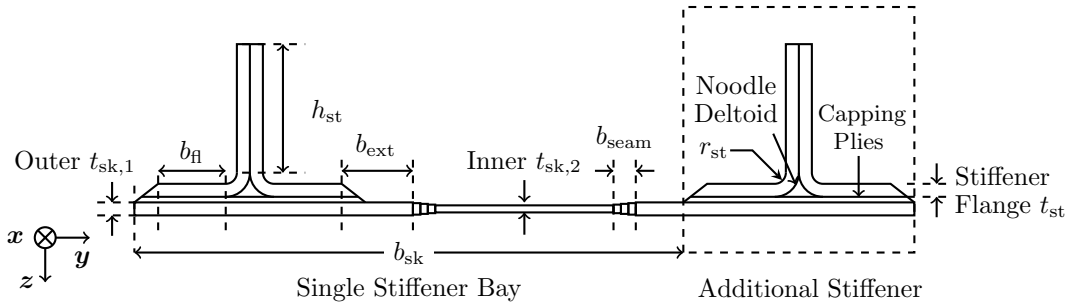

Figure 4.4: Cross-section of the DST panel labelled with geometric variables.

Table 4.1: Stage I: Table of design variables

Panel Type	Skin	Stiffener
Baseline	$(\xi_{1,2}^{A,D})_{\text{sk}}$, t_{sk}	t_{st}, h_{st}, b_{fl}
DST	Outer $(\xi_{1,2}^{A,D})_{\text{sk},1}$, $t_{\text{sk},1}$, b_{ext}	t_{st}, h_{st}, b_{fl}
	Inner $(\xi_{1,2}^{A,D})_{\text{sk},2}$, $t_{\text{sk},2}$	

4.5.2 Applied Load

The design running load N_x is prescribed as a compressive force per unit width, homogenised across a single stiffener bay. Both the skin and stiffeners are load-bearing. The total load applied to the panel must therefore be adjusted to account for the fact that two stiffeners are modelled. Specifically, variations in the axial stiffness of the additional stiffener and the attached skin section, resulting from changes in the design variables, will attract varying levels of running load into the panel. The overall applied load P_x is

calculated by adding an additional contribution to the load associated with the additional stiffener section $(\mathrm{EA})_{\mathrm{st}}$ proportional to the axial stiffness of a single stiffener section divided by that of a complete stiffener bay $(\mathrm{EA})_{\mathrm{bay}}$. The additional stiffener region and stiffener bay are marked on Fig. 4.4. For a structure composed of N plates, the axial stiffness is expressed as:

$$(\mathrm{EA})_i = \sum_{i=1}^{N} b_i \left(A_{11,i} - \frac{A_{12,i}^2}{A_{22,i}} \right) \tag{4.9}$$

where subscript i refers to the strip number in VIPASA, see Section 4.5.3.

Obtaining both $(\mathrm{EA})_{\mathrm{st}}$ and $(\mathrm{EA})_{\mathrm{bay}}$, the overall applied load is calculated as:

$$\mathrm{P}_x = N_x \, b_{\mathrm{sk}} \left(1 + \frac{(\mathrm{EA})_{\mathrm{st}}}{(\mathrm{EA})_{\mathrm{bay}}} \right) \tag{4.10}$$

4.5.3 Buckling Constraints

Buckling constraints are applied to prevent the stiffener or skin buckling prematurely before the design load is reached. The finite strip program, VIPASA (Vibration and Instability of Plate Assemblies including Shear and Anisotropy) [153], is used to predict the buckling behaviour of the panel. The use of VICONOPT (VIpasa with CONstraints and OPTimisation) in the previous Chapter (see Chapter 3 in particular Section 3.4.1) also validated the use of VIPASA for the accurate buckling analysis of DST structures. VIPASA is selected here instead of VICONOPT, as the extra features of VICONOPT when compared to VIPASA, i.e. greater accuracy for plates loaded under shear, are not applicable in this problem, and VIPASA is more computationally efficient.

Buckling modes are assumed to vary sinusoidally in the longitudinal direction (x in Fig. 4.1a) with half-wavelength λ, the number of modes, N, is specified by the user and the half-wavelength values are taken as $\lambda = \ell$, $\ell/2$, ..., ℓ/N where $\ell = \mathrm{L}/2$ is the effective length of the panel. As a result of this assumption, the displacements, rotations and, correspondingly, the forces and moments at the longitudinal edge also vary sinusoidally. In the absence of shear load or bend-twist coupling, VIPASA modeshapes correspond to simply-supported transverse boundary conditions. In order to obtain buckling results for the stiffened panel structure with clamped end boundary conditions as indicated in Fig. 4.1, the VIPASA model has a length of half the actual panel length, as the effective length, ℓ, for a column with both ends fixed is equivalent to half that of a column with both ends pinned [169], as illustrated in Figure 4.6. The structure of the stiffened panel is created through the connection of plate substructures, as illustrated in Fig. 4.5. The stiffener radii are modelled using an arc of three connected plates to simulate the curvature, as previous work has shown accuracy of the buckling load prediction is affected by this modelling refinement [170].

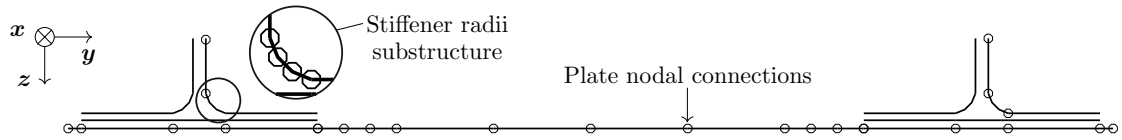

Figure 4.5: Diagram of VIPASA strip model, illustrating the connected plate substructure and detail of the stiffener radii arc.

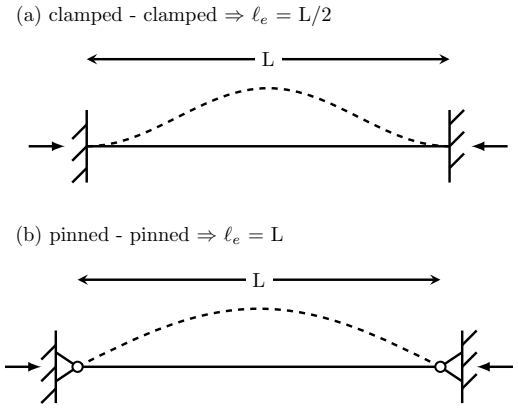

Figure 4.6: Effective lengths for alternative boundary conditions.

The exact stiffness matrices for an individual plate are explicitly obtained as a function of the edge forces and displacements using classical plate theory [171]. The subsequent transcendental eigenproblem is solved using the iterative Wittrick-Williams algorithm [172], an efficient modelling approach which guarantees convergence on all specified eigenvalues. The analysis returns a list of eigenvalues, the buckling loads and, for the final analysis, a modeshape plot associated with each i^{th} half-wavelength specified. Total computation time for a single run, with the modeshape plotting function disabled, is approximately 0.052 seconds. Buckling factors F_i are calculated by dividing these eigenvalues by the applied in-plane loading. Hence a buckling constraint is evaluated as follows:

$$1 - F_i \leq 0 \tag{4.11}$$

An example plot exhibiting bucking factor vs. half-wavelength for an optimised constant stiffness stiffened panel is shown in Fig. 4.7. The results relating to the global, local and stiffener buckling modes are highlighted in red. A sufficiently large range of half-wavelengths is assessed in this analysis to encompass critical global, local skin and local stiffener buckling modes.

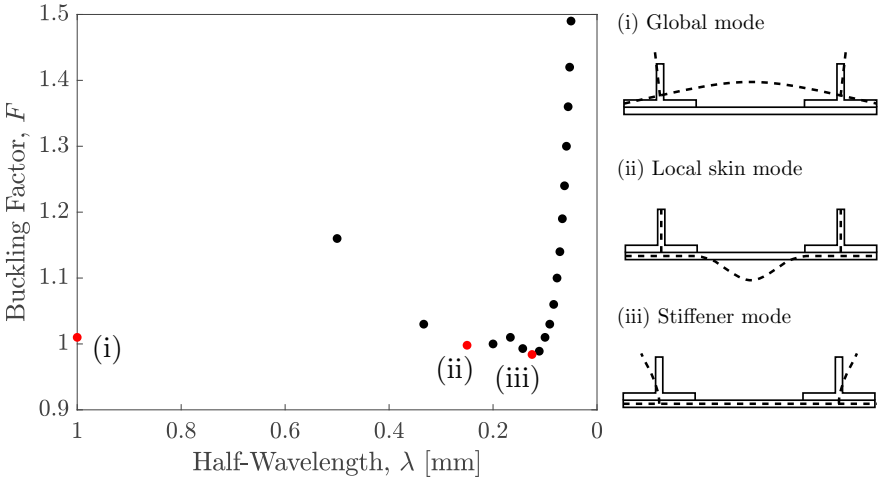

Figure 4.7: Buckling factor F vs. half-wavelength λ example plot for the first 20 half-wavelengths (N = 20) for an optimised constant stiffness stiffened panel with $\ell = 1\,\text{m}$, $b_{\text{sk}} = 0.3\,\text{m}$ and $h_{\text{st}} = 56\,\text{mm}$.

4.5.4 Strain Constraint

The axial strain of the entire structure is limited to an allowable value, ϵ_{max}, which is based on industrial limits for damage tolerance, see Section 4.7. The smeared panel axial stiffness is calculated using Eq. (4.9) which models the regions as connected parallel springs, dividing by the width of the panel, and the strain ϵ_x is returned using Eq. (4.1). The strain constraint is then evaluated using the design strain ϵ_{max} as follows:

$$\frac{\epsilon_x}{\epsilon_{\text{max}}} - 1 \leq 0 \tag{4.12}$$

4.5.5 Lamination Parameter Feasible Regions

Lamination parameters are interdependent variables. No bijective function exists between any combination of in-plane, in-and-out-of-plane or out-of-plane parameters, so for a given point in the $\xi^A_{1,2}$ space, there exists a number of possibilities for the selection of $\xi^D_{1,2}$, and vice-versa. A number of non-linear constraints define the outer limit for the selection of lamination parameters and also the relationships between the in-plane, coupling and out-of-plane regions. Some manufacturing constraints can also be accounted for at this stage. For symmetric laminates composed of standard angles (0°, ±45°, 90°), the constraint relating the in-plane and out-of-plane parameters are as follows [121]:

$$2\,|\,\xi^j_1| - \xi^j_2 - 1 \leq 0 \quad j = A, D \tag{4.13}$$

Additional constraints that link the in-plane and out-of-plane lamination parameters for standard angle laminates are derived in [117]. These constraints form conceptually similar boundaries to the feasible region illustrated in Fig. 4.8, however, spanning the full

six-dimensional space of in-plane and out-of-plane lamination parameters corresponding to standard angle laminates. Herencia et al. then accounted for symmetric laminates, defining 10 constraints [122]. Setting $\xi_3^{A,D}$=0, and eliminating constraints which are never active gives rise to the following 8 constraints:

$$(\xi_i^A - 1)^4 - 4(\xi_i^A - 1)(\xi_i^D - 1) \leq 0 \qquad i = 1, 2 \tag{4.14a}$$

$$(\xi_i^A + 1)^4 - 4(\xi_i^A + 1)(\xi_i^D + 1) \leq 0 \qquad i = 1, 2 \tag{4.14b}$$

$$(2\xi_1^A - \xi_2^A - 1)^4 - 16(2\xi_1^D - \xi_2^D - 1)(2\xi_1^A - \xi_2^A - 1) \leq 0 \tag{4.14c}$$

$$(2\xi_1^A + \xi_2^A + 1)^4 - 16(2\xi_1^D + \xi_2^D + 1)(2\xi_1^A + \xi_2^A + 1) \leq 0 \tag{4.14d}$$

$$(2\xi_1^A - \xi_2^A - 3)^4 - 16(2\xi_1^D - \xi_2^D - 3)(2\xi_1^A - \xi_2^A - 3) \leq 0 \tag{4.14e}$$

$$(2\xi_1^A + \xi_2^A + 3)^4 - 16(2\xi_1^D + \xi_2^D + 3)(2\xi_1^A + \xi_2^A + 3) \leq 0 \tag{4.14f}$$

4.5.6 Lamination Parameter Manufacturing Constraints

In order to account for unanticipated off-axis loading, it is common industrial practice to maintain a 10% minimum of the overall laminate thickness of each standard angle ply (0°, ±45°, 90°). This common practice reduces the feasible regions in the in-plane and out-of-plane lamination parameter space as illustrated in Fig. 4.8. The limits of the constrained out-of-plane region are defined by 6 points, each representing the extreme stacking sequence combinations of 0°/±45°/90° plies, as described by Liu [173], however, a triangular feasible region can be approximated for simplicity. For the in-plane parameters, the space is considerably reduced due to the 10% rule, but little reduction is observed in the out-of-plane feasible region.

As all variables are transformed onto the unit interval, the application of upper and lower bounds to the lamination parameter variables scales the entire region to now lie between these bounds, given in Table 4.2. In doing this, all feasible regions constraints defined in Eqs. 4.13 and 4.14 are automatically scaled to fall within these bounds, including those linking the in-plane and out-of-plane parameters.

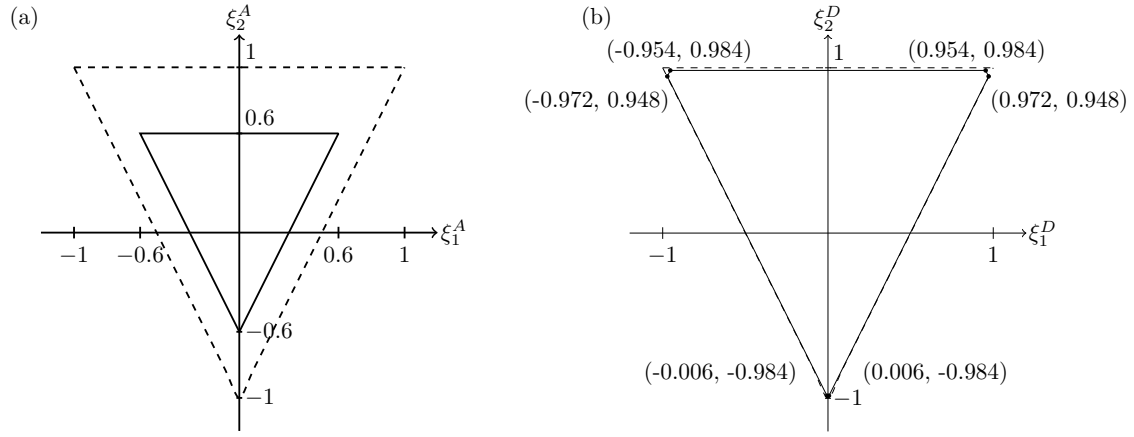

Figure 4.8: Reduced feasible region for the (a) in-plane (membrane) and (b) out-of-plane (flexural) lamination parameters considering the use of only standard angles (0°,±45°, 90°) and imposing the 10% rule. The original boundary, denoted by dotted lines, is given for comparison.

Table 4.2: Lamination parameter upper and lower bounds.

	ξ_1^A	ξ_2^A	ξ_1^D	ξ_2^D
Lower Bound	-0.6	-0.6	-0.972	-0.984
Upper Bound	0.6	0.6	0.972	0.984

4.5.7 Geometric Constraints

A linear constraint is enforced to ensure the stiffener spacing remains fixed to value b_{st}, under variations in the flange length and extension of the skin outer regions beyond the stiffener flange. Another linear constraint ensures the difference in thickness between the outer and inner skin regions is not too large. This constraint is based upon current industrial guidelines which enforce a ratio of 10:1 between transition width and thickness variation in components where the taper is transverse to the loading direction [174]. This linear constraint is defined as:

$$|t_{\text{sk},1} - t_{\text{sk},2}| \leq \frac{b_{\text{seam}}}{10} \tag{4.15}$$

4.6 Stage I: Optimisation Algorithms

Two optimisation algorithms are employed to solve the minimum mass problem subject to the constraints as previously defined: a gradient-based method and a Particle Swarm Optimisation (PSO) routine. The computational efficiency and quality of final solution obtained by both approaches are compared for five numerical case studies.

4.6.1 Gradient-Based Optimisation

An in-built MATLAB function *fmincon* is employed to find the minimum mass of the specified laminate geometry, subject to the previously defined linear and non-linear constraints, and upper and lower variable bounds. Within the function *fmincon*, a Sequential Quadratic Programming (SQP) algorithm is selected to find the local minima of the objective function subject to the constraints. This algorithm strictly enforces the upper and lower variable bounds at each iteration, and uses a Lagrangian approach for constraint handling. The efficiency and accuracy of a gradient-based approach is generally superior to alternative optimisation methods as, although the gradients must be calculated at each step for each variable, convergence is reached in fewer iterations [98]. Analytical expressions for assessing the derivatives of the objective function and constraints are supplied when possible. As the buckling performance of the stiffened panel structure is analysed using VIPASA, a finite-difference method is used to evaluate the gradient function, which is acceptable in this case as the time for a single VIPASA analysis with 30 half-wavelengths is approximately 0.052 seconds.

4.6.2 Particle Swarm Optimisation

Particle Swarm Optimisation, first introduced by Kennedy and Eberhart in 1995 [168], belongs to a subset of population-based meta-heuristic stochastic optimisation techniques known as Evolutionary Algorithms (EA). PSO is based on biological examples of bird flocking and animal swarming behaviour, where interactions between each member of the group influence motion towards an optimal position. Replicating this in the algorithm, a population of particles travel through the design space, influenced by a combination of the best solutions discovered on previous iterations and parameters introducing a measure of randomness to imitate natural behaviour. The meta-heuristic nature of the particle swarm method erases the dependency of the optimiser on gradient information, and therefore is less likely to be trapped in local optima.

Particle swarm optimisation uses iterations of candidate solutions to inform the next round of the process. A specified number of particles are defined, and their positions are the input variables from which a fitness value is calculated using the objective function. A combination of the overall global best candidate solution and the individual particles best solution, and some calculated inertial vector, a social and a cognitive parameter inform the next motion of the particle. The selection of the inertial, social and cognitive parameters affect both the speed of convergence and the exploration of the design space. The original PSO method was applied to unconstrained unbounded problems, but this has been extended by a number of authors to solve both constrained and bounded problems, and is generally achieved by using penalty functions [175].

As with the gradient-based method, lamination parameters are used to both reduce the number of variables needed to describe the laminate stiffnesses, and to represent the discrete ply variables continuously. Although the lamination parameters are no longer

needed to simplify the design space to reduce the possibility of local optima, PSO is generally best suited to problems formulated using continuous variables, and the speed of convergence increases with a smaller dimensional space [176].

4.6.2.1 Algorithm Formulation

The stochastic nature of the algorithm is implemented through the addition of randomly generated parameters in the calculation of the velocity vector. The next particle position is calculated based on this velocity. The optimisation iterations continue, either until a level of specified convergence is reached or the maximum number of iterations are completed.

Particles are defined with both position x and velocity v vectors, with lengths equivalent to the number of input variables. The position of each particle represents a single solution within the design space and accordingly this position is used to obtain the objective function value y. Each particle i retains the knowledge of its own best previous position in the space, known as the local best p^i, and the overall swarm best position, the global best p^g.

The local and global best solutions are subsequently used to update the velocity vector, to inform the motion of the particle to the next position. For k iterations and i number of particles, the velocity vector is calculated as follows:

$$v^i_{k+1} = wv^i_k + c_1 r_1 (p^i_k - x^i_k) + c_2 r_2 (p^g_k - x^i_k) \tag{4.16}$$

where w is an inertial vector, c_1 is the cognitive parameter and c_2 is the social parameter. The selection of the inertial, cognitive and social parameters affects the rate of convergence and quality of the final solution. Larger values for the social and cognitive parameters may cause the swarm to prematurely converge to known best solutions which may be local optima, where conversely a larger inertial vector results in larger particle velocities that encourage probing of the entire design space, but discourage convergence. The variables r_1 and r_2 are randomly generated numbers between 0 and 1. A maximum velocity parameter, $V_{\max}$, limits the value of particle velocity to avoid particles straying from the boundaries of the search space.

The velocity vector then updates the position of the swarm:

$$x^i_{k+1} = x^i_k + v^i_{k+1} \tag{4.17}$$

After each iteration, the retained global and local best solutions are compared to the new particle solutions and updated if the objective function is improved. The algorithm proceeds iteratively until the maximum number of generations, $\mathrm{n_{gen}}$, is reached, or until some prescribed measure of convergence between the particle solutions is reached. In this case, the swarm is said to be converged when difference between the maximum and

minimum solutions in the current generation of particles is below a minimum tolerance value, y_{tol}:

$$y_{\text{tol}} = y^{\max} - y^{\min} \tag{4.18}$$

As the entire algorithm consists of two simple equations, PSO has the advantage of being easy to implement, however, these advantages are obtained at the cost of higher computational inefficiency due to the rate of convergence when compared with gradient-based methods. There is also no explicit procedure for implementing constraints or ensuring solution feasibility, which are necessary to enforce for any practical engineering problem [177].

4.6.2.2 Constraint Handling

Evolutionary Algorithms (EA), including PSO, were initially developed to solve single objective, unconstrained problems and as such there is no standard method for directly handling constraints. Consequently, several methods have been adopted for the imposition of constraints in EAs and a review of these can be found in [175]; a more specific review pertaining only to PSO can be found in [178]. The approaches are sorted into three main categories: penalty functions, methods that preserve feasibility and methods that clearly distinguish feasible from infeasible solutions. These approaches are illustrated in Figure 4.9. Hybrid methods combining at least two of the approaches are also used. From these approaches, no single approach was identified for general application to all problems and instead *a posteriori* information about the behaviour of the problem or the design space was most useful in selecting an appropriate method. Reviewing the known features of this particular engineering problem, each approach can be evaluated for its suitability.

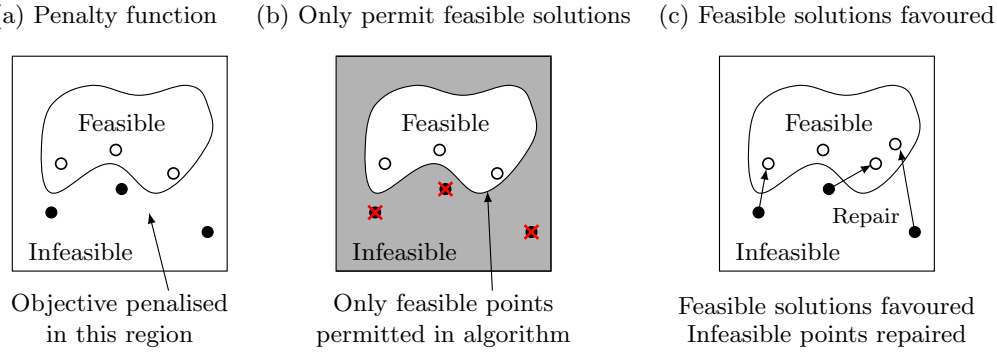

Figure 4.9: Constraint handling approaches for PSO.

Penalty functions, where a penalty value based on constraint evaluation is added to the fitness value, are simple to apply but can be difficult to condition. This difficulty is most apparent in optimisation problems with small and discontinuous feasible regions, as the algorithm struggles to find feasible points and the penalties inflate the fitness values for infeasible points causing the swarm to diverge or converge to a non-optimal solution [177]. Penalty functions are widely employed for constraint handling in evolutionary algorithms, but do not ensure the feasibility of solutions.

The approach of preserving feasibility involves both exclusively generating feasible solutions and restricting the search to only within the feasible regions of the design space. In contrast, the method of differentiating between feasible and infeasible solutions allows the generation of infeasible solutions, but favours feasible designs by insuring the best infeasible solution is always worse than the worst feasible solution. Infeasible solutions can be 'repaired' through repositioning the point back within the feasible region, using the position of the known feasible points [179]. This is achieved in an iterative process where the infeasible solution is repositioned, the constraints are assessed, and if found to still be infeasible, this is repeated. This can therefore decrease the computational efficiency of the PSO significantly, particularly if the feasible region is small or disjointed.

Due to the buckling mode switching behaviour known to occur in the design of stiffened panels and the discontinuous design space, it is difficult to satisfactorily force the feasibility of all particle positions in each algorithm iteration, or to fully realise the extents of the feasible design space in order to repair infeasible solutions. The mode switching behaviour is handled as with the gradient-based approach, where a sufficiently large range of half-wavelengths is analysed in order to encompass critical global, local skin and local stiffener buckling modes, and each returned buckling load related to each wavelength is assessed as a constraint. However, it is noted that if the particle population is initialised within the given bounds of the design space and satisfying all constraints, then feasibility is more likely to be maintained during the optimisation routine [180]. As the initialisation process can be conducted by generating and evaluating designs at random, the limits of the feasible design space with respect to all dimensions need not be known *a priori*.

Solution feasibility, with respect to both linear and non-linear constraints, is therefore implicitly enforced in a two step procedure as described by Hu and Eberhart [180]:

(i) All initial starting points are within the feasible region, and satisfy all the constraints. Successive cohorts of particles are generated randomly, then assessed against the constraints, those who meet the criteria are saved. This process is repeated until the number of feasible particles is equal to the specified number of particles in the swarm.

(ii) The best local and global positions are selected based on a better fitness value and if the particle strictly satisfies all constraints.

Initialising Start Points

Part (i), initialising the population with feasible particles, is highly inefficient when completely randomly generated. In order to expedite the process, the initial design lamination parameters representing each region ($\xi_{1,2}^{A,D}$) are explicitly calculated from evenly spaced sampling of discrete stacking sequence combinations with n number of plies, which guarantees feasibility with respect to all linear and non-linear lamination parameter constraints, as given in Eqs 4.13 and 4.14. The stacking sequences are generated using the four stan-

dard angle plies, creating symmetric and balanced laminate configurations, where the ±45° plies are assumed to occur as adjacent pairs to minimise ξ_3^D, which is assumed to be zero in the feasible region constraints. Fig. 4.10a illustrates the evenly spaced sampling of the in-plane lamination parameter region using $n = 1000$ ply laminate sequences, and associated out-of-plane lamination parameters are plotted in Fig. 4.10b. The sampling strategy ensures that start points are seeded from all regions of the lamination parameter space.

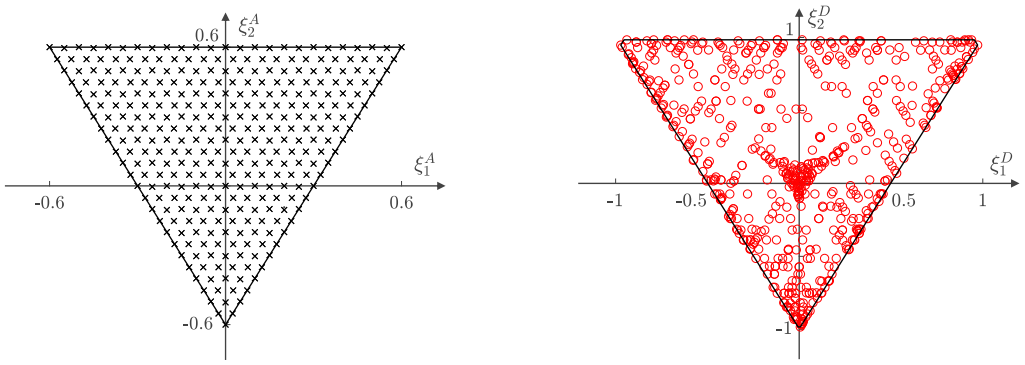

Figure 4.10: (a) In-plane lamination parameter generation, using $n = 1000$. (b) Out-of-plane lamination parameter generation, using $n = 1000$.

The feasible lamination parameter points $\xi_{1,2}^{A,D}$ are used to create random start points, assigned to the Outer and Inner skin regions, where the other variables are randomly generated between the specified lower and upper bounds. The start points are assessed against the buckling performance, strain and geometric constraints, and feasible start points are stored until the number of feasible points is equal to the size of the population.

Bound Handling

The range of values that each variable is allowed to assume is defined by the upper and lower bounds. These values can be arbitrary, or prescribed based on manufacturing restrictions, industrial design rules, or the limits of feasibility.

Lamination parameters, as through thickness integrals of the sine or cosine of each ply orientation, are bounded to lie between -1 and 1 (note all these are subsequently scaled to fit the 10% design rule lower and upper bounds, as described in Table 4.2). Although enforcing these bounds strictly limit the optimisation variables to the minimum and maximum feasible values, they still allow particles to assume infeasible positions in the lamination parameter design space as they ignore the interdependency between the parameters. For symmetric laminates composed of standard angles, two linear equations describe the outer boundary between the in-plane and the out-of-plane lamination parameters:

$$2\,|\,\xi_1^j| - \xi_2^j - 1 \leq 0 \qquad j = A, D \tag{4.19}$$

Eight other non-linear equations, presented previously as Eqs 4.14, link the in-plane and out-of-plane lamination parameter space. Together, these ten equations are usually implemented as constraints that are evaluated to assess the feasibility of the solution. In this methodology, the two linear equations in Eq 4.13 are implemented as bounds rather than 'constraints' in order to promote feasibility of particle solutions. As seen in Fig 4.11, although the upper and lower bounds are correctly applied, not all values within these limits are feasible in terms of laminate parameter space. The feasible space is reduced to half the size described by the bounds, which is a significant proportion of candidate solutions.

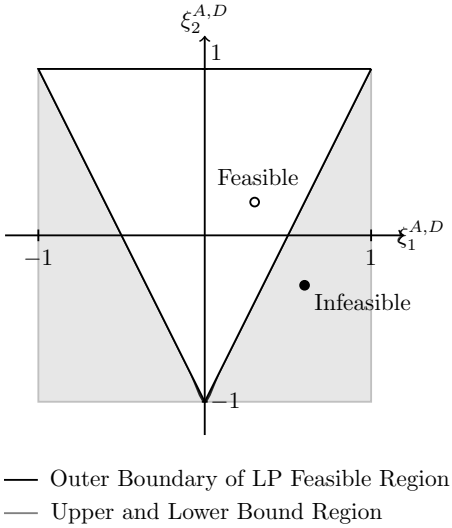

Figure 4.11: Lamination parameter in-plane, out-of-plane feasible regions, indicating the difference between the original bounds and the feasible region boundary.

Particles positioned in the infeasible region are set back on the closest boundary, in a direction perpendicular to the feasible perimeter. For those particles positioned in the infeasible region where this perpendicular rule is not applicable, these are set back on the nearest vertex of the feasible region. This method has the effect of accurately assessing solutions close to or on the boundary, which is suitable for the optimisation of DST structures, as the literature review indicated that optimised designs are generally $\pm 45°$ or $0°$ dominated and therefore positioned on the boundary. The velocity of the infeasible particles must also be updated, otherwise it is likely that the velocity on the next iteration will create the same motion to leave the feasible region. A review of bound handling techniques, critiquing methodologies for adjusting both position and velocity of particles in the infeasible region can be found in [181]. In this implementation, the velocities are reset to zero for repositioned particles, thereby absorbing the particles back into the lamination parameter feasible region, and allowing their next motion to be informed by the feasible positions of the local and global best only.

The upper and lower position bounds for all other variables are simply enforced by repositioning particles outside these on the nearest crossed boundary, and applies to all variables.

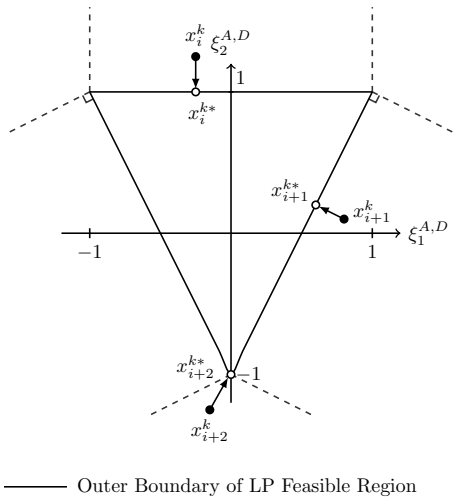

Figure 4.12: Bound handling in the in-plane lamination parameter space.

This is referred to as the Nearest method. So for each dimension d, the particle is set back on the boundary as follows:

$$\text{If } x_k^i > X^{i,max} \text{ then } x_{k+1}^i = X^{d,max}$$

$$\text{If } x_k^i < X_{i,min} \text{ then } x_{k+1}^i = X^{d,min}$$

Only the particles that violate the in-plane and out-of-plane lamination parameters bounds, as illustrated in Figs. 4.11 and 4.12, or the lower or upper bounds of the problem variables, as given in Table 4.1, are repositioned on the nearest boundary of the known feasible region. The performance and geometric constraints of all particles are then re-evaluated, and those that still violate any of the applied constraints are not allowed to be stored as best solutions/ positions but are retained for the next generation. This allows the particles to move through the infeasible design space but the motion is only influenced only by feasible best solutions. Infeasible points with respect to buckling loads are not repaired, as the extent of the feasible regions with respect to the performance constraints is not known, and implementing repair strategies further decrease the computational efficiency of the algorithm [179].

4.7 Algorithm Comparison: Gradient Based and PSO

The presented optimisation methodologies are applied to the case of a DST stiffened panel as illustrated in Fig. 4.1. The panels are designed using AS4-8552 CFRP, with the material properties E_{11}= 114.3 GPa (compressive modulus), E_{22}= 8.8 GPa, G_{12}= 4.9 GPa, ν_{12}= 0.314, ρ= 1580 kg/m^3, and a ply thickness of 0.196 mm [182]. Five different case study designs are used to test the algorithms, the variables used for each case are presented in Table 4.3. The stiffener spacings, design running loads and panel lengths are selected to be representative of designs found on a commercial mid-range aircraft wing. The design space is likely discontinuous in terms of feasible designs which affects the use of the gradient-

Table 4.3: Case study parameters

Case	N_x (kN/mm)	b_{sk} (mm)	L (m)
1	0.5	300	1
2	1	300	1
3	1	300	2
4	2	400	1
5	2	400	2

based solver, so ultimately running the gradient-based approach a repeated number of times from different, randomly selected, start points ensures that a global optimum is returned. For both optimisation algorithms, each panel example is therefore re-run ten times with alternative start points or randomly generated initial swarm positions.

Both optimisation algorithms are implemented using the fixed parameters in Table 4.4. The strain constraint is set at 4500 µstrain based on industrial limits for damage tolerance [183]. The stiffeners are assumed to have elastic properties equivalent to the industrial standard angle stacking sequence percentage ratio of 60%/30%/10% for 0°/45°/90° respectively [105]. The seam region width (b_{seam}) is fixed at 30 mm, re-using the width from the previous experimental study in Chapter 3. This width is conservative as shear stress is transferred with a distance three times the ply thickness, but it is still comparatively small when compared with minimum turning radii for curvilinear fibre designs. The inner radius of the stiffener foot is fixed at 5 mm, for formability.

Table 4.4: Fixed parameters for methodology comparison.

Parameter	Value
ϵ_{max} (µstrain)	4500
b_{seam} (mm)	30
r_{st} (mm)	5

The geometric variables are bounded between values deemed appropriate for the design problems in question, as given in Table 4.5, and lamination parameter bounds are as detailed previously in Table 4.2. The lower bound for the stiffener flange, b_{fl}, is set as 35 mm which is the minimum length that allows for bolted repairs.

Table 4.5: Variable upper and lower geometric bounds, t refers to bounds applied to each thickness variable.

	t	h_{st}	b_{fl}	b_{ext}
		(mm)		
Lower Bound	2	5	35	1
Upper Bound	15	60	70	100

The PSO algorithm parameters are listed in Table 4.6. Usual population sizes for PSO lie between 20 and 40 particles, with smaller population sizes preferred as it significantly lowers the computation time with respect to initialisation of the start points, as, even with the generated lamination parameter variables, not all candidate start points are feasible. However, as the design space is large and complex, a larger swarm size was selected to promote algorithm performance [184]. The inertial vector, cognitive and social parameters are set as used by Hu and Eberhert in [180], which were implemented to solve similar constrained non-linear optimisation problems. The inertial vector is implemented as a random dynamic parameter, which encourages searching of the full design space and avoids premature convergence.

Table 4.6: PSO algorithm implementation parameters. The inertial vector updates each k^{th} iteration, where r_k is a randomly generated number between 0 and 1.

PSO Parameters	
Population Size, n_{pop}	40
Number of Generations, n_{gen}	300
Convergence Tolerance, y_{tol}	0.05
Inertial Vector, w	$0.5 + (\text{r}_k/2)$
Cognitive Parameter, c_1	1.49445
Social Parameter, c_2	1.49445
Maximum Velocity, V_{max}	0.8

4.7.1 Algorithm Comparison Results & Discussion

The best results from the ten optimisation runs for each case study are presented in Table 4.7, comparing the results from the gradient-based and PSO algorithms, alongside the lowest buckling factor for each final optimum solution. Convergence plots for both algorithms for a single case study are presented in Figure 4.13. For each case study, measures of reliability, the number of feasible solutions from the total number of runs, robustness, the average final objective function value, and efficiency, the average number of function evaluations and iterations taken to obtain a solution, are presented in Table 4.8.

Table 4.7: Comparison of the best optimised solution from ten runs of each case study, for both algorithms.

	Mass	Outer Skin					Inner Skin					Stiffener				Lowest
Method	(kg)	ξ_1^A	ξ_2^A	ξ_1^D	ξ_2^D	$t_{\text{sk},1}$	ξ_1^A	ξ_2^A	ξ_1^D	ξ_2^D	$t_{\text{sk},2}$	b_{fl}	h_{st}	t_{st}	b_{ext}	F
Case 1: $N_x = \mathbf{0.5\,kN/mm}$, $b_{\mathbf{sk}} = \mathbf{300\,mm}$, $\mathbf{L = 1\,m}$																
G-B	2.32	0.4997	0.4835	0.5228	0.4767	5.4	-0.3433	0.0867	-0.1894	-0.6174	2.5	42.6	27	2.0	1	0.996
PSO	2.32	0.5974	0.5948	0.8377	0.9048	3.8	-0.6000	0.6000	-0.1636	0.0529	3.0	37.8	21.5	3.2	1	1.015
Case 2: $N_x = \mathbf{1\,kN/mm}$, $b_{\mathbf{k}} = \mathbf{300\,mm}$, $\mathbf{L = 1\,m}$																
G-B	3.01	0.5525	0.5950	0.7344	0.9259	6.2	-0.0711	-0.4578	-0.0105	-0.9747	3.2	35	23.1	4.1	1	1.004
PSO	3.02	0.6000	0.6000	0.1078	0.2932	4.7	0.0000	-0.6000	-0.0061	-0.9622	3.1	35.5	20	5.5	7	1.000
Case 3: $N_x = \mathbf{1\,kN/mm}$, $b_{\mathbf{sk}} = \mathbf{300\,mm}$, $\mathbf{L = 2\,m}$																
G-B	6.19	0.4468	0.3801	0.3488	0.1388	6.4	0.0000	-0.6000	-0.0090	-0.9781	3.4	36.2	53.9	2.8	1	0.995
PSO	6.60	0.1971	0.2091	-0.2058	0.5689	5.1	0.0000	-0.5999	-0.0356	-0.7704	3.0	36.1	46.6	4.4	20.1	1.003
Case 4: $N_x = \mathbf{2\,kN/mm}$, $b_{\mathbf{sk}} = \mathbf{400\,mm}$, $\mathbf{L = 1\,m}$																
G-B	7.20	0.5585	0.5966	0.7610	0.9328	10.3	0.3488	0.0975	0.1801	-0.5998	7.3	35	20.9	8.7	1	1.007
PSO	7.37	0.5979	0.5998	0.2286	0.0463	10.0	0.3854	0.1771	-0.0279	-0.3078	7.1	35.5	21.8	9.0	21.5	1.009
Case 5: $N_x = \mathbf{2\,kN/mm}$, $b_{\mathbf{sk}} = \mathbf{400\,mm}$, $\mathbf{L = 2\,m}$																
G-B	13.94	0.5363	0.5915	0.6654	0.9073	9.4	0.0838	-0.1770	0.0066	-0.9071	6.4	35	47.8	7.5	1	0.999
PSO	14.24	0.6000	0.6000	0.5363	0.1054	8.2	0.1085	-0.1803	0.0638	-0.4199	7.1	35	49.7	7.6	14.6	1.001

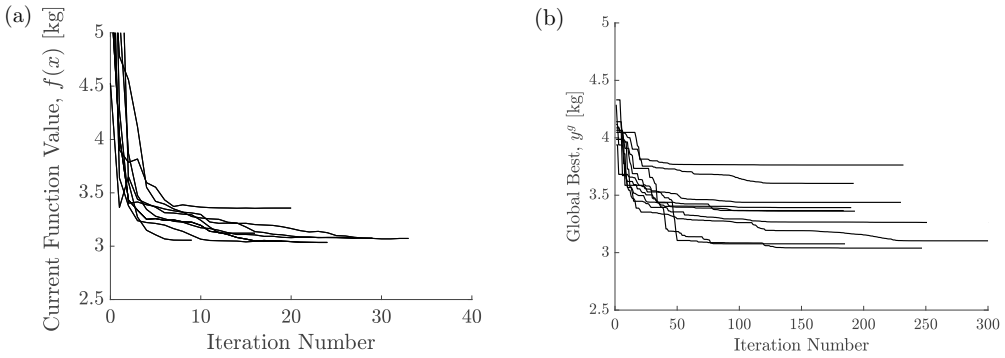

Figure 4.13: Comparison of (a) gradient-based vs (b) PSO algorithm convergence for ten runs, for case study 2: $N_x = 1\,\text{kN/mm}$, $b_{\text{sk}} = 300\,\text{mm}$, and L = 1 m.

Table 4.8: Reliability, robustness and efficiency comparison between the gradient-based (G-B) and PSO algorithms for ten runs.

	Feasible Solutions		Average Mass		Average Func Evals		Average Iterations	
Case	G-B	PSO	G-B	PSO	G-B	PSO	G-B	PSO
1	9	9	2.36	2.43	48	7 000	17	175
2	8	9	3.07	3.26	53	8 336	20	208
3	9	9	6.25	6.75	52	8 120	20	203
4	9	10	7.48	7.78	63	8 280	21	207
5	9	8	14.39	15.01	61	11 000	16	275

Ten runs, from randomly generated start points, were found to guarantee the return of the global optimum when using the gradient based approach. It can be seen from Fig. 4.13a that the global optimum mass was returned five out of ten runs. This is supported by the panel mass results reported in Tables 4.7 and 4.8, where the average masses returned from ten runs are very close to the global optimum values which indicates that the global optimum is returned multiple times.

The constraint and bound handling approach implemented in the particle swarm algorithm is observed to work effectively in limiting the designs to the feasible region, as reported in Table 4.7, and producing optimised designs where the critical buckling load factor is close to one. In particular, the bound handling technique for the lamination parameter feasible region is seen to allow the particles to appropriately explore the regions close to feasible boundary, as several optimum solutions lie on the bounds.

Comparing performance in Table 4.7, the gradient-based solver is able to return the lowest minimum mass solution for each of the case studies trialled. PSO returns similar solutions as the gradient-based approach for the studies with lower in-plane load, stiffener spacing and panel length, but struggles to find the global optimum when these parameters increase. As the lower and upper bounds for each variable are held constant for each case study, the feasible design space is reduced when the case study load parameters increase as laminate

thickness and the other geometric variables will increase to bear the load without buckling. The PSO algorithm enforces strict feasibility of initialised particles and stored solutions so, as the feasible design space between the bounds is reduced, the algorithm may struggle to search the space effectively.

Predictably, the gradient-based solver uses significantly fewer iterations and function evaluations than PSO, differing by two orders of magnitude. This disparity grows further as the function evaluations required to initialise random feasible particles are not included in the count in Table 4.8. The reliability of the two algorithms is similar for each case study, and no relationship between the case study parameters (i.e. load, stiffener spacing) and number of converged feasible solutions is observed. The average objective function value (mass of the panel) is always lower for the gradient-based approach than the PSO, and close to the optimum result as given in Table 4.7. From the comparison convergence plots for case study 2, in Figure 4.13, it can be observed that the gradient based approach converges rapidly to the same mass value. The PSO algorithm tends to find a 'best' solution within 50-100 iterations, but does not converge until approximately 200 iterations.

It is interesting to note that for case studies 1 and 2, the mass value returned is the same for both optimisers, but the distribution in mass across the regions of the stiffened panel are different. This is clear evidence of the presence of local optimal solutions. Despite the poor efficiency and lack of robustness of the PSO, it is able to locate alternative solutions, whereas the gradient-based approach tends to converge to the same design point repeatedly, as indicated by the average mass in Table 4.7. Ultimately, a gradient-based approach is appropriate for the efficient and accurate optimisation this problem, but the designer needs to recognise the presence of multiple local optima that still exist despite using lamination parameters to define the stiffnesses of the laminate regions. The designs will have to be re-run from different start points for each problem.

4.8 Stage II: Stacking Sequence Design

Stage II of the optimisation routine deals with finding discrete stacking sequences from the returned continuous lamination parameters and thicknesses describing the material properties of each laminate region. In previous work, the return of laminate stacking sequences from lamination parameters using of meta-heuristic solvers is common. Genetic algorithms compose the majority of the optimisation strategies used to return stacking sequences from continuous lamination parameters.

In Stage II of the optimisation, a Genetic Algorithm is used to find stacking sequences that best match the continuous optimal thickness and lamination parameters. In order to satisfy the performance constraints, the ply thicknesses are rounded up to to result in an integer number of plies, n_{ply}. The 'Outer' and 'Inner' stacking sequences are returned by separate GA runs, with no constraint to match with the stacking sequence in one region with that in the other. In Stage I, the lamination parameters and thicknesses of

the stepped seam are assumed to be linear variations between those of the 'Outer' and 'Inner' regions. In Stage II, the seam stacking sequences are obtained by targeting a linear variation in the returned ply stacking sequence percentages for the 'Inner' and 'Outer' regions, with some manual adjustment to ensure blended transition, achieved in three discrete steps, maintaining continuous plies across the width where possible.

4.8.1 Objective

The objective function is to minimise the Euclidean distance between the target lamination parameters (ξ_{opt}) and the calculated lamination parameters (ξ_{ga}) for the candidate stacking sequence, which is expressed following the example of Diaconu and Sekine [117]:

$$f(\boldsymbol{x}) = \sum_{i=1}^{4} w_i^A \, (\, \xi_{i,ga}^A - \xi_{i,opt}^A)^2 + \sum_{i=1}^{4} w_i^D \, (\, \xi_{i,ga}^D - \xi_{i,opt}^D)^2 \tag{4.20}$$

where $\boldsymbol{x}$ is a vector of design variables representing the ply orientations.

All eight in-plane and out-of-plane lamination parameters $\xi_{1-4}^{A,D}$, where $\xi_{3,4}^{A,D} = 0$ consistent with Stage I assumptions, are used in the calculation of the objective function to ensure extension-shear and bend-twist coupling characteristics are minimised. Weighting parameters (w^A, w^D) can be applied to prejudice the optimiser to better match specific lamination parameters than others. In this case, the in-plane parameters were targeted to a greater extent than the out-of-plane component of the stiffness variables. Two penalty terms, $g_{10\%}(\boldsymbol{x})$ and $g_{\text{contiguity}}(\boldsymbol{x})$, are added to the fitness function to account for the 10% rule and ply contiguity constraints.

4.8.2 10% Rule Constraint

The 10% rule has previously been enforced through the restriction of the lamination parameter feasible region. In general, this ensures that the genetic algorithm generated stacking sequences do not violate this rule. For thin laminates it is well known that matching lamination parameters with a small amount of discrete plies is difficult [124]. To ensure that the 10% rule, initially enforced in Stage I, is not subsequently violated to achieve a better match, a penalty function is applied in Stage II to maintain at least a 10% proportional of each ply angle. This function is expressed as:

$$g_{10\%}(\boldsymbol{x}) = \sum_{j=1}^{4} \Pi_j \begin{cases} \Pi_j = 1, & \text{when } n_j < 0.1\, n_{\text{ply}} \\ \Pi_j = 0, & \text{otherwise} \end{cases} \tag{4.21}$$

where n_j is the total number of plies with the j^{th} orientation and Π_j .

4.8.3 Stacking Sequence Rules

The following rules are applied to the stacking sequence design for the stiffened panel. Some are taken from Niu [67], and they have been supplemented with additional considerations due to the discrete tailoring across the width:

(i) Laminates are balanced and symmetrically stacked about the midplane, to prevent both warping of the laminate during cure and coupling of in-plane and out-of-plane elastic response.

(ii) $\pm 45°$ plies are positioned on the outer surface of the laminate for increased damage tolerance.

(iii) A maximum 4-ply contiguity is enforced to prevent high transverse stress gradients in the laminate and to avoid delaminations.

(iv) Plies on the bond-line between skin and stiffener are of the same orientation, and not in the principal direction (i.e. 0°) to ensure load is transferred through shear.

Symmetry is enforced by optimising half the stack, with the remaining plies mirroring these variables about the mid-plane. The outer plies are pre-assigned to $\pm 45°$ to satisfy constraints (ii) and (iv). A penalty function is employed to enforce the ply contiguity constraint as per [107, 122]:

$$g_{\text{contiguity}}(\boldsymbol{x}) = \Theta \tag{4.22}$$

where Θ is the total number of instances within the stacking sequence where more than four plies of the same orientation are stacked contiguously.

4.8.4 Stage II: Example Results & Discussion

The genetic algorithm is employed to return discrete stacking sequences for the optimal Stage I designs generated in Section 4.7. Each design is generated using a population of 40, 200 generations, a crossover probability of 0.7, and each generation retains 6 elite candidates. Weighting for the lamination parameters is set to give the same importance to the in and out-of-plane parameters; w_i^A, $w_i^D = 1$. Separate runs are required to return the stiffener, 'Outer' and 'Inner' skin stacking sequence designs.

The target (Stage I) and final (Stage II) lamination parameters for the panel skin regions, and the stacking sequences that correspond to these parameters, alongside final stiffener stacking sequences, are given in Table 4.9. Also presented in Table 4.9 are the geometric variables, lowest buckling factor and total panel masses generated at each stage of the optimisation routine. The stacking sequence rules established in Section 4.8.3 are adhered to through the use of constraints and problem formulation, as illustrated by the stacking sequence designs in Table 4.9.

The original Stage I optimisation assumes no extension-shear or bend-twist coupling, but coupling terms are present in some of the discrete stacking sequences. Balanced designs

are not always obtained as meeting the 10% rule constraint in prioritised, leading to designs with unequal numbers of $\pm 45^\circ$ plies. Symmetry is strictly enforced, eliminating $\mathbf{B}$ matrix terms. Overall, $\xi_3^{A,D}$ terms corresponding to the discrete designs are small, with returned values between ± 0.010, as the genetic algorithm targets designs that eliminate these terms. The final buckling and strain constraints are evaluated including the corresponding coupling behaviour, and although some reduction in final buckling factors is observed, this is minimal. Loss in performance can also be attributed to the difference between the stiffness properties of the closest matching discrete stacks and the continuous lamination parameters returned in Stage I.

Table 4.9: Comparison of target and solution lamination parameters, and corresponding discrete stacking sequence solutions, generated using the GA.

	Mass	Outer Skin					Inner Skin					Stiffener				Lowest
Method	(kg)	ξ_1^A	ξ_2^A	ξ_1^D	ξ_2^D	$t_{\text{sk},1}$	ξ_1^A	ξ_2^A	ξ_1^D	ξ_2^D	$t_{\text{sk},2}$	b_{fl}	h_{st}	t_{st}	b_{ext}	F
Case 1: N_x **= 0.5 kN/mm,** b_{sk} **= 300 mm, L = 1 m**																
Stage I	2.32	0.4997	0.4835	0.5228	0.4767	5.4	-0.3433	0.0867	-0.1894	-0.6174	2.5	42.6	27	2.0	1	0.996
Stage II	2.44	0.4286	0.4286	0.4346	0.3794	5.488	-0.2857	0.1429	-0.2157	-0.4869	2.744	43	27	2.156	1	0.9561
	Outer: $[\pm 45/0_3/90/0_4/45/0/90/\text{-}45]_S$ Inner: $[\pm 45/90/45/90/0/90]_S$ St: $[\mp 45/0/90/0/\overline{0}]_S$															
Case 2: N_x **= 1 kN/mm,** b_{sk} **= 300 mm, L = 1 m**																
Stage I	3.01	0.5525	0.5950	0.7344	0.9259	6.2	-0.0711	-0.4578	-0.0105	-0.9747	3.2	35	23.1	4.1	1	1.004
Stage II	3.14	0.3750	0.5000	0.3984	0.4568	6.272	-0.1111	-0.3333	0.0425	-0.8765	3.528	35	24	4.116	1	0.9327
	Outer: $[\pm 45/0_4/90/0_2/90/0_3/\pm 45/90]_S$ Inner: $[\pm 45/\mp 45/45/90/\text{-}45/0/90]_S$ St: $[\mp 45/0/90/0/45/0_2/90/0/\overline{45}]_S$															
Case 3: N_x **= 1 kN/mm,** b_{sk} **= 300 mm, L = 2 m**																
Stage I	6.19	0.4468	0.3801	0.3488	0.1388	6.4	0.0000	-0.6000	-0.0090	-0.9781	3.4	36.2	53.9	2.8	1	0.995
Stage II	6.27	0.4242	0.3333	0.4293	0.4293	6.468	0.0000	-0.5294	0.0147	-0.9495	3.528	37	54	2.94	1	0.9596
	Outer: $[\pm 45/0_2/45/90/0_4/\text{-}45/90/0_2/90/0/\overline{-45}]_S$ Inner: $[\pm 45/\mp 45_2/0/90/\text{-}\overline{45}]_S$ St: $[\mp 45/0_3/45/0/\overline{90}]_S$															
Case 4: N_x **= 2 kN/mm,** b_{sk} **= 400 mm, L = 1 m**																
Stage I	7.20	0.5585	0.5966	0.7610	0.9328	10.3	0.3488	0.0975	0.1801	-0.5998	7.3	35	20.9	8.7	1	1.007
Stage II	7.23	0.4151	0.5849	0.4309	0.5724	10.388	0.3514	0.1351	0.1926	-0.4988	7.448	35	21	8.82	1	0.9288
	Outer: $[\pm 45/0_4/90/0_3/90/0/90/0_2/45/0_4/90/0/\text{-}45/90/\text{-}45/0/\overline{-45}]_S$ Inner: $[\mp 45_3/0/45/0_4/90_2/0_3/\text{-}45/\overline{0}]_S$															
	St: $[(\mp 45/0)_3/45/0_4/90/0_2/\text{-}45/0_3/90/\overline{90}]_S$															
Case 5: N_x **= 2 kN/mm,** b_{sk} **= 400 mm, L = 2 m**																
Stage I	13.94	0.5363	0.5915	0.6654	0.9073	9.4	0.0838	-0.1770	0.0066	-0.9071	6.4	35	47.8	7.5	1	0.999
Stage II	14.27	0.4167	0.5000	0.3832	0.5020	9.408	0.0588	-0.1765	0.0588	-0.8018	6.86	35	48	7.644	1	0.9326
	Outer: $[\pm 45/0_2/90/0_4/0/45/0/90/0_4/\text{-}45_2/0_2/90_2/45/0]_S$ Inner: $[\mp 45_2/\pm 45/45/0/\text{-}45_2/45/90/0_3/90_2]_S$															
	St: $[\mp 45/\text{-}45/0/45/0_2/45/0/\text{-}45/0_2/45/0_2/(90/0)_2/\overline{0}]_S$															

4.9 Conclusions

- A two-level optimisation methodology has been implemented for the optimisation of discretely tailored stiffened panels. Buckling performance is assessed using the efficient Strip Model VIPASA, suitable for prismatic design of composite plate structures.
- Lamination parameters are used to describe the stiffness of each region in the first stage of the optimisation. Considering balanced, symmetric laminates, each region requires only four parameters and one thickness variable to describe the laminate stack. The feasible region for the lamination parameters considering the 10% rule (see Chapter 2) is simply constrained by scaling the bounds.
- A particle swarm optimisation is implemented to the solve the Stage I problem, and is compared to a gradient-based algorithm. The gradient-based approach outperformed the PSO in every respect, quality of solution, convergence rate, robustness and reliability. However, the existence of multiple local optima was confirmed.
- A convex design space is created using lamination parameters with respect to buckling of simple plates. However, for the minimum mass optimisation of composite stiffened panels, the feasible design space is discontinuous and non-convex with respect to the constraints. In order to obtain a global optima with an highly efficient gradient-based approach, the problem will have to be run multiple times with randomly generated start points.
- A genetic algorithm is implemented to return discrete stacking sequences from the continuous lamination parameters and geometric variables, subject to laminate design rules and the 10% minimum percentage constraint which are enforced through penalty constraints.

Chapter 5

Stiffened Panel: Analysis

5.1 Introduction

Using the optimisation methodology implemented in Chapter 4, a numerical study is conducted using a stiffened panel component. Several examples are optimised for minimum mass using the same loading and stiffener spacing, but present alternative optimised tailoring concepts for comparison. The principal panels discussed in detail are an optimised baseline case and a fully discretely tailored case, where Discrete Stiffness Tailoring is applied in the skin. The intent on generating these designs is not only to compare the analytical results for differences in performance and panel mass, but to experimentally test an optimised tailored design. To that end, the optimisation routine is adapted to account for additional practical manufacturing limitations, and the fully discrete tailored stiffened panel design was manufactured and tested to failure. The analytically and experimentally obtained buckling loads and modeshapes are compared, providing validation of the optimisation strategy.

5.2 Numerical Study

A T-stiffened panel of length L, illustrated in Figure 5.1, is selected as a suitable representative aircraft structure for the demonstration of DST. The panel carries a compressive uni-axial running load N_x, with clamped transverse (loading) edges and free longitudinal edge boundary conditions. All panel cases have a fixed stiffener spacing (b_{sk}) of 300 mm, and the industrial standard angle stacking sequence percentage ratio, 60%/30%/10% for $0°/\pm45°/90°$ respectively [105], predetermines the elastic properties of the stiffeners for Stage I. Stiffness and/or thickness tailoring is applied to the panel skin, which is divided into an 'Outer' region, to which the stiffener is bonded, and an 'Inner' region, the length of skin between the stiffeners. The laminate properties are varied between each region over a seam distance, b_{seam}.

The established optimisation methodology is applied to five distinct T-stiffened panel cases as presented in Fig. 5.2: an optimised baseline, an industrial baseline, tapered constant stiffness, DST tapered panel and DST constant stiffness panel. The industrial baseline case utilises the industrial skin ply angle ratio of 44%/44%/12%, and as such, this example best approximates a current commercial standard design for comparative purposes,

whereas the baseline optimum design represents the best, minimum-mass, solution if the constant stiffness properties of the skin are allowed to vary. Previous work in [1] established that allowing for both laminate stiffness and thickness variation across the width of a compression panel, a 40% reduction in mass can be achieved compared to a constant stiffness design. Hence, three tailored designs, Fig 5.2c-e, investigate the mass reduction that can be attributed to the independent variation of the laminate thickness or stiffness properties, and the reduction when both variables are allowed to optimise together in a single skin panel design. The design variables for each panel type are collated in Table 5.1.

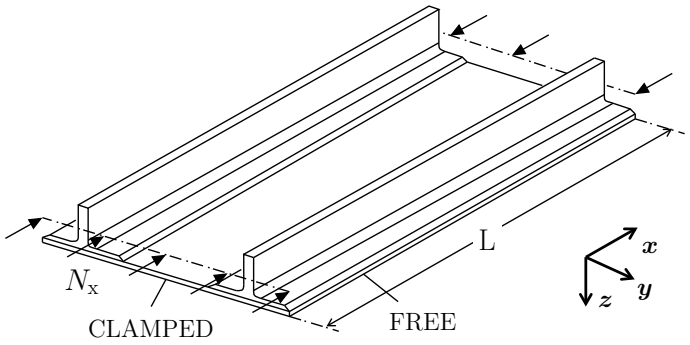

Figure 5.1: Isometric view of the stiffened panel geometry, indicating boundary conditions and loading.

Table 5.1: Table of design variables to be optimised for each panel type. Variables relating to the stiffener geometry apply to all cases.

Panel Type	Skin	Stiffener
(a) Baseline Optimum	$(\xi_{1,2}^{A,D})_{\text{sk}}$, t_{sk}	
(b) Baseline Industrial	t_{sk}	
(c) Tapered Skin Constant Stiffness	$(\xi_{1,2}^{A,D})_{\text{sk}}$, $t_{\text{sk},1}$, $t_{\text{sk},2}$, b_{ext}	t_{st}, h_{st}, b_{fl}
(d) DST	Outer: $(\xi_{1,2}^{A,D})_{\text{sk},1}$, $t_{\text{sk},1}$, b_{ext}	
	Inner: $(\xi_{1,2}^{A,D})_{\text{sk},2}$, $t_{\text{sk},2}$	
(e) DST Constant Thickness	t_{sk}, Outer: $(\xi_{1,2}^{A,D})_{\text{sk},1}$, b_{ext}	
	Inner: $(\xi_{1,2}^{A,D})_{\text{sk},2}$	

The first stage of the optimisation routine is applied to the panels defined using the fixed parameters in Table 5.2. The design compressive load per unit width of 1 kN/mm is selected to represent the loading experienced near the tip of a wing on a standard narrow bodied aircraft and the maximum strain allowable is set at 4500 µstrain based on industrial limits for damage tolerance [183]. As this numerical study is performed with the objective of manufacturing and testing the DST design case, the original 1 m length is shortened to include a 25 mm length of potted resin on each loading edge ensuring creation of a clamped boundary condition.

For the DST panels, the seam region width (b_{seam}) is fixed at 30 mm, this is selected to

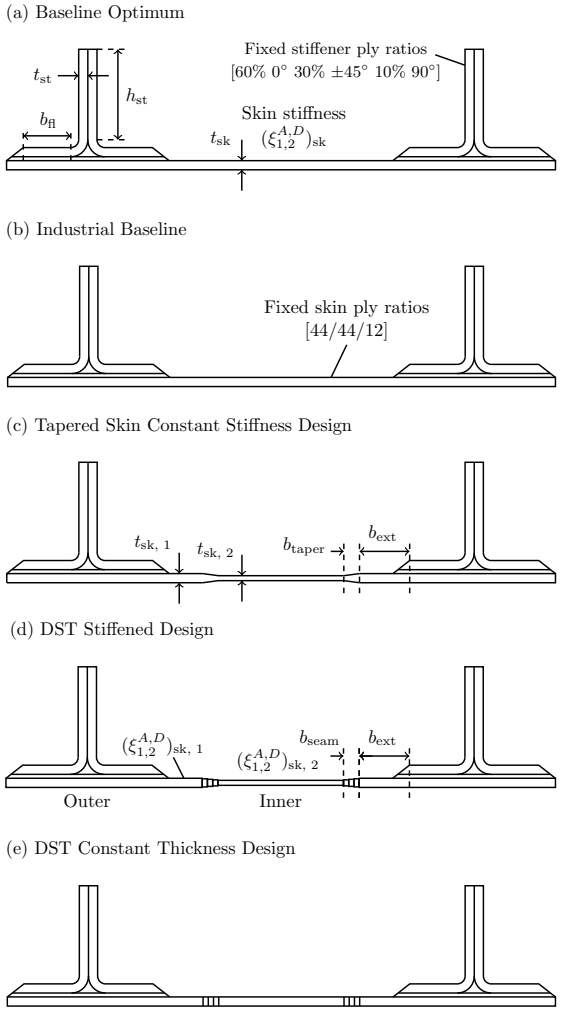

Figure 5.2: Cross-sections of the a) baseline optimum, b) industrial baseline, c) tapered skin constant stiffness design, d) DST fully optimised, and e) DST constant skin thickness panel cases.

be arbitrarily large as the transfer of load due to shear stress requires a relatively small overlap. The tapered, constant stiffness skin panel design uses the same width for the taper (b_{taper}), for consistency. The geometric optimisation variables are bound by minimum and maximum ranges as given in Table 5.3. The lamination parameter bounds, describe the ultimate limits for the feasible region. The thickness bounds are applied consistently to the appropriate variables. Structural width bounds are arbitrarily selected to envelope a reasonable design space, excepting the stiffener flange width lower bound (b_{fl}), as this is the minimum length that allows for bolted repairs.

The panels are optimised using the material properties of AS4-8552 CFRP, E_{11}= 114.3 GPa (compressive modulus), E_{22}= 8.8 GPa, G_{12}= 4.9 GPa, ν_{12}= 0.314, ρ= 1580 kg/m^3 [182]. For the second stage GA, a ply thickness of 0.196 mm is used to create the discrete stacks. The DST stiffened optimum, Fig. 5.2d, was manufactured with the same material.

Table 5.2: Fixed parameters: Numerical study

Parameter	Value
N_x, kN/mm	1
$\epsilon_{\max}$, µstrain	4500
b_{sk}, mm	300
b_{seam}/ b_{taper}, mm	30
r_{st}, mm	5
L, mm	1

Table 5.3: Variable upper and lower geometric bounds.

	t	h_{st}	b_{fl}	b_{ext}
		(mm)		
Lower Bound	2	5	35	1
Upper Bound	10	60	70	100

An amendment to the general optimisation methodology is necessary to account for available tooling for the creation of the radii of the stiffener block. After the initial Stage I results, the returned continuous stiffener thickness is rounded up to the nearest whole millimetre. The whole millimetre restriction is imposed by commercially available tooling required for manufacturing the stiffener radii mould. This new stiffener thickness and the original stiffener lamination parameters are submitted to a genetic algorithm (as per Stage II), from which a full stacking sequence is obtained. The calculated lamination parameters from the retrieved stack are then resubmitted as fixed to the gradient based optimiser, from which new skin and structural width optimum results are obtained. Whilst the whole millimetre constraint increases the final panel mass, as this is consistently applied to all panel cases, it can be assumed that all cases are penalised equally and are still comparable. All runs of the Stage II GA uses a population of 40, 200 generations, a crossover probability of 0.7, and each generation retains 6 elite candidates. Weighting for the lamination parameters is selected to give greater importance to the in-plane parameters; $w_i^A = 1.5$ and $w_i^D = 1$.

5.3 Numerical Results

The optimum designs obtained at each stage of the optimisation routine are presented in Table 5.4, and the final discrete stacking sequence designs are detailed in Table 5.5. As the objective function to be minimised is the mass of a single stiffener bay, the mass of a single bay section is presented for comparison, and the percentage difference between the optimised baseline case (Type a) and the implemented tailoring concept (Types b - e) is given in brackets. Reasonable agreement between the lamination parameters obtained at the first and second stages was generally achieved, see Table 5.4, with the exception of the

in-plane parameters for the baseline stiffener design, and the tapered constant stiffness skin design, as the small discrete number of plies in this case limit the procurement of a suitable matching candidate. To achieve a blended design between the 'Inner' and 'Outer' skin region for the discretely tailored cases, a linear variation in the standard angle ply percentages and thicknesses was assumed. In practice, the linear variation between inner and outer regions functions well, as the stiffness is gradually varied across a structure to avoid stress concentrations around ply drop-offs, and the 10% rule is easily maintained across the seam. In order to allow a more gradual transition of total laminate stiffness and thickness, unbalanced laminate configurations were permitted for Seam 2 and 3 for the DST cases, listed in Table 5.5.

Table 5.4: Thicknesses, lamination parameters and structural widths for the optimum stiffened panel designs returned at the two stages of the optimisation routine.

Panel Type	Stage	Panel Part	t	In-Plane		Out-Of-Plane		h_{st}	b_{fl}	b_{ext}
			(mm)	ξ_1^A	ξ_2^A	ξ_1^D	ξ_2^D	(mm)	(mm)	(mm)
(a)	I	St. flange	1.7	0.5000	0.4000	0.3050	-0.3140	35	44.9	-
		Skin	6.2	0.2318	-0.1281	-0.0129	-0.9073			
	II	St. flange	2.156	0.2727	0.2727	0.2186	-0.4846	35	45	-
		Skin	6.272	0.2500	0.000	0.0537	-0.7500			
(b)	I	St. flange	1.7	0.5000	0.4000	0.3050	-0.3140	35	57.1	-
		Skin	6.5	0.3200	0.1200	0.3150	-0.3300			
	II	St. flange	2.156	0.2727	0.2727	0.2186	-0.4846	35	58	-
		Skin	6.664	0.2941	0.0588	0.2697	-0.4053			
(c)	I	St. flange	6.4	0.5000	0.4000	0.3050	-0.3140	35	20.9	1
		Inner skin	5.1	0.1758	-0.2484	0.0854	-0.7892			
		Outer skin	2.1	0.1758	-0.2484	0.0854	-0.7892			
	II	St. flange	7.056	0.4444	0.3333	0.3121	-0.3086	35	20	1
		Inner skin	5.096	0.0769	-0.2308	0.0469	-0.8261			
		Outer skin	2.352	0.0000	-0.3333	-0.0278	-0.9259			
(d)	I	St. flange	4.2	0.5000	0.4000	0.3050	-0.3140	35	20.8	1
		Inner skin	3.1	-0.0004	-0.5920	0.0187	-0.8461			
		Outer skin	6.1	0.5778	0.5947	0.8481	0.9223			
	II	St. flange	4.9	0.4400	0.3600	0.3202	-0.2605	35	21	1
		Inner skin	3.136	0.0000	-0.5000	0.006	-0.9840			
		Outer skin	5.88	0.4667	0.4667	0.4927	0.2865			
(e)	I	St. flange	6.5	0.5000	0.4000	0.3050	-0.3140	35	18.1	1
		Inner skin	3.5	0.0190	-0.5620	-0.0090	-0.9780			
		Outer skin	3.5	0.5725	0.5941	0.8246	0.9207			
	II	St. flange	7.056	0.4444	0.3333	0.3121	-0.3086	35	19	1
		Inner skin	3.528	0.0000	-0.5556	-0.0247	-0.9451			
		Outer skin	3.528	0.5556	0.5666	0.4184	-0.0590			

Table 5.5: Optimal final stacking sequence solutions for each panel type, with the respective standard angle percentages given for each layup. The final structural widths for each type and mass for a single stiffener bay are also presented.

Panel Type	Stacking Sequence - No. of Plies 0°/±45°/90° (%)	h_{st} (mm)	b_{fl} (mm)	b_{ext} (mm)	Mass (kg)
(a)	St. flange $[\pm 45/0_2/90/\overline{0}]_S$ - 11 plies	50	35	-	3.61
	46/36/18				
	Skin $[\mp 45_3/\pm 45/0/90/0_3/90/0_2]_S$ - 32 plies				
	37.5/50/12.5				
(b)	St. flange $[\pm 45/0_2/90/\overline{0}]_S$ - 11 plies	50	35	-	3.89
	46/36/18				(+7.8%)
	Skin $[\mp 45/0/\mp 45/0/\pm 45/0/\mp 45/0/90/0_2/90/0]_S$ - 34 plies				
	41/47/12				
(c)	St. flange $[\pm 45/0_2/90/\overline{0}]_S$ - 11 plies	50	35	1	3.47
	46/36/18				(-3.9%)
	Inner Skin $[\mp 45/\pm 45/\mp 45/0/\pm 45/(90/0)_2]_S$ - 26 plies				
	23/62/15				
	Outer Skin $[\mp 45/\pm 45/90/0]_S$ - 12 plies				
	17/66/17				
(d)	St. flange $[\pm 45/0/\mp 45/0_3/90/0_3/\overline{90}]_S$ - 25 plies	21	35	1	3.09
	56/32/12				(-14.4%)
	Inner skin $[\mp 45/\pm 45/\mp 45/0/90]_S$ - 16 plies				
	12.5/75/12.5				
	Seam 1 $[\mp 45/0/\pm 45/0/\mp 45/0/90]_S$ - 20 plies				
	30/60/10				
	Seam 2 $[\mp 45/0_2/+45/90/0_2/\mp 45/0/\overline{90}]_S$ - 23 plies				
	43.5/43.5/13				
	Seam 3 $[\mp 45/0_3/+45/90/0_3/\mp 45/0/\overline{90}]_S$ - 27 plies				
	52/37/11				
	Outer skin $[\mp 45/0_4/90/0_4/90/\mp 45/0]_S$- 30 plies				
	60/27/13				
(e)	St. flange $[\mp 45/\mp 45/0_2/\pm 45/0_4/90/0_3/90/0]_S$ - 34 plies	19	35	1	3.21
	56/33/11				(-11.1%)
	Inner skin $[\mp 45/\pm 45_2/90/\text{-}45/0_2/45/90/\mp 45_2/\pm 45]$ - 18 plies				
	11/78/11				
	Seam 1 $[\mp 45/0/\mp 45/0/90/\text{-}45/0_2/45/90/0/\pm 45/0/\pm 45]$				
	33/56/11 18 plies				
	Seam 2 $[\mp 45/0_2/45/0/90/\text{-}45/0_2/45/90/0_2/\text{-}45/0/\pm 45]$ - 18 plies				
	44.5/44.5/11				
	Seam 3 $[\mp 45/0_4/90/\text{-}45/0_2/45/90/0_4/\pm 45]$ - 18 plies				
	56/33/11				
	Outer skin $[\mp 45/0_4/90/0_2]_S$ - 18 plies				
	67/22/11				

The VIPASA buckling analysis is performed for N = 30 modes, taking half-wavelength lengths of $\lambda = \ell$, $\ell/2$, ..., $\ell/30$, where $\ell = L/2$ is the effective panel length. The resulting modeshape plots for each half-wavelength are returned, indicating if the mode occurs locally in the skin or stiffener web, or globally, alongside the buckling load factors for each case. The buckling factors, applied load and critical buckling strain for the designs are presented in Table 5.6. The final panel designs for concepts (a) and (d) are illustrated in Fig. 5.3.

Table 5.6: Theoretical VIPASA critical buckling factors (F_i) and strain values (ϵ_x) for the final discrete optimised designs.

Panel Type	Applied Load, P_x	Buckling Factors			Critical Buckling
	(kN)	Global	Skin	Stiffener	Strain ϵ_x (µstrain)
(a) Baseline	411.9	-	1.006	1.578	2177
(b) Ind. Baseline	424.9	-	1.002	1.089	1953
(c) Taper	496.4	1.116	1.109	-	2717
(d) DST	516.8	0.999	0.971	-	2310
(e) DST Const. t	523.9	0.999	0.998	-	2369

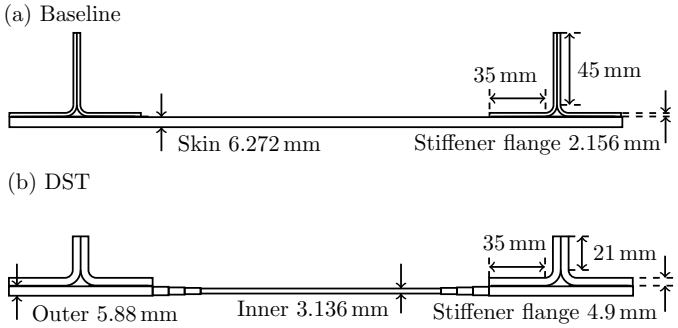

Figure 5.3: Cross-section comparison of the (a) Baseline and (b) DST optimum Stage II discrete designs.

5.4 Discussion

Comparing different tailoring strategies, it is found that when both stiffness and thickness are allowed to vary simultaneously, a 14.4% reduction in mass can be achieved compared to an optimised baseline case, which improves to 20.5% when compared to thickness optimised baseline panel that uses industrial ply percentages. Variation in stiffness across the skin width procures a far greater reduction in mass than simply varying the thickness, 11.1% compared to 3.9% respectively. The scale of the mass reduction achieved applying stiffness tailoring to a stiffened panel is less than half that of a discretely steered compression plate, theoretically estimated at 40% [1]. Considering that a stiffened panel is already an efficient structural arrangement for bearing compressive load, it is logical to assume the effect of stiffness tailoring would be less significant than for a simple panel.

The achievable mass reduction for both the all panel types is limited by the lower bound

for bolted repairs as the $b_{\text{fl}} = 35\,\text{mm}$ minimum is reached at all stages of the optimisation routine, the results of which are given in Tables 5.4 and 5.5. For the tapered constant stiffness and DST design, the constraint which limits the difference in thickness between the 'Inner' and 'Outer' regions was active, which suggests that a more significant mass saving could be achieved if there was some relaxation of the industrial taper constraints. The extension of the 'Outer' skin beyond the stiffener flange (b_{ext}) also returned the lower bound, resulting in an immediate transition beyond the edge of the stiffener foot, illustrated in Fig 5.3b. This result suggests that a rapid transition from the outer to inner skin design is ideal which is a distinct advantage of the discrete tailoring technique over continuous fibre steering.

Focusing on the baseline and DST results, concepts (a) and (d) respectively, cross-sections of the final panel designs are illustrated in Fig. 5.3 which shows the significant difference in the distribution of mass and stiffness between each panel type. The discrete stiffness tailoring redirects the stiffness, and therefore load, in the panel through the stiffener and the 'Outer' skin region, which is composed of the largest possible proportion of 0° plies allowed by the 10% rule. The 'Inner' skin region conversely is created of the maximum proportion of ±45° plies with little laminate thickness, as needed only for buckling resistance in the free skin region. In contrast, the optimum baseline skin design ply percentages are typical of the aerospace industrial skin ratio of 44%/44%/12% which bear the significant majority of the compressive load, while the stiffener contributes a small amount of stiffness to the panel, but significant resistance to a global mode due to an increased second moment of area. The 10% rule indirectly maintains some fully continuous plies across the width of the skin panel that provide some seam strength, despite inhibiting the feasible lamination parameter space for the DST skin design.

A local skin buckle is the critical buckling mode for both the baseline and DST optimised panel designs, which are listed for all panel types in Table 5.6. Due to the poor matching between the continuous lamination parameters and discrete stacking sequences for the tapered constant stiffness design, the buckling factors and critical strain values are excessive and no longer optimal. Reviewing the modeshape plots for the specified half-wavelengths, the DST case exhibits both global and skin buckling, whereas the baseline case buckles in skin and stiffener local modes. The baseline panel is too stiff and its second moment of area too large to result in global buckling at the given panel length, and the stiffener buckling occurs at 150% of the design load, exhibiting a large amount of redundancy and excess mass in the baseline design. In contrast, the reserve for the global and skin modes in the DST case are both close to one, and stiffener buckling is made impossible by the stiffener thickness and stubby web height of the DST design. By tailoring the skin to increase the buckling capacity of the panel, the stiffener height can be greatly reduced as the contribution of the web to the second moment of area is no longer needed. With the application of DST, stiffener sizes can be potentially reduced, alongside a possible increase in the stiffener spacing. No panel design returned a critical buckling strain close to the

maximum strain allowable imposed, given in Table 5.6, as the applied loading and fixed stiffener spacing in this numerical case do not generate high strains.

5.5 Conclusions

In this chapter, the novel concept of Discrete Stiffness Tailoring was presented as a means by which the optimal distribution of laminate stiffness and thickness can be achieved in order to realise easily manufacturable lower weight aerospace structures. Using the optimisation methodology developed previously, five different design concepts were investigated for a single load and stiffener spacing case study, representative of an aerospace upper wing cover.

- A 14.4% reduction in mass is obtained compared to a baseline constant stiffened case for a specific design loading, when the tailoring philosophy is applied to the panel skin, and stiffness and thickness are allowed to vary simultaneously. Tailoring redistributes the load to the stiffener region, resulting in more efficient use of material.
- Tailoring only stiffness across the width results in approximately three times the percentage mass saving than tapering the laminate thickness alone. The greatest material efficiency is obtained when both stiffness and thickness are allowed to optimise simultaneously.
- The optimised transition between the 'Outer' region, underneath the stiffener bondline, and the 'Inner' free skin region is shown to occur immediately beneath the stiffener flange tip. This immediate transition is facilitated by DST.
- Discrete Stiffness Tailoring is not constrained by a minimum fibre turning radius, which tend to be on the order of hundred of millimetres, and therefore a sharp transition in stiffness properties can be effected.
- For discretely stiffened panels, the global and local buckling modes occur almost concurrently, as would be expected as the efficiency of the material is increased, although no stiffener mode is active as the stiffener height is too short for this particular load case.

Chapter 6

Stiffened Panel: Experimental Validation

6.1 Introduction

The optimised DST stiffened panel design, with thickness variation, from the numerical study in Chapter 5 is manufactured and experimentally tested, in order to validate the optimisation methodology implemented in Chapter 4. The manufacturing process and testing methdology are described. The critical buckling load and strain, and buckling modeshapes are compared to VIPASA and FE analysis.

The FE analysis included in this Chapter is the combined work of C. Scarth and T. Maierhofer, as presented in [185].

6.2 Manufacturing

This section details the manufacture of the optimised DST panel (optimised skin stiffness and thickness) from the previous numerical study and the testing process for the panel.

Skin and stiffeners were formed and cured separately, then secondary bonded together using Redux liquid shim from Hexcel. The stiffeners were laid up using a custom aluminium mould and the stiffener noodles formed from rolled 0° prepreg, in line with current industrial practice [186]. The noodle region is indicated in Fig. 4.4. The skin panel was laid up on a steel plate which creates a flat surface to which the stiffeners are attached, and a stepped surface on the opposite side, as per Fig. 6.1. This skin manufacturing procedure creates a cross-sectional geometry different to that modelled in the optimisation method and causes the position of the laminate neutral axis to vary across the width. The effect of the neutral axis change as a subsequence of the manufacturing method was found to have a negligible impact on the buckling behaviour of the panel, as the two models were created and compared in VIPASA prior to the experimental test. It is noted that in this laboratory-scale test, the inner surface was manufactured as flat to facilitate bonding of the stiffeners to this surface. In reality, a flat outer skin surface is necessary for optimal aerodynamic performance, but is not considered in this work. It is emphasised that the same optimisation methodology could be applied to a panel with flat outer surface.

The transition of the stacking sequence from 'Outer' to 'Inner' skin region is detailed in Figure 6.2. Continuous ±45° plies are maintained across the width of the structure. Some asymmetrical stacking sequences are present in the seam region, but these regions

are very small in comparison to the full panel width, and no warping was seen post-cure. Once the stiffeners were bonded, however, the finished panel skin was observed to have a small amount of positive out-of-plane curvature away from the stiffeners, measured at approximately 1 mm in amplitude over 600 mm of panel length and was therefore assumed to have developed during the secondary bonding process. The imperfection was measured using a Digital Image Correlation (DIC) system, which is discussed in greater depth later within this Section. The integrity of the bondline between the stiffener foot and skin panel was analysed using an ultrasonic scan (C-scan) pre-test, and no defects were observed.

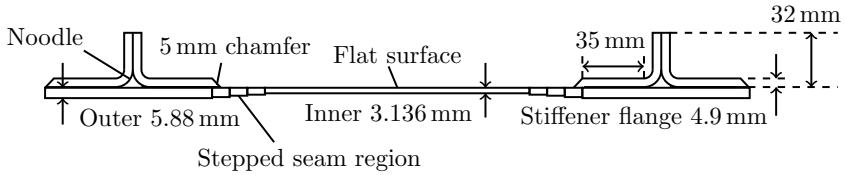

Figure 6.1: Manufactured panel cross-section geometry, illustrating the flat and stepped skin panel sides.

Table 6.1: Stacking sequences and geometry for experimental DST panel, detailing the stepped seam transition from 'Outer' to 'Inner' skin regions.

Panel	Stacking Sequence - No. of Plies	h_{st}	b_{fl}	b_{ext}
Type	0°/±45°/90° (%)	(mm)	(mm)	(mm)
DST	St. flange $[\pm 45/0/\mp 45/0_3/90/0_3/\overline{90}]_S$ - 25 plies	21	35	1
	56/32/12			
	Inner skin $[\mp 45/\pm 45/\mp 45/0/90]_S$ - 16 plies			
	12.5/75/12.5			
	Seam 1 $[\mp 45/0/\pm 45/0/\mp 45/0/90]_S$ - 20 plies			
	30/60/10			
	Seam 2 $[\mp 45/0_2/+45/90/0_2/\mp 45/0/\overline{90}]_S$ - 23 plies			
	43.5/43.5/13			
	Seam 3 $[\mp 45/0_3/+45/90/0_3/\mp 45/0/90/2]_S$ - 27 plies			
	52/37/11			
	Outer skin $[\mp 45/0_4/90/0_4/90/\mp 45/0]_S$- 30 plies			
	60/27/13			

The final stiffener height (base to web top, including capping plies) was trimmed to 32 (+0.1) mm, the panel lengths and loading edges were machined to parallelism tolerances of 0.1 mm and 0.05 mm respectively, as suggested by Compression-After-Impact (CAI) composite standard test method ASTM D7137 [163] which is appropriated in the absence of a specific procedure. The fully manufactured panel was then potted in resin 25 mm deep at both loading edges, to avoid end brooming failure. The resin blocks were manufactured using a blend of Araldite 2011 A/ 2011 B/ HV997-1, 100:45:45 parts by weight. Although the creation of a clamped end condition is aided by these blocks, the true experimental boundary condition is indeterminate. As the strut-like global buckling

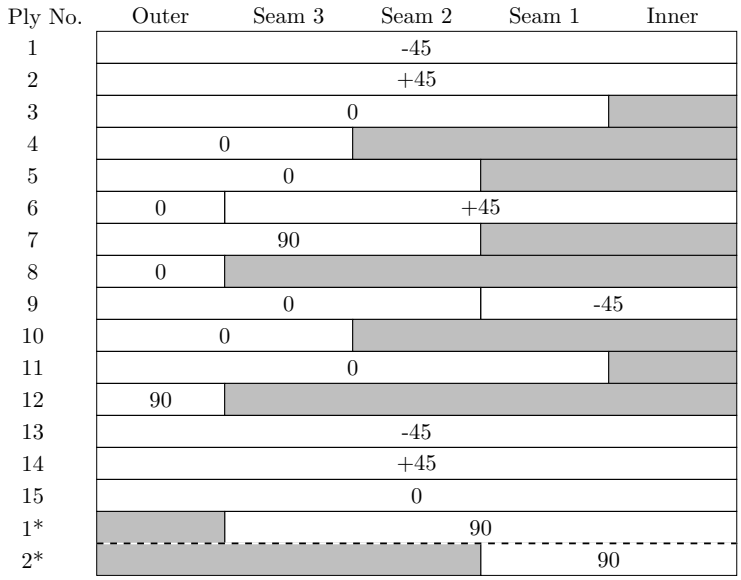

Figure 6.2: Stacking sequence transition detail. The dashed line denotes the midplane of the stack and plies 1-15 are mirrored around this, noting the two central plies are asymmetrically added.

factor for the DST case approaches one at the original design length L = 1000mm, in order to avoid this mode arising due to the uncertain end conditions, the experimental test panel length was shortened to 850 mm. The test panel length, accounting for the resin blocks, is therefore 800 mm. VIPASA results for a shortened panel length are also presented in Table 6.2. The buckling reserve factor for the L/2 half-wavelength is increased by 30% by shortening the panel length by 200 mm, however, the increase is not as significant as approximations using the Euler (strut) buckling equation would suggest (+50%). The effect of the length change on the global modes is illustrated in Fig. 6.3. The original (strut-like) global mode returned when $\lambda = L/2$ is no longer equivalent to the mode with $\lambda = L/2$ for the shorter panel which is dominated by plate-like buckling of the skin between stiffeners. The strut-like mode for the shorter panel will occur at a higher eigenvalue, and hence the results are not directly comparable. It is important to note that the post-buckling capacity is also artificially increased by shortening the panel.

Table 6.2: Theoretical VIPASA critical buckling factors (F_i) and strain values (ϵ_x) for the final DST design for alternative panel lengths. *Note that buckling for $\lambda = L/2$ changes to a skin-dominated plate mode as a result of the panel shortening.

Panel Type	Applied Load P_x (kN)	Panel Length, L (mm)	Buckling Factors Global* ($\lambda = L/2$)	Skin ($\lambda = L/6$)	Stiffener	Critical Buckling Strain ϵ_x (µstrain)
DST	516.8	1000	0.999 (strut)	0.971	-	2310
		800	1.296 (plate)	0.965	-	2296

A speckle pattern was created on the front and back faces of the skin panel using a combination of a stencil and random permanent marker dots, pictured in Fig. 6.4. An

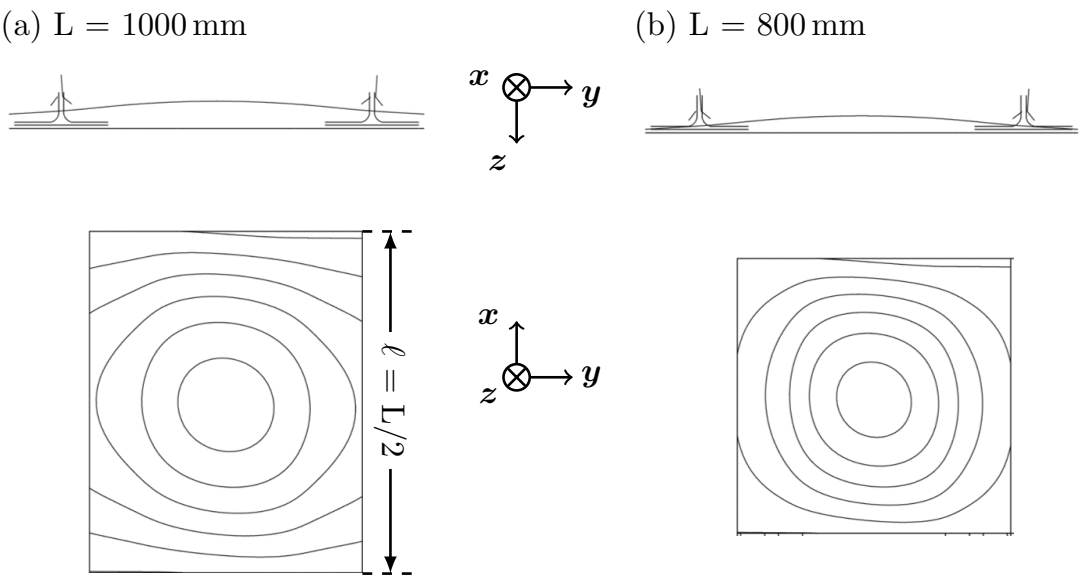

Figure 6.3: Effect of reducing the panel length, L, on the global buckling mode-shape.

annotated front view of the panel is presented in Fig. 6.5, indicating the resin potting and the stiffener webs. The tops of the stiffener webs were deliberately left white in order to accentuate the development of any delaminations within the web stack. Two pairs of low-speed stereo cameras were used for Digital Image Correlation (DIC) of the buckling modeshapes and surface strains. A pair of high speed DIC cameras were also used to capture the instantaneous failure of the panel.

Figure 6.4: DIC speckle pattern.

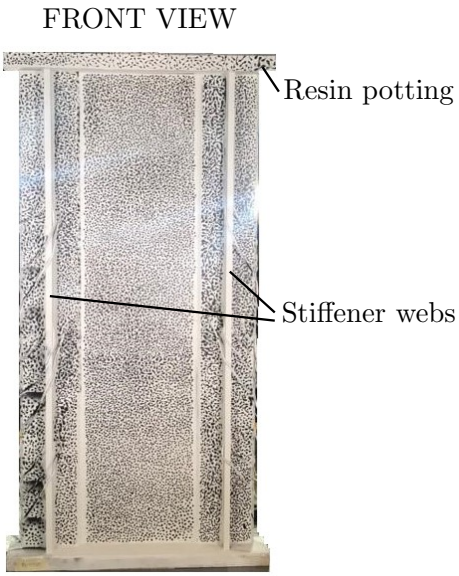

Figure 6.5: Annotated front view of stiffened panel.

Thirteen pairs of strain gauges were employed to accurately determine the onset and development of buckling. These are particularly useful for monitoring the stiffeners as

these are not captured by DIC. A strain gauge map is supplied in Figure 6.6f. The gauges attached to the stiffener blade are placed approximately 3 mm from the free edge. The strain gauges were also used to shim and correct the cross-head to ensure uniform loading across the panel. A 25 mm thick machined steel plate was placed in-between the potted end and shims, in order to evenly spread the distribution of load over the panel width.

A Dartec 2000 kN testing machine under displacement control was used to perform the tests. Initial tests were run to 110% of the predicted buckling load at a displacement rate of 0.4 mm/min, and then a final test was conducted to failure.

6.3 Finite Element Analysis

Finite element analysis is conducted to provide validation of the optimised DST panel buckling load obtained using VIPASA, and for comparison with experimental results. A linear eigenvalue buckling analysis using a subspace solver is performed using the commercial software ABAQUS. The skin and stiffener are modelled using four-node general purpose shell elements (S4R) with three integration points within each ply, as these account for transverse shear which is likely to be influential due to laminate thicknesses considered [105]. The element size is in the region of 5 mm to guarantee the convergence of the first five modes to three significant figures. The stiffeners are attached to the skin using tie constraints to simulate bonding. A second FE model is created to include the noodle region illustrated in Fig. 4.4. The noodle is modelled using six-node 3D wedge elements (C3D6), the elements are assigned the homogeneous properties of 0° unidirectional plies and tie-constraints are used to attach the noodle surfaces to the inner shell surfaces of the stiffener and the capping plies.

Replicating the experimental potted end conditions, the panel is restrained from displacement and rotation in all axes at one end, and all degrees of freedom except longitudinal displacements in the y-axis are restrained on the loading edge as labelled in Fig. 4.4. Secondary tensile strains in the x-direction are therefore induced which results in a more conservative model than VIPASA, where no transverse loads are applied. The panel transverse edges are unconstrained. The load is applied as a uniform end shortening.

6.4 Results & Discussion

Plots of strain against compressive load, measured using the strain gauges, are shown in Fig. 6.6. Out-of-plane displacement plots obtained from DIC, illustrating the development of experimental modeshapes are presented in Fig 6.7. Analytical 2D buckling modeshapes determined using VIPASA and finite element analysis, along with an experimentally obtained modeshape are shown in Fig. 6.8. Cross-sectional plots of buckling modes, obtained from experimental DIC data are shown in Fig. 6.9. Cross-section buckling modeshape plots, comparing the experimentally obtained critical mode as presented in Fig. 6.8, and the analytically obtained

Due to the pre-existing skin panel geometric imperfection, slight deviation of the upper strain gauges (15 & 22) on the 'Inner' skin region was observed from a load of 50 kN in Fig. 6.6d, indicating bending of the inner skin region, which is also recorded in the DIC z-displacement plots, Fig. 6.7a. The increased bending is restrained by the support of the stiffeners in the opposing direction, and the skin buckling is suppressed, before occurring at approximately 479 kN. Two experimental buckling modes are identified from the DIC analysis: a critical skin mode which developed initially, and a global mode which develops before the failure of the panel, presented in Fig 6.7c & f respectively. The onset of experimental buckling at 479 kN is evaluated from a change in gradient of the averaged 'Inner' skin gauges, given in Fig. 6.6a. From the averaged strain gauge results in Fig. 6.6 it can be seen that despite the onset of local skin buckling, there is no significant loss in the overall panel stiffness, not until a higher load where global mode is present and well developed. At a load of 536 kN, the experimental modeshape is composed of 4 full sinusoidal waves, confined to the 'Inner' skin region as observed in Figs. 6.8c & d. The centre of the panel developed a local modeshape as out-of-plane bending was already present due to the influence of the geometric imperfection, this is more clearly seen in the cross-section plot in Fig. 6.9. The analytically obtained modeshapes are highly comparable to each other as the shape is confined to the local buckling of the 'Inner' skin between the stiffeners, and both are composed of three full sine-waves down the length of the panel.

Analytical, FEA and experimental critical buckling loads, strains and the recorded overall axial stiffness of the panel are presented in Table 6.3. Comparing the stiffnesses, the FEA result is 8% more conservative than that obtained using VIPASA. This discrepancy is due to the difference in the applied boundary conditions, as transverse strains are induced in the FE analysis, promoting buckling at a lower load. The experimental buckling load of 479 kN is bounded by the VIPASA and FE results with differences of +3.8% and -4.8% respectively, which may be accounted for by geometric differences between the models and the actual manufactured design, the boundary conditions and premature experimental buckling due to the initial imperfection. Good agreement between the VIPASA and experimental results provides validation of the optimisation methodology which allows this approach to be applied to a study of stiffened panel designs, varying the stiffener spacing and compressive running loads, or to alternative structures.

A homogenised axial stiffness, obtained using Eq. (4.9) from Chapter 4 and a smeared panel thickness, were used to calculate a stiffness of 70.4 GPa for the VIPASA model and FEA returns a similar but lower stiffness value of 69.5 GPa, as presented in Table 6.3. An experimental stiffness of 73.2 GPa was obtained from the initial gradient of the averaged skin panel strain gauges. Minor features, such as the noodle and the stiffener flange chamfer, exist in reality but were not initially modelled and contribute to the increased stiffness of the experimental panel. The noodle volume was estimated from the stiffener radius using equations from [186], and modelling this additional material increased the axial stiffness in both the VIPASA and FEA models by 1.5%, decreasing the discrepancies be-

tween the stiffnesses returned by the analytical models and experimental test. This minor stiffness increase nevertheless increases the predicted buckling loads by 4.4%, eliminating discrepancy between the FEA prediction and fully developed experimental buckling load. Including the noodle, however, increases the difference between the experimental and VIPASA results. The differences between the experimental, FE and VIPASA buckling loads is a consequence of three factors: the experimental buckling load is lowered due to the imperfection, the VIPASA analysis does not account for induced transverse strains, so the predicted load is higher, and the experimental longitudinal boundary condition is indeterminate, realistically between simply-supported and clamped conditions, which also lowers the experimental load in comparison to the analytical and numerical results.

Post the initial local skin mode, a global mode developed at approximately 536 kN which was determined through the distinct and significant divergence of the 'Inner' skin strain gauges (17 & 24) presented in Fig. 6.6d. The gradients of the lines before and after divergence are extrapolated, and the buckling load is taken from the point at which these intersect. The initiation of the global mode is also coincident with a discontinuous jump recorded at 542 kN in all strain gauges. The switch between modes is recorded in the DIC z-displacement plots captured at 536, 539 and 542 kN in Figs. 6.7c-e, as the local skin wavelengths are now integrated in a larger central buckle. Cross-sections in Fig. 6.9b show displacement across the width also suggesting a shift to a global mode after 542 kN. The strain gauges on the stiffener web presented in Fig 6.6b indicate that the stiffeners never buckle locally as predicted by the numerical study, but the stiffener webs mid-length are placed under significant compressive strain from the development of the large mid-length buckle due to the global mode.

Following global buckling, the panel was loaded until failure which occurred at a compressive load of 630 kN, 24% higher than the skin buckling load. Images from the high-speed cameras capturing the experimental panel failure are presented in Fig 6.11. Post-buckling, the compressive strain recorded by the mid-length stiffener web gauges (3 & 4 in Fig. 6.6b) increased significantly to approximately 6750 µstrain, and this consequently led to the compressive material failure of the left-hand stiffener web, as indicated in Fig. 6.11a. Crumpling of the left-hand stiffener resulted in fragmentation of the potted resin ends as labelled in Fig. 6.11a and the failure of the secondary bond between both stiffeners and the buckled skin panel, Figs. 6.11b & 6.11c. Post-test examination of both the de-bonded right-hand stiffener and skin panel found no clear outward signs of damage. However, it is impossible to establish the benefit of stiffness tailoring on post-buckling capacity as this is improved through shortening the panel length L to 800 mm. It is noted that the transverse seam regions were able to carry the design load and a significant amount of post-buckling load to failure, for which the panel was not designed, without accruing visible damage. This underlines the potential benefit of DST despite the potential weakness of the transverse discontinuities.

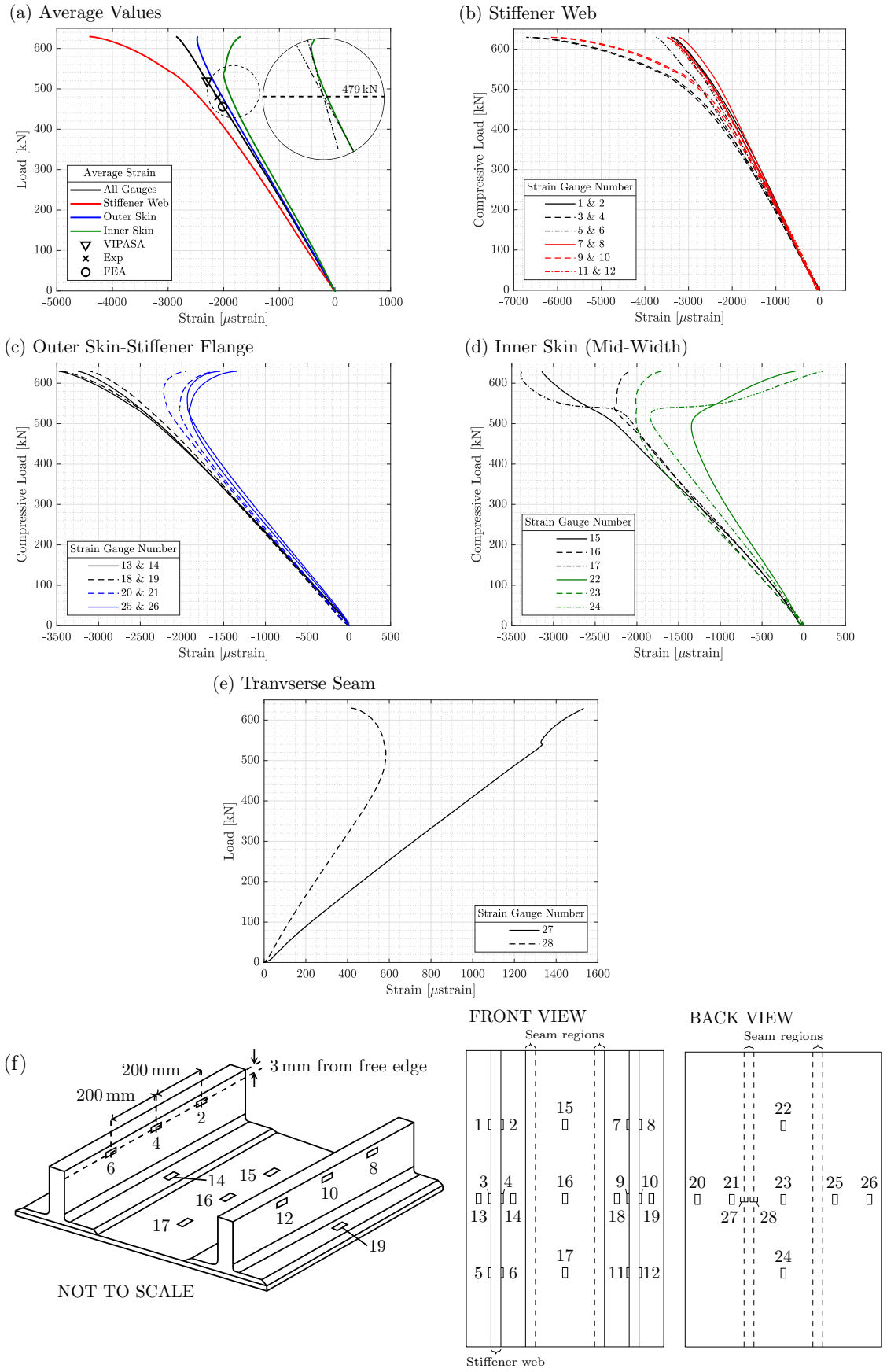

Figure 6.6: Compressive load vs strain. The strain gauge numbers in the legends correspond to the positions labelled on the strain gauge map in (f).

(a) Skin bending

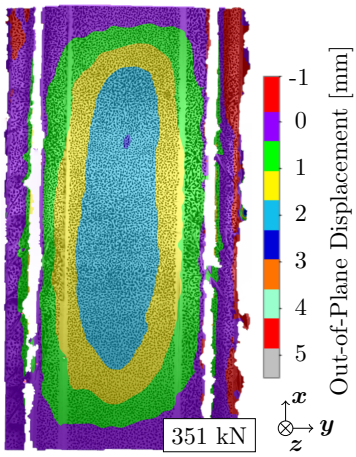

(b) Initial skin buckling mode

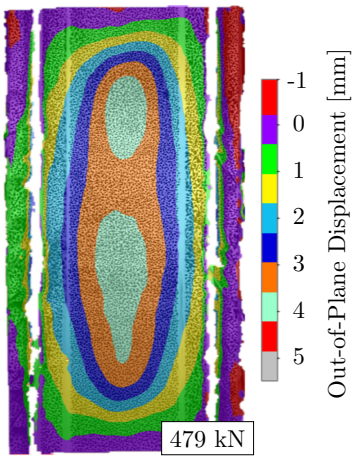

(c) Fully developed skin buckle

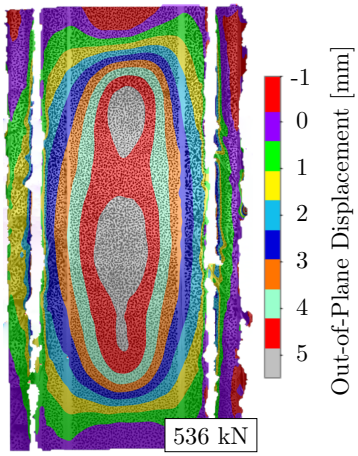

(d) Mid-modeshape switch

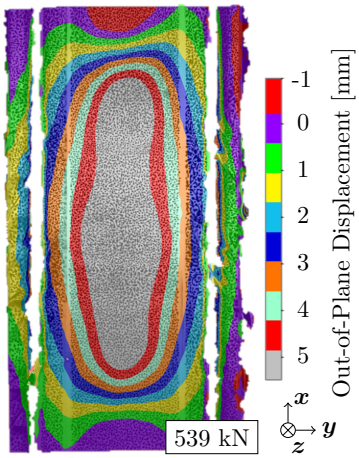

(e) Euler mode

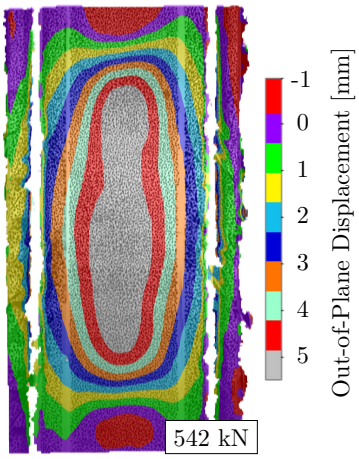

(f) Pre-failure

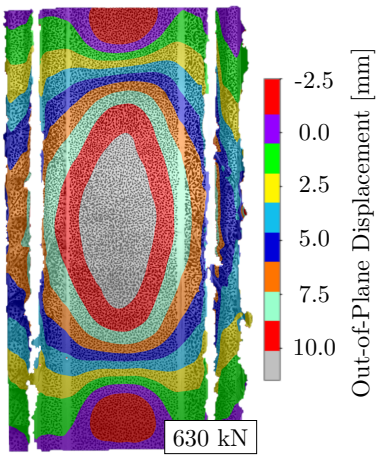

Figure 6.7: Out-of-plane displacements from the experimental test. Note that the sub-figure (f) has a different legend as the out-of-plane displacements are significantly larger.

(a) VIPASA: 498 kN

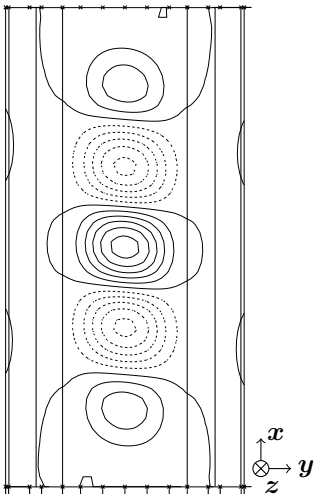

(b) FE Analysis: 456 kN

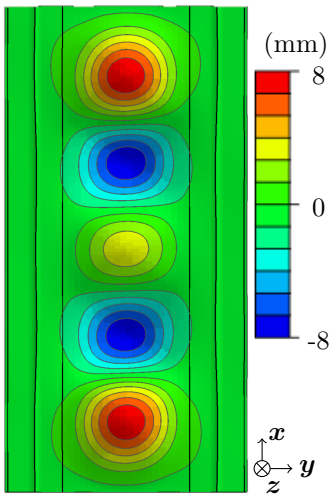

(c) Exp. Front Side: 536 kN

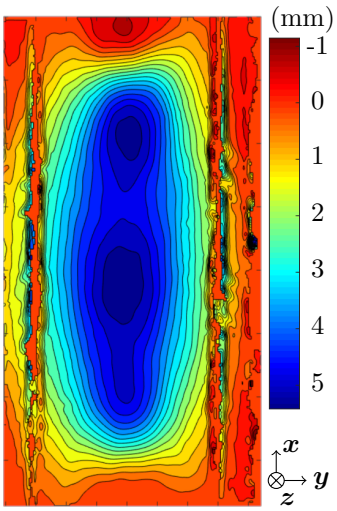

(d) Exp. Back Side: 536 kN

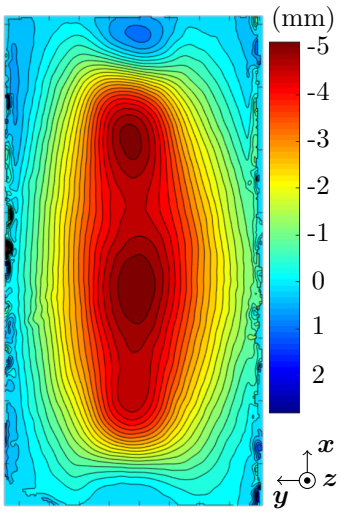

Figure 6.8: Comparison of 2D analytical and experimental buckling mode-shapes. For (c) and (d) red denotes negative z-displacement and blue represents positive z-displacement, consistent with labelled axes.

Table 6.3: Comparison of experimental and analytical results for the DST stiffened panel design with a length of 800 mm and clamped boundary conditions. Updated results including the stiffener noodle are also presented.

	Exp.	VIPASA	FEA	VIPASA + Noodle	FEA + Noodle
Buckling load (kN)	479	498 (+3.8%)	456 (-4.8%)	520 (+7.9%)	479 (-)
Buckling strain (µstrain)	2113	2296	2008	2300	2019
E_{xx} (GPa)	73.2	69.3	69.5	70.4	70.8

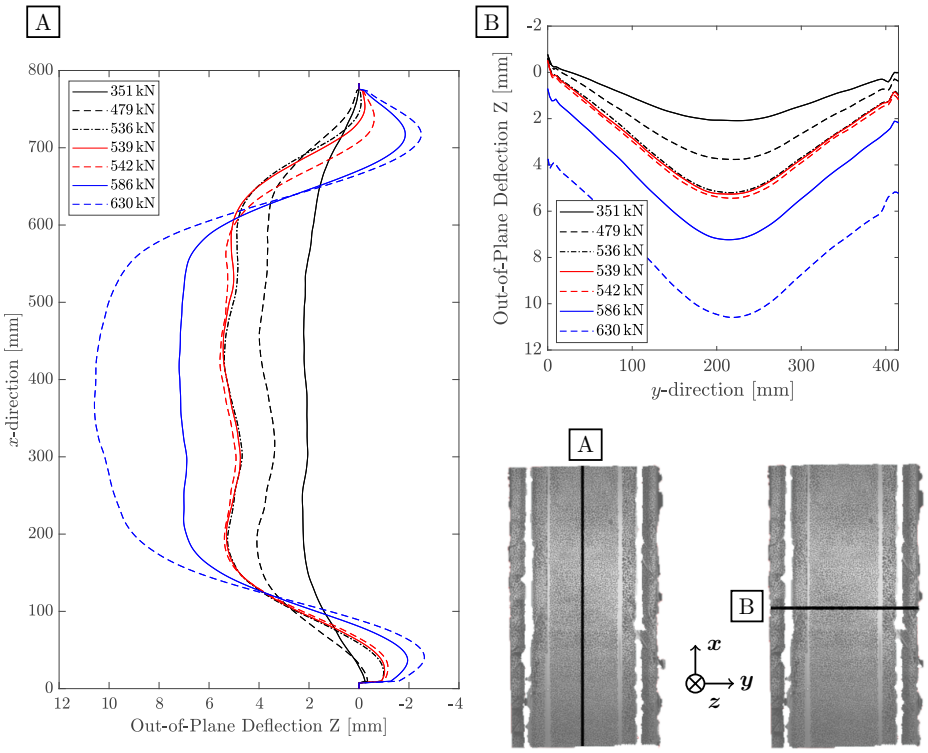

Figure 6.9: Out-of-plane displacement (Z) cross-section plots, showing development of the local skin and global modeshape with increased load. **A** is sampled from the xz plane, and **B** from the yz plane, and the position of the respective cutting planes are indicated on the panel diagrams.

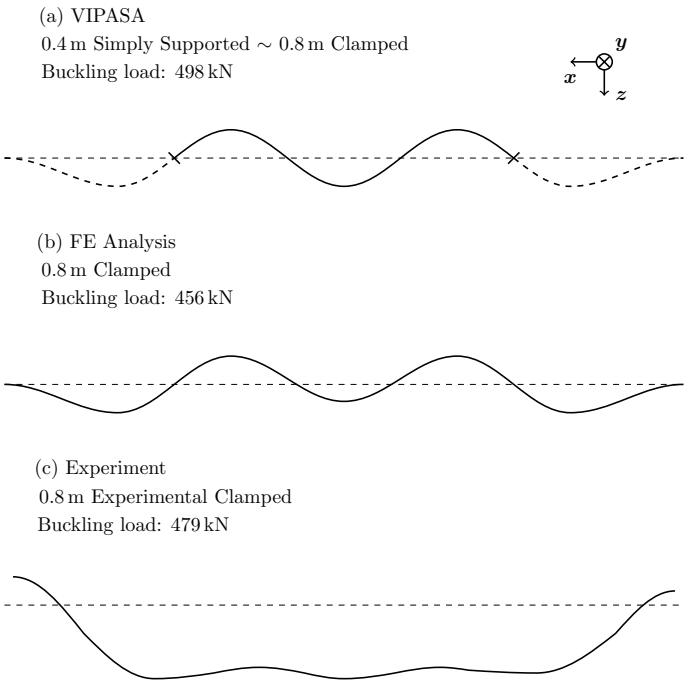

Figure 6.10: Cross-section mid-width buckling modeshape plots in xz plane for the analytical (a) VIPASA, (b) FEA and (c) experimental results.

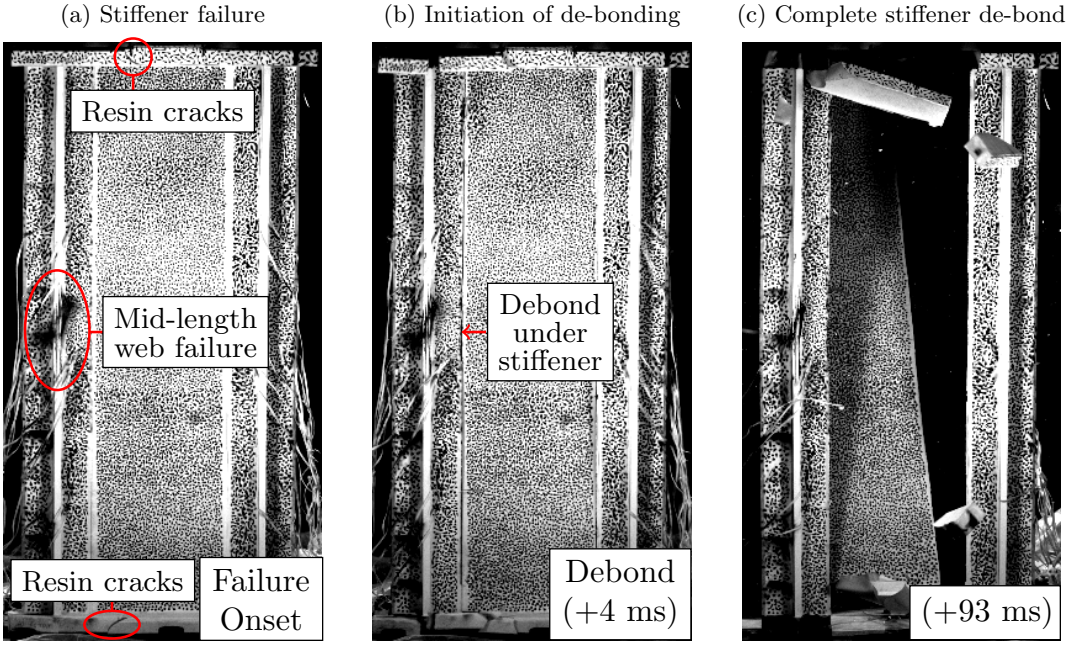

Figure 6.11: High-speed camera images of the panel failure at 630 kN. The initial failure of the left-hand mid length stiffener web is indicated, along with the cracking in the top and bottom resin potted ends.

6.5 Conclusion

A discretely stiffness tailored panel, optimised for minimum mass in the previous Chapter, was manufactured and tested in order to validate the implemented two-stage optimisation methodology, and to demonstrate the novel tailoring concept experimentally for a representative aircraft structure for the first time.

- The optimised DST buckling load, obtained using the VIPASA model, was within 4% of that obtained experimentally. Good agreement between the analytical and experimental critical skin buckling modes was observed, although the experimental result was affected by a manufactured imperfection in the skin panel.
- Including the stiffener noodle in the analytical models increased the buckling load by 4.4%, despite only increasing the overall axial stiffness by 1.5%. Industrial practise excludes modelling the load bearing contribution of the noodle, but this work demonstrates the conservatism of this approach.
- Panel failure occurred at a load 24% greater than the skin buckling load, however as the panel length was shortened from the optimised design, the post-buckling capacity is increased. This, however, suggests some potential for optimising for post-buckling behaviour using DST.
- Failure was a result of material failure in the stiffener web. The seams within the tailored skin panel exhibited no sign of damage, despite the weak resin regions between the discontinuous plies, thus providing greater confidence in the transverse

strength of a seamed region.

Chapter 7

Study: Infinitely Wide Panels

7.1 Introduction

In the previous Chapter, the established optimisation routine was validated by the design and test of a minimum-mass stiffened panel with Discrete Stiffness Tailoring. In this Chapter, the optimisation routine implemented in Chapter 4 is used to conduct a parametric numerical study of infinitely wide stiffened panels, where the panel length, stiffener bay width and in-plane compressive loading are varied, where the magnitude of in-plane loading is selected to simulate forces experienced across a single aircraft span. The VIPASA model is updated such that, instead of longitudinal free edges, the stiffener bay now has periodic boundary conditions that allow for the development of transverse buckling modeshapes, better replicating a realistic composite structure. The optimisation methodology is also amended to allow for the selection of Non-Standard Angles (NSAs), and to implement blending methodology between the discrete regions, ensuring maximum continuity of plies and preserving transverse structural integrity.

7.2 Optimisation Methodology Adaptation

The original optimisation methodology, implemented in Chapter 4 for the design of a minimum-mass T-stiffened compression panel, is performed in two stages. The first stage is a gradient-based lamination parameter optimisation, restricted to standard angle designs (0°, ±45°, 90°). The stiffened panel is composed of a single skin, and two stiffeners attached at either longitudinal edge, and hence the VIPASA model for the assessment of the critical buckling load is based on free longitudinal and clamped transverse boundary conditions. The second stage is comprised of a standard genetic algorithm that returns discrete stacking sequences. Blending of the stacking sequences between the discrete skin regions is not implemented as a constraint in either stage, and manual manipulation of the stacking sequences is necessary to achieve a manufacturable design and to maintain maximum continuity of plies across the width. From the initial experimental work conducted in Chapter 3, transverse strength and integrity is preserved through the presence of continuous plies, and therefore it is critical to consider a blending constraint when designing discrete stiffened structures.

The literature review found that previous work by Bloomfield [123] proved a greater mass

saving is obtained for panels, constrained by minimum buckling requirements, formed of non-standard angle fibre orientations, compared to strictly selecting from the tradition standard angle set. NSA designs also better facilitate the manufacture of defect-free parts than traditional angle plies [147, 187].

The aim of this numerical study is to now:

(i) Quantify the average percentage mass reduction due to stiffness tailoring compared to a baseline optimum design. The mass reduction illustrates the suitability of discrete stiffness tailoring for the different design cases, where the load, panel length and the stiffener spacing are varied.

(ii) Investigate the effect of allowing the selection of non-standard angle designs on the reduction in mass attained by the DST designs.

(iii) Implement a blending constraint to maximise the number of continuous plies shared between adjacent regions, and to quantify the continuity present in each design.

In order to achieve the aims listed above, the major amendments to the optimisation methodology are as follows:

(i) The VIPASA stiffened panel model is updated so that the longitudinal edges are subjected to periodic boundary conditions, which replicate the conditions for a stiffened panel on an aircraft wing.

(ii) The equations that enforce the lamination parameter feasible regions and constraints are updated to include the exclusively non-standard angle regions.

(iii) The process to return a discrete stacking sequence is now completed in two steps, instead of a single, standard, genetic algorithm. The returned in-plane lamination parameters and continuous laminate thicknesses are used to analytically determine the ply angles, and the proportion of each angle that compose the discretely tailored skin laminate. Hence, a discrete number of plies of each orientation is returned, matching the optimal in-plane stiffness. The solutions are submitted to a permutation genetic algorithm, which optimises the ply order to match the out-of-plane optimum lamination parameters, subject to blending and stacking sequence rule constraints.

The two optimisation routines from Chapter 4 and the current Chapter are illustrated in Fig. 7.1 for comparison. Each Stage will be discussed in greater detail in the subsequent sections.

7.3 Stage I: Gradient Based

The objective function is to minimise the mass of a single stiffener bay. Each design case is run ten times, with randomly generated start points, with the gradient-based optimiser *fmincon*, ensuring the global optimum is found.

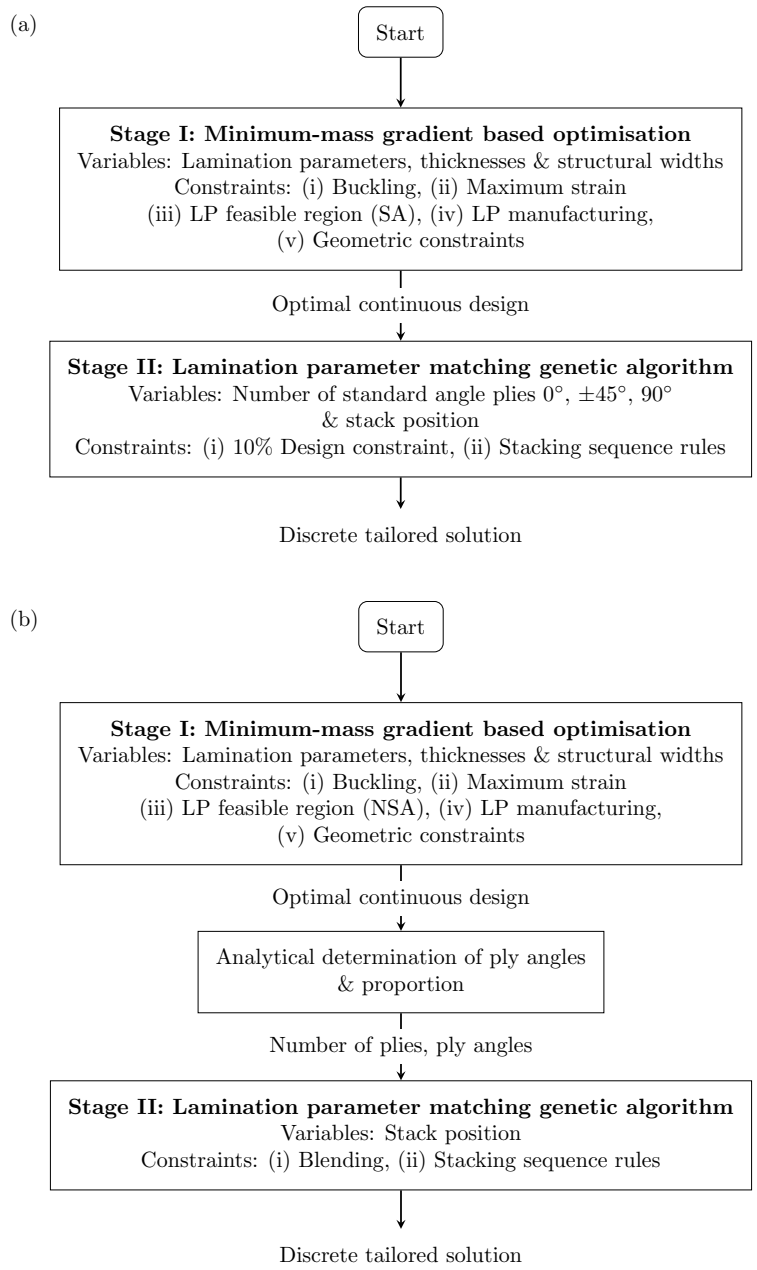

Figure 7.1: Flowchart comparison between (a) the original optimisation methodology as presented in Chapter 4 and (b) the adapted version implemented in this Chapter.

7.3.1 VIPASA Infinitely Wide Model

A T-stiffened panel, assumed by VIPASA model theory to be infinitely wide, is composed of repeating stiffener bay sections of width b_{sk} as illustrated in Fig. 7.2. Longitudinal half-wavelengths λ are defined as in Chapter 4, where $\lambda = \ell, \ell/2, ..., \ell/\text{N}$, where ℓ is the effective length of the panel and N is the number of user defined sinusodial modeshapes in the x-direction, as marked in Fig. 7.2. For infinitely wide VIPASA models, transverse buckling modeshapes are also assumed to vary sinusoidally in the y-direction. As the number of repeating sections tends to infinity, the values for the transverse half-wavelengths λ_{T} are taken with respect to the bay section width: $\lambda_{\text{T}} = b_{\text{st}}/\eta$, where η is a range of N_{T} number

of values that vary from zero to one in equally spaced intervals.

The VIPASA analysis returns the corresponding eigenvalue, buckling load and mode-shape plot for each combination of i^{th} longitudinal half-wavelength and j^{th} transverse half-wavelength specified, creating a list of N x N_T results. Buckling factors are again calculated by dividing the eigenvalue by the applied in-plane loading, and the buckling constraints are evaluated as follows:

$$1 - F_{ij} \leq 0 \tag{7.1}$$

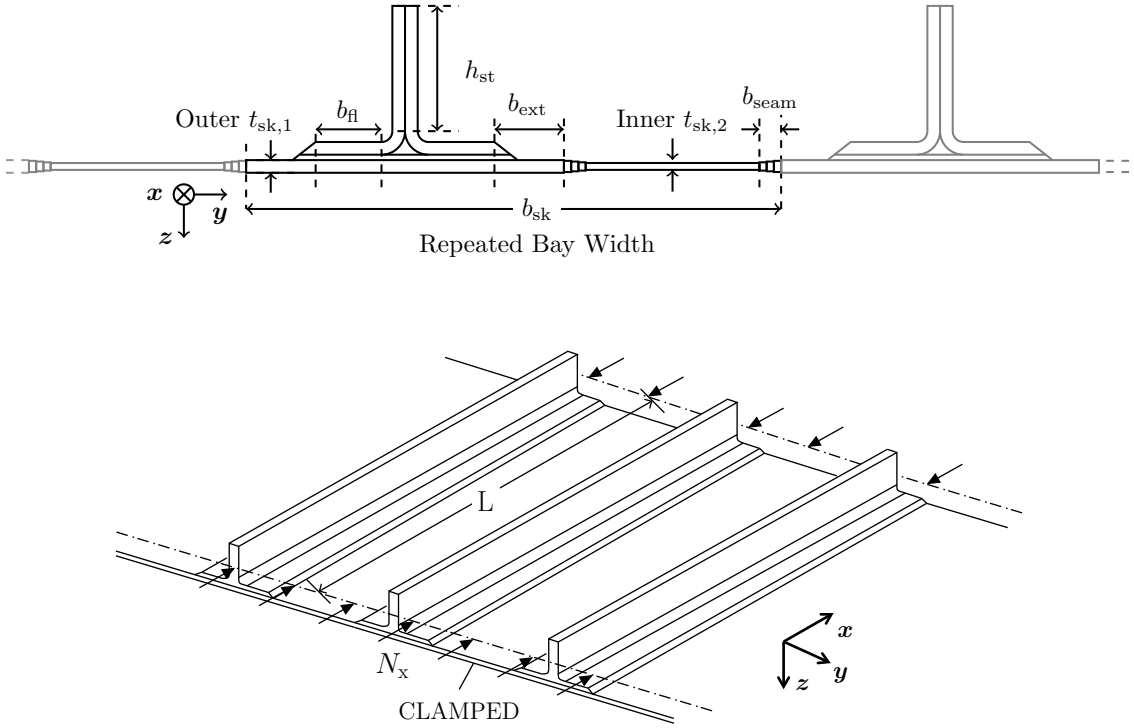

Figure 7.2: Infinitely wide panel model.

7.3.2 Lamination Parameter Feasible Regions: Non-Standard Angles

As lamination parameters are interdependent variables, a series of equations are required to define the outer bounds for the in-plane, coupling and out-of-plane lamination parameters, and the relationships between these terms. Traditional standard angle designs that are symmetric and balanced, and where ±45° plies are placed in pairs to minimise bend-twist coupling, can be defined using only four lamination parameters, $\xi_{1,2}^{A,D}$, which are bounded by the linear constraints indicated in Fig 7.3. By including non-standard angle designs, composed of an angle $\pm\theta^\circ$ in a percentage proportion $p_{\pm\theta^\circ}$ and another angle $\pm\phi^\circ$ in a proportion (1 - $p_{\pm\theta^\circ}$), the volume of the design space is expanded by 30%. This extended set of ply orientations has shown to benefit the buckling performance of composite plates, leading to more efficient structures [148].

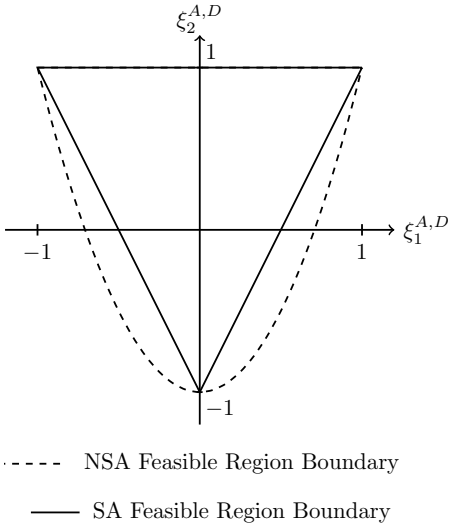

Figure 7.3: Standard and non-standard angle feasible in-plane and out-of-plane feasible regions.

The constraints defining the feasible region for all possible ply angle combinations for in-plane and out-of-plane lamination parameters are as follows:

$$2\,(\xi_1^j)^2 - \xi_2^j - 1 \leq 0 \quad j = A, D \tag{7.2}$$

Additional non-linear constraints have been derived by Wu, Raju and Weaver [86], defining the interdependent feasible parameter space for the in-plane ($\xi_{1,2}^A$) and out-of-plane ($\xi_{1,2}^D$) lamination parameters with no ply angle restriction:

$$5\,(\xi_1^A - \xi_1^D)^2 - 2\,(1 + \xi_2^A - 2\,(\xi_1^A)^2) \leq 0 \tag{7.3}$$

$$(\xi_2^A - 4t\xi_1^A + 1 + 2t^2)^3 - 4\,(1 + 2|t| + t^2)^2\,(\xi_2^D - 4t\xi_1^D + 1 + 2t^2) \leq 0 \tag{7.4}$$

$$(4t\xi_1^A - \xi_2^A + 1 + 4|t|)^3 - 4\,(1 + 2|t| + t^2)^2\,(4t\xi_1^D - \xi_2^D + 1 + 4|t|) \leq 0 \tag{7.5}$$

where t = [-1, -0.75, -0.5, -0.25, 0, 0.25, 0.5, 0.75, 1].

The NSA feasible region is scaled to fit the limits of the SA 10% rule upper and lower bounds for both the in-plane and out-of-plane lamination parameters, as displayed in Figure 7.4. While the 10% rule has physical significance in standard angle designs, this rule now acts to enforce minimum requirements for stiffness in orthogonal laminate directions for the NSA cases.

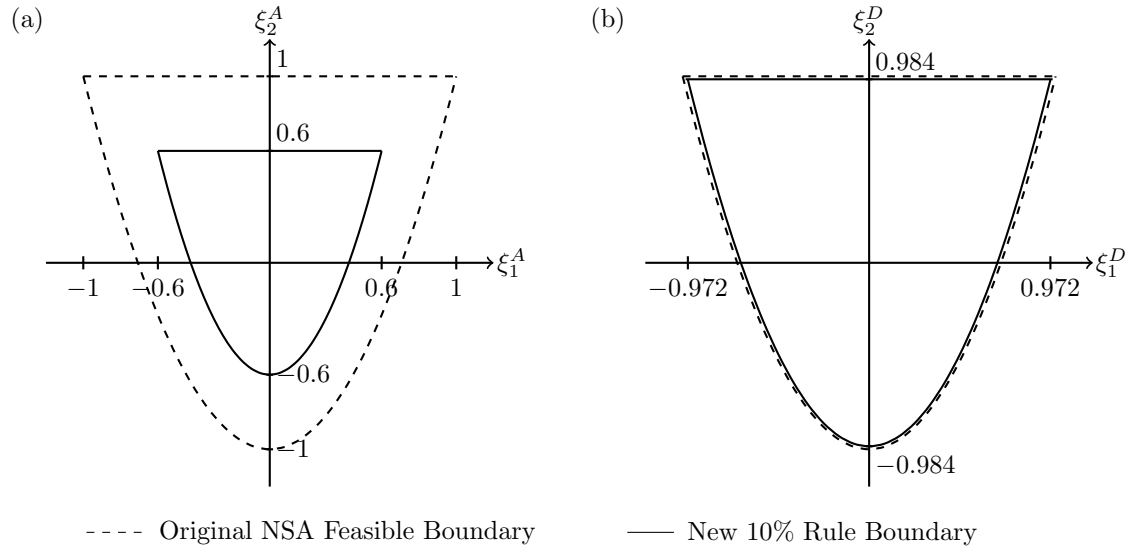

Figure 7.4: Non-standard angle feasible region for (a) in-plane (membrane) and (b) out-of-plane (flexural) lamination parameters, scaled to fit the bounds of the 10% ply percentage rule as applied to standard angle designs.

7.4 Blending of Composite Structures

The term 'blending' was first coined by Kristindottir et al. to describe the matching of the laminate stacking sequences defining different adjacent regions of a structure, to remove significant discontinuities that are either impossible to manufacture or critically reduce structural integrity [78]. In this definition of blending, plies are dropped from a single key region (the region requiring the thickest laminate in order to satisfy performance constraints) and not reintroduced in other areas of a structure, with no other ply additions, as per Zabinsky et al. [188]. A simplified blended definition was introduced by Adams et al., where plies were only dropped on the outer or inner surface of the stack, as depicted in Fig. 7.5a and b. This simplification, albeit necessary due to the computational expense of simultaneously optimising the laminate elastic properties for a given loading whilst incorporating the blending constraint using a genetic algorithm, restricts the design space significantly.

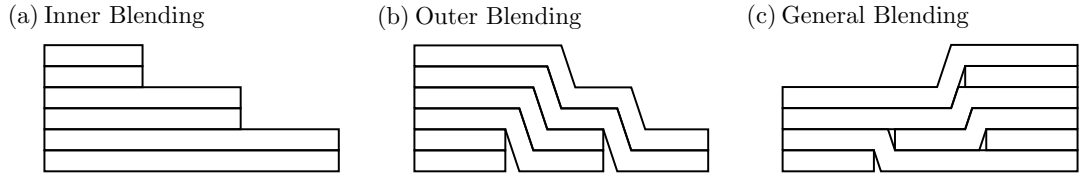

Figure 7.5: Examples of blending (a) Inner (b) Outer (c) General

Guide based algorithms have been commonly applied to the problem of blending, first appearing in the work of Adams et al. [143]. A laminate 'guide' stacking sequence is selected, and from this all regions of the panel are created through the ply deletion dependent on the local loading, using a single genetic algorithm. This preserves the through-thickness position of plies in order to maintain continuity and blending across a structure, resulting in

perfectly blended designs. Using an approach based on matching sublaminates, perfectly blended solutions were obtained with less severe weight penalties than the guide-based approach [189]. Other approaches enforce a minimum requirement of continuity between laminate regions, which generally is computed as a fraction of common layers divided by the total thickness, rather than completely blended solutions [134], which are more appropriate to problem of designing DST laminates. This type of blending is referred to as general blending, as illustrated in Fig 7.5c.

Genetic algorithms are most commonly used in the majority of work producing optimised blended stacking sequences for whole composite structures. GAs are well-suited to the design of discrete stacking sequences as they can easily handle discrete variables, and providing that a high level of diversity within the population is maintained, are not prone to becoming trapped in local minima if the design space is non-convex. Local minima can also be avoided by re-running the optimisation several times, encouraging the population to cover the full design space to avoid local optima, and selecting the best converged result. For complex problems such as structural optimisation, however, the evaluation of the objective function and constraints for a single candidate can require computationally expensive simulations. Repeated evaluation is required for each member of the population and for each iteration of the algorithm, when combined this becomes unreasonable, and makes application of a GA unsuitable for one stage optimisation techniques. Consequently, many designers implement a two-stage optimisation approach, where laminate performance is first optimised using continuous variables (lamination parameters), and then a second level algorithm returns a discrete stacking sequence matching the continuous optimal solution, with some blending constraint. It must be noted that a certain degree of structural continuity can be enforced in the first stage of a multi-step optimisation routine by limiting the variation in lamination parameters between adjacent regions, which limits loss of performance due to stacking sequence retrieval [145].

Aside from gradient-based or meta-heuristic algorithms, branch and bound methods have also been applied for the lay-up optimisation of composite structures [190, 191]. The branch and bound method is a deterministic optimisation technique for discrete and combinatorial problems, where candidate solutions are created by sequentially assembling plies. The ply orientations are limited to a discrete set of angles, often the four standard angles, and all possible designs are created using an enumeration tree structure, where a single stacking sequence solution corresponds to a full branch of the tree. Infeasible branches are 'pruned', removing them from the tree structure, thereby reducing the size of the problem and therefore making the methodology less inefficient. In particular, branch and bound methods have been shown to handle complex blending cases, satisfying blending constraints and other laminate design rules, that genetic algorithms with penalty functions struggle to solve [190].

Discrete stiffness tailoring allows for significant variation in laminate stiffness between adjacent regions of a structure through the discrete alteration of ply angles and thicknesses,

which can be effected over a very short transitional length. This tailoring is achieved at the expense of transverse strength, where discrete alterations in the ply angle introduce weaknesses within the structure. Therefore, the presence of continuous plies in adjacent regions should be prioritised when designing the discrete stacking sequences in Stage II of the optimisation routine. In Chapter 4, the genetic algorithm is free to select the proportion of plies and the stacking sequence order in order to match the optimum lamination parameters for a single laminate region. In order to enforce a blending constraint, the two panel skin regions will have to be optimised simultaneously. This however is complicated by the use of non-standard angles, where a single lamination parameter point can be represented by a several alternative laminate designs.

On the basis that the relationship between in-plane lamination parameters and the proportion of pre-specified ply angles is linear, it becomes simple to return percentages in which either standard or non-standard angles constitute the full stack, and in this way the problem is simplified and therefore becomes combinatorial in nature. Note that although it is linear, the relationship is not singular, and several different compositions of various ply angles in different percentages will create the same in-plane response. The blending constraint will be formulated as a penalty function based on some assessment of continuity constraint between the two laminate designs.

7.5 In-Plane Stiffness Matching

In Chapter 4, a standard genetic algorithm is implemented to return a discrete stacking sequence to match the continuous in-plane and out-of-plane lamination parameters defining the skin regions and stiffener, which were optimised for performance in Stage I. The standard algorithm is free to select the number of plies of each standard angle which compose the stack, alongside the ordering of these plies.

In this Chapter, the optimisation methodology is altered to exploit the linear dependence of the in-plane lamination parameters on fibre orientation in order to return axial stiffness matched standard and non-standard angle ply proportions, and these plies are then submitted to a permutation genetic algorithm. This is based on work conducted by Liu et al. [192], which utilises a scheme which first targets the correct in-plane lamination parameters by assessing the correct percentage of each standard angle, and then a second inner loop composed of a permutation genetic algorithm attempts to match the flexural optimised lamination parameters.

7.5.1 Standard Angles

The in-plane lamination parameter feasible region, with standard angle ply percentages mapped on the design space, is presented in Figure 7.6. Due to the linear relationship between standard angle ply and in-plane lamination parameters, as demonstrated in the ply angle percentage map, it becomes simple to determine the exact proportions of each

angle that constitute a single stack. The expressions that link the proportions of each standard angle and the in-plane lamination parameters, as per [192] are as follows:

$$\xi_1^A = p_0 - p_{90} \tag{7.6}$$

$$\xi_2^A = p_0 + p_{90} - p_{\pm 45} \tag{7.7}$$

where p_0, p_{90} and $p_{\pm 45}$ represent the proportion of 0°, 90° and ±45° plies in the laminate stack respectively, where $p_0 + p_{90} + p_{\pm 45} = 1$, representing the full laminate stack.

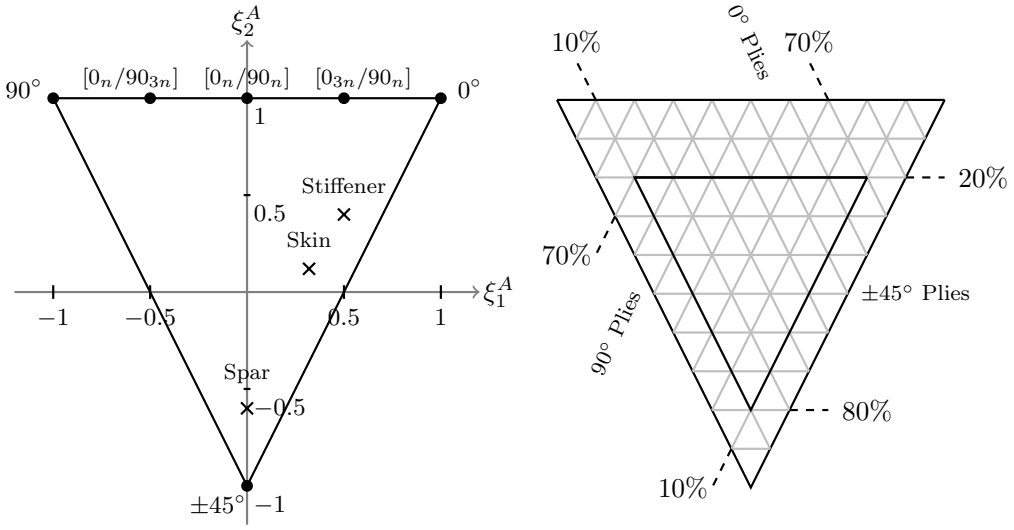

Figure 7.6: In-plane lamination parameter region for standard angles, where the equivalent parameters for typical aerospace components are marked. Standard angle percentages are mapped on the design space.

7.5.2 Non-Standard Angles

The in-plane lamination parameter feasible region, with corresponding laminate non-standard angle designs set on the outer boundary, is presented in Figure 7.7. The in-plane lamination parameter outer boundary parabola represents laminate designs composed only of all 0°, all 90°, or of a single angle ply ±θ°. The linear bound enforcing the ξ_2^A upper limit represents laminate designs composed of solely 0° and 90° plies in linearly varying proportions. Returning a matched in-plane stiffness becomes more complicated when including non-standard angle cases as there may be several combinations of angle plies that satisfy the axial stiffness. There is also a limitation on the number of different angles that can constitute a single design, in terms of ease of manufacture. Therefore, a solution is proposed by which the 'Outer' and 'Inner' in-plane lamination parameters are used to identify the most optimum combination of two angle ply pairs. All points on a single straight line, traversing the feasible region, can be described by a linearly varying proportion of the two pairs of angle plies, or a single pair of angle plies and the correct ratio of [0°/90°] that can be ascertained analytically. This linear variation of stiffness with the in-plane lamination

parameters can be exploited to benefit the design of blended laminates with non-standard angles.

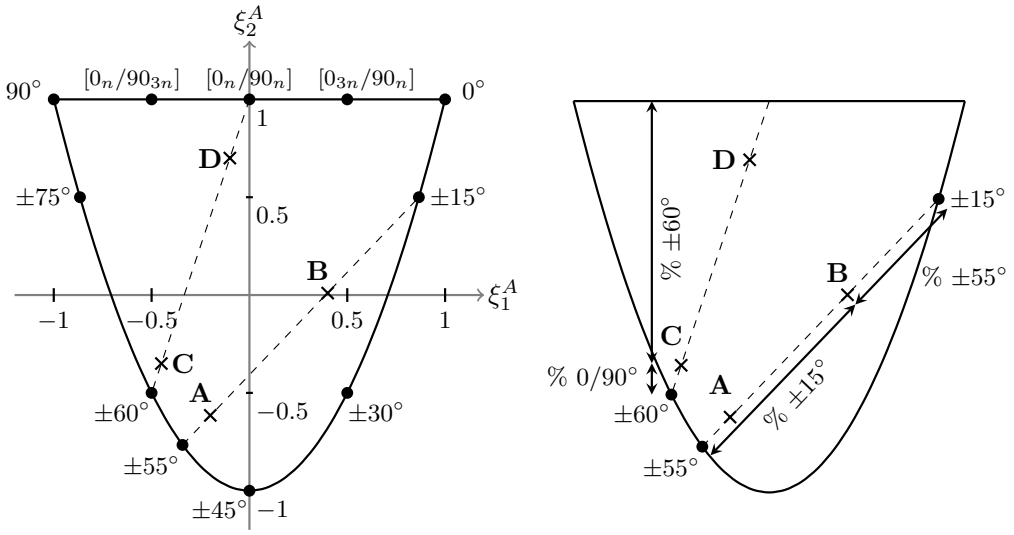

Figure 7.7: In-plane lamination parameter region, annotated with example non-standard angle designs, A and B, and C and D. The right hand figure illustrates how to determine ply proportions of example points using the in-plane lamination space.

An 'Outer' and an 'Inner' laminate design, for example, are represented by Point A and Point B respectively in Fig. 7.7. By connecting the two points, and extrapolating to the outer boundary, it can be analytically determined that these designs are composed of only [±15°/ ±55°] in varying proportions. The proportion of each non-standard angle in a given stacking sequence can be explicitly calculated as a the proportion of the line that spans the entire feasible region. In this case, the line lengths corresponding to the proportions of ±15° and ±55° that compose design B are marked in Fig. 7.7, as fractions of the line that spans the entire feasible region from ±15° to ±55° on the outer parabola.

For lamination parameter points that, when connected, do not both cross the parabolic outer boundary, a separate formulation is required to create laminate designs that are composed of some angle ±θ°, 0° and 90° plies. For example, Points C and D in Figure 7.7 represent designs are composed of [0°/90°/±60°] plies. General expressions that link the in-plane parameters, and proportions of zero, ninety and ±θ° plies are as follows:

$$\xi_1^A = p_\theta \cos(2\theta) + p_0 - p_{90} \tag{7.8}$$

$$\xi_2^A = p_\theta \cos(4\theta) + p_0 + p_{90} \tag{7.9}$$

where $\xi_{1,2}^A$ are the in-plane lamination parameters and $p_{\pm\theta}$, p_0 and p_{90} represent the percentages of ±θ°, 0° and 90° plies respectively.

7.6 Stage II: Permutation Genetic Algorithm

The in-plane stiffness matching method generates exact continuous proportions of each ply angle that together constitute a single laminate stack. The continuous percentages are converted into discrete numbers of each ply, and deciding a final arrangement of each ply angle now becomes a combinatorial problem. Hence, a permutation genetic algorithm is implemented, to optimise the stacking sequence with respect to the out-of-plane lamination parameters, where blending between laminate designs is implemented as a penalty constraint. Compared to a conventional genetic algorithm, re-defining the discrete numbers of ply angles reduces the dimensionality of the design space, and permutation GAs have been shown to out-perform standard GAs in efficiently finding the optimal arrangement of ordered variables [111]. The improvement in the efficiency of permutation GAs arises from the removal of objective and penalty functions related to constraints enforcing set proportions of each ply angle. In this case the speed of the algorithm is increased by pre-selecting the numbers of each ply angle but is also subject to an extra blending constraint when compared to the previous Chapter, which ultimately results in a similar runtime but outputs a blended final design.

As with a standard genetic algorithm, generations of candidate solutions are created through the selection of elite individuals from the previous iteration, and through the creation of new children from mutating single individuals or crossing a pair of individuals together. As the stacking sequence design is now limited to variations of specific proportions of certain angle plies, the mutation and crossover functions must be rewritten to produce new candidates that meet these requirements. The customised functions are implemented within the existing MATLAB *ga* architecture.

The algorithm is also adapted to optimise the discrete stacking sequences of two laminates simultaneously, whilst enforcing a blending constraint, in the case of two laminates arranged adjacently to each other. The laminates are assumed to share some proportion of angle plies, but are allowed to have different thicknesses. A single vector of design variables $\boldsymbol{x}$ represents the ply orientations of two stacking sequence designs:

$$\boldsymbol{x} = \underbrace{[X_1, X_2, ..., X_n]}_{\text{Laminate 1}} \underbrace{[X_{n+1}, X_{n+2}, ..., X_{2n}]}_{\text{Laminate 2}} \tag{7.10}$$

where n is the number of plies needed to describe half the thickest laminate stack, due to laminate symmetry. Extra 'empty' plies are added to the portion of the vector that represents the thinner laminate. These placeholder empty plies represent dropped plies in the design and their presence is required for the blending constraint evaluation.

Encoding the laminate is necessary for use in the genetic algorithm. In this instance, integer values from one to N_θ represent the orientation of each ply, where N_θ is the number of distinct angle plies composing the laminate designs. Positive and negative ply angles are represented by separate integer values, i.e. $45°$ is encoded as 3 and $-45°$ as

4. The zero encoding represents an empty ply. The permutation GA is applicable for standard and non-standard angle laminate design.

The initial population of candidates are generated through random permutations of the vector of angle plies. Note that the creation and subsequent manipulation of candidate solutions during cross-over and mutation for Laminate 1 and Laminate 2 designs are isolated from each other, in order to maintain the correct proportion of plies in each laminate design.

7.6.1 Cross-over Function

An even numbered selection of candidate solutions from the previous generation are randomly selected to be cross-over parents. These parents are subsequently randomly paired together in order to create new candidate solutions. Developed by Goldberg and Lingle [193], a partially mapped crossover subroutine is implemented. Two break-point vector indices are randomly defined, and a vector string between, and including, the two indices from one parent is transplanted into a child vector, in the same string position. The second parent is then used to populate the empty elements, provided that the stipulated numbers of each ply angle are not exceeded if added to the child vector. Missing genes are then randomly assigned to the empty elements, to produce a complete cross-over child.

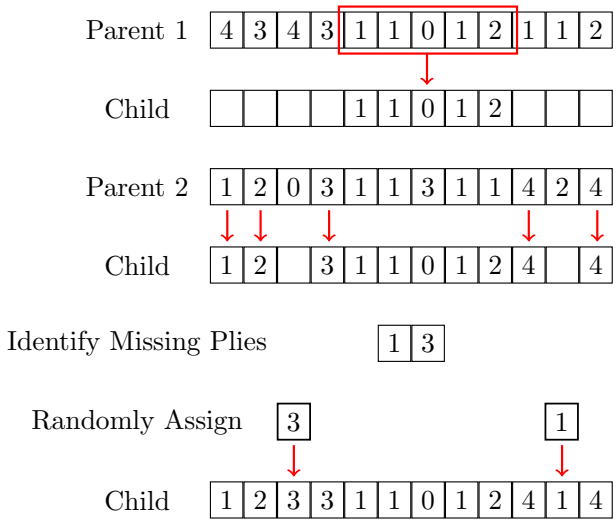

Figure 7.8: Diagram illustrating the process of the partially mapped crossover.

7.6.2 Mutation Function

The mutation function traditionally alters a minor portion of a previous candidate solution randomly. In order to maintain the same proportion of angle plies in each laminate design, this function is altered to switch a user-defined percentage of genes, p_{mutate}, at random. A binary encoded mutation index, where the probability of a given element having a value of 1 is p_{mutate}, is created to define the genes to be switched as demonstrated in Fig 7.9.

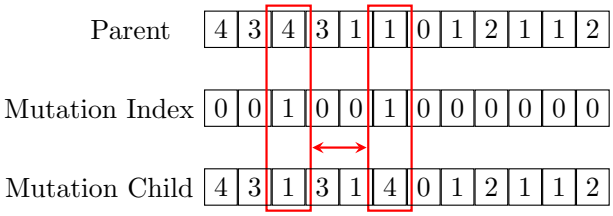

Figure 7.9: Diagram illustrating the creation of children through mutation.

7.6.3 Objective Function

The objective function is to minimise the summation of the Euclidean distances between the target out-of-plane lamination parameters and the out-of-plane lamination parameters calculated for the candidate stacking sequences:

$$f(\boldsymbol{x}) = \sum_{j=1}^{2} \sum_{i=1}^{4} w_i^D (\xi_{i,ga}^D - \xi_{i,opt}^D)^2 \tag{7.11}$$

As the proportions of each angle ply are constant for each candidate solution, ξ_{1-4}^A are fixed values and are not included in the objective function.

7.6.4 Blending Penalty Constraint

Blending is defined as the degree to which two stacking sequences 'match' each other, where maintaining continuous plies from one region to another is prioritised as it preserves transverse strength. A metric for 'composition continuity' was introduced by Liu and Hafkta [134], where the number of continuous plies is divided by the total laminate thickness, and a minimum percentage of blended plies is enforced as an optimisation constraint. Adams et al. [194] compute a Levenstein distance, also known as the edit distance, to produce a numerical metric for blending. The Levenstein distance is calculated through the summation of the number of edits, d, these being either additions, deletions or substitutions, required to transform one variable string to another, as illustrated in Figure 7.10. As candidate solutions are encoded as as strings within the genetic algorithm, this approach is suitable for blending constraint evaluation.

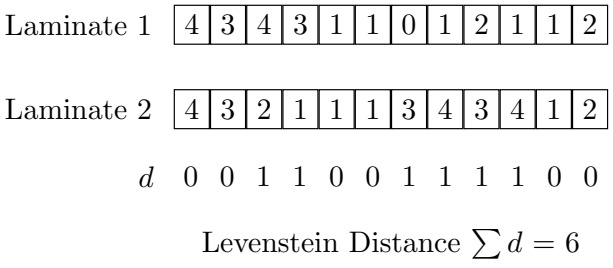

Figure 7.10: Example calculation of the Levenstein distance as a blending metric.

By comparing the quantities of each angle ply that compose Laminate 1 and Laminate 2 respectively, a minimum possible obtainable edit distance $d_{\min}$ can be calculated. As greater values of d represent largely unblended designs, the minimum value $d_{\min}$ conversely represents a maximum attainable blended laminate solution. The calculated Levenstein distance for a candidate solution is hence normalised to lie on the unit interval:

$$g_{\text{blend}}(\boldsymbol{x}) = \frac{\sum_{i=1}^{n} d_i - d_{\max}}{n - d_{\max}} \tag{7.12}$$

This metric is applied as a penalty constraint, which is added to the objective function for each evaluation.

7.6.5 Stacking Sequence Rules

The following stacking sequence rules are applied to the laminate design as per Niu [67]:

(i) Laminates are balanced and symmetrically stacked about the midplane, to prevent both warping of the laminate during cure and coupling of in-plane and out-of-plane elastic response.

(ii) A maximum 4-ply contiguity is enforced to prevent high transverse stress gradients in the laminate and to avoid delaminations.

(iii) The two outer plies are continuous across the two regions, covering any internal seams or ply drops, for increased damage tolerance. Load bearing (0° and 90°) degree plies are prohibited from occurring in the surface of the laminate.

Symmetry is enforced by optimising half the stack, with the remaining plies mirroring these variables about the mid-plane.

A penalty function is employed to enforce the ply contiguity constraint as per [107, 122]:

$$g_{\text{contiguity}}(\boldsymbol{x}) = \Theta \tag{7.13}$$

where Θ is the total number of instances within the stacking sequence where more than four plies of the same orientation are stacked contiguously. A similar penalty function is used to enforce the blending of the outer two plies and to impede the selection of 0° plies as outer plies, where a penalty of one is added to the objective function for each violation.

7.6.6 Blending Test Case

The design of the DST panel (type (d)) in Chapter 5 was created by returning each regional stacking sequence individually, and then manually combining the two to form a blended laminate, preserving continuous plies. Applying the blending constraint to this problem maximises the number of shared plies, with minimal difference between the two designs in terms of lamination parameters, evaluated using the objective function as expressed in Eq. 7.11, given in Table 7.1. As the objective function is the sum of all Euclidean distances

between the optimal and target $\xi^D_{1,2}$ terms representing the Inner and Outer stacks, the quantitative difference between the two generated designs is very small. As the stacks are symmetric, the half stacks for each design are given for comparison in Fig 7.11.

Table 7.1: Table of lamination parameters corresponding to discrete stacking sequences (see Fig 7.11) generated with a standard GA and permutation GA with blending constraint, targeting the DST design presented in Chapter 5, panel type (d). The designs are assessed using the objective function defined in Eq. 7.11 with a weighting of one, and the number of shared plies.

	Region	ξ^A_1	ξ^A_2	ξ^D_1	ξ^D_2	$f(x)$	Shared Plies
Target	Outer	0.5778	0.5947	0.8481	0.9223		
	Inner	-0.0004	-0.5920	0.0187	-0.8461		
GA	Outer	0.4667	0.4667	0.4679	0.2652	0.5923	4
	Inner	0.0000	-0.5000	-0.0117	-0.9688		
Perm. GA	Outer	0.4667	0.4667	0.4341	0.2119	0.6788	6
	Inner	0.0000	-0.5000	0.0703	-0.8516		

(a) Standard GA - No blending

Outer	-45	45	0	0	0	90	0	0	0	0	45	0	0	90	-45
Inner	-45	45				45	-45				45	-45		90	0

(b) Permutation GA - Blending constraint

Outer	-45	45	0	0	0	90	0	0	0	45	-45	0	90	0	0
Inner	-45	45			45	-45			0	45	-45		90		

Figure 7.11: Example of a blended solution, compared with a standard GA result with no blending. Continuous plies, discretely altered plies and dropped plies are coloured black, blue and red respectively.

7.7 Parametric Study

The modelled T-stiffened panel, presented in Section 7.3.1, is characteristic of commercial aircraft upper wing covers that are used to carry compressive loads. For a medium-range aircraft with an approximate Maximum Take-Off Weight (MTOW) of 100,000 kg, the design compressive running limit load N_x is assumed to vary from 0.5 kN/mm at the wing tip, to 3 kN/mm approaching the wing root, as indicated in Fig 7.12.

The longitudinal length, L, of the panel is varied between 1 m and 2 m in length, which is consistent with rib spacing, the longitudinal distance between clamped connections to the supporting wing structure. The original numerical study utilised a stiffener bay width, b_{sk}, of 300 mm as this is representative of aircraft designs. The motivation for applying discrete stiffness tailoring to the stiffened panel skin is to create an efficient use of material and ultimately to reduce the structural mass. As a result of stiffness tailoring, it may be possible to reduce the required number of stiffeners per metre width using DST, whilst

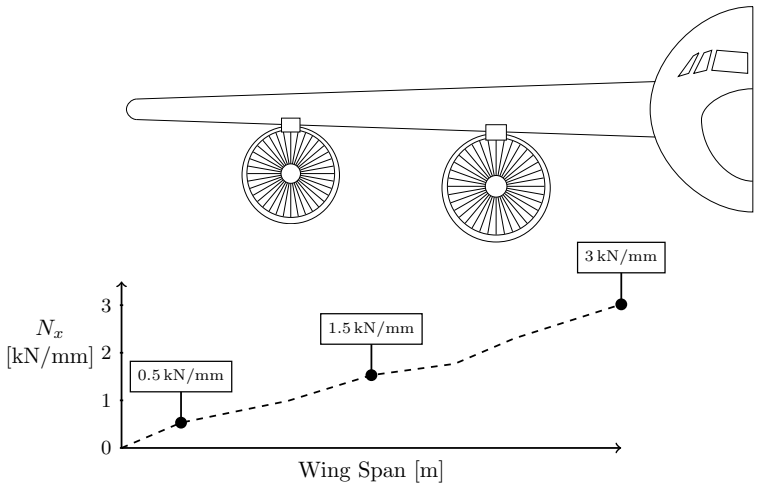

Figure 7.12: Generalised variation in compressive load experienced across the span of a wide-body aircraft wing.

achieving the same material efficiency. Fewer stiffeners constitute reduced manufacturing time, and so to this end, three additional stiffener bay widths of 350, 400 and 450 mm are investigated.

Baseline panel designs optimised for minimum mass are also presented for comparison with the discretely steered studies, for each load case. The baseline cases are generated using the two-step optimisation procedure as developed in Chapter 4, but using the infinitely wide VIPASA boundary conditions, as described in Section 7.3.1. Two DST designs: one restricted to standard angle designs, and the other allowed to select non-standard angle designs, are also optimised for comparison. All case study designs are evaluated using N = 45 and N_T = 15, which are the number of longitudinal and transverse wavelengths respectively. The number of longitudinal and transverse wavelengths were selected to sufficiently cover global, stiffener and skin buckling modes, by ensuring that the smallest wavelength is representative of the smallest stiffener height length. A sensitivity analysis was conducted to guarantee that the range of values of λ and λ_T analysed returned the critical buckling load.

All panel types are optimised using the fixed parameters in Table 7.2 and the variables bounds as given in Table 7.3. Discrete stacking sequence solutions for the 'Inner' and 'Outer' regions of the DST panel skin designs are generated using the in-plane stiffness matching procedure and permutation GA as described in Sections 7.5 and 7.6. Each run of the permutation GA, as per the algorithm parameters selected previously, uses a population of 40 candidate solutions where four elite children are retained each generation, 80% of the children are created through crossover, and all other children are created through mutation. A mutation percentage of ten percent is used for generating mutated children. The original GA from Chapter 4 is used to return the stiffener discrete stacking sequence, using standard angle plies. The stiffness properties of the T-stiffener are again predetermined using the industry standard ratio of 60%/30%/10% for 0°, ±45° and 90°

respectively. Discrete stiffener stacking sequences are created through the use of the standard genetic algorithm, where laminate design rules are enforced through penalty functions, previously implemented in Chapter 4.

Table 7.2: Fixed parameters: Infinitely wide panel study

Parameter	Value
ϵ_{max} (μstrain)	4500
b_{seam} (mm)	30
r_{st} (mm)	5

Table 7.3: Variable upper and lower geometric bounds; t refers to bounds applied to each thickness variable.

	t	h_{st}	b_{fl}	b_{ext}
		(mm)		
Lower Bound	2	10	35	1
Upper Bound	25	100	70	100

7.8 Results

For comparison between the design cases, a metric of material efficiency is calculated by dividing the total applied load, $P = N_x\, b_{sk}$, by the mass of an optimised stiffener bay. Larger values of material efficiency for equivalent panel geometries represent more optimal, reduced mass, designs. Surface plots of material efficiency are presented in Figure 7.13, varying stiffener spacing and panel length, for the three in-plane running load cases: 0.5, 1.5 and 3 kN/mm, for standard angle baseline, non-standard angle and standard angle blended optimum designs. The same colour map is used for material efficiency surface plots, to aid comparison. The percentage difference in panel mass between the baseline and DST NSA optimum designs for each in-plane loading case are presented in Fig. 7.13 (vi).

In and out-of-plane optimum lamination parameters which represent the DST skin designs, for both SA and NSA results, and the optimum baseline skin parameters are plotted alongside the demarcated lamination parameter feasible boundary for $N_x = 0.5$, 1.5 and 3 kN/mm for all variations in panel length and stiffener spacing are presented in Fig. 7.14. These figures illustrate general trends in the optimal stiffnesses selected for each design, dependant on the in-plane loading.

Percentages of blended plies in the final designs, continuous across the 'Outer' and 'Inner' regions, which are calculated as a proportion of the thickest laminate skin thickness, are presented in Figure 7.15. Results are given for all panel lengths and stiffener spacings for each of the three loading cases considered.

Stacking sequence designs and final panel geometries for specific cases are presented in Table 7.4, alongside the buckling factors corresponding to global, local skin and stiffener buckling, and the critical buckling strain. Baseline, DST standard angle and DST non-standard angle designs are compared for low and high in-plane load cases, and for different panel lengths. The total mass of each panel design is also presented to quantify the mass reduction due to stiffness tailoring.

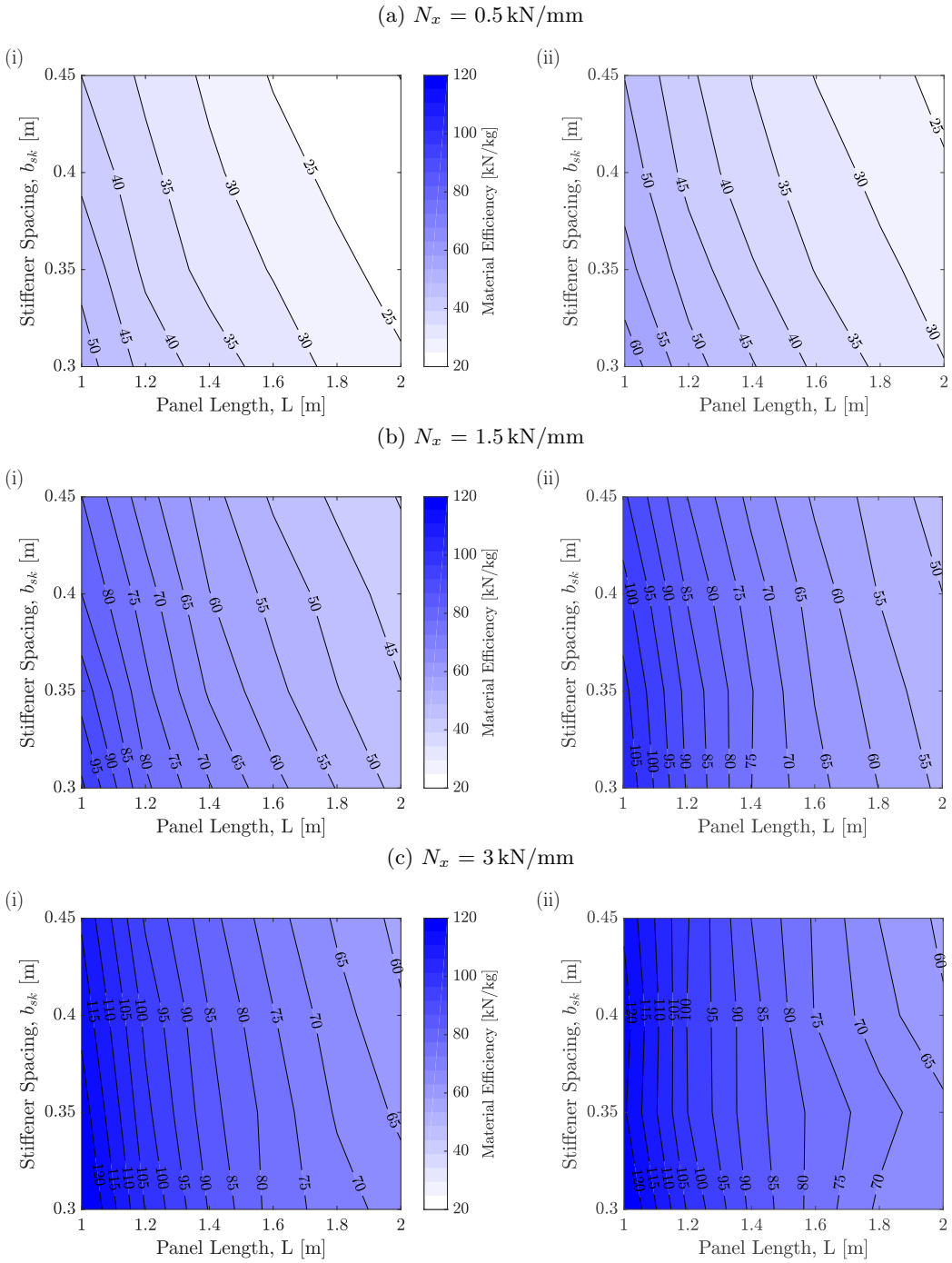

Figure 7.13: Surface plots of material efficiency (applied load divided by total panel mass) for the (i) baseline and (ii) DST NSA optimum stiffened panel designs for different running loads: N_x (a) 0.5, (b) 1.5 and (c) 3 kN/mm.

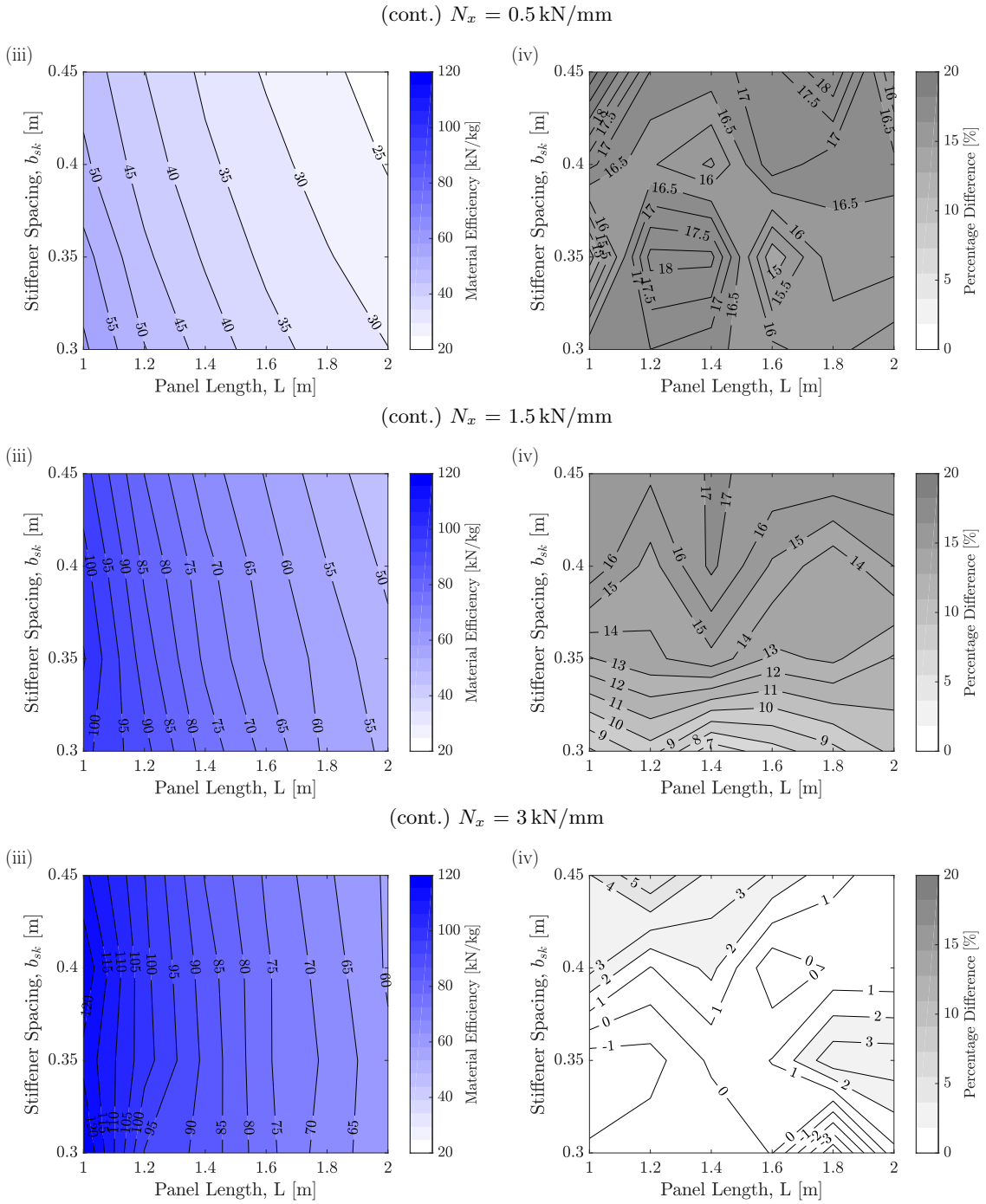

Figure 7.13 (cont.): Surface plots of material efficiency (applied load divided by total panel mass) for the (iii) DST standard angle optimum stiffened panel design for different running loads: N_x (a) 0.5, (b) 1.5 and (c) 3 kN/mm. (iv) Percentage difference in mass between (i) baseline and (ii) DST NSA panel designs.

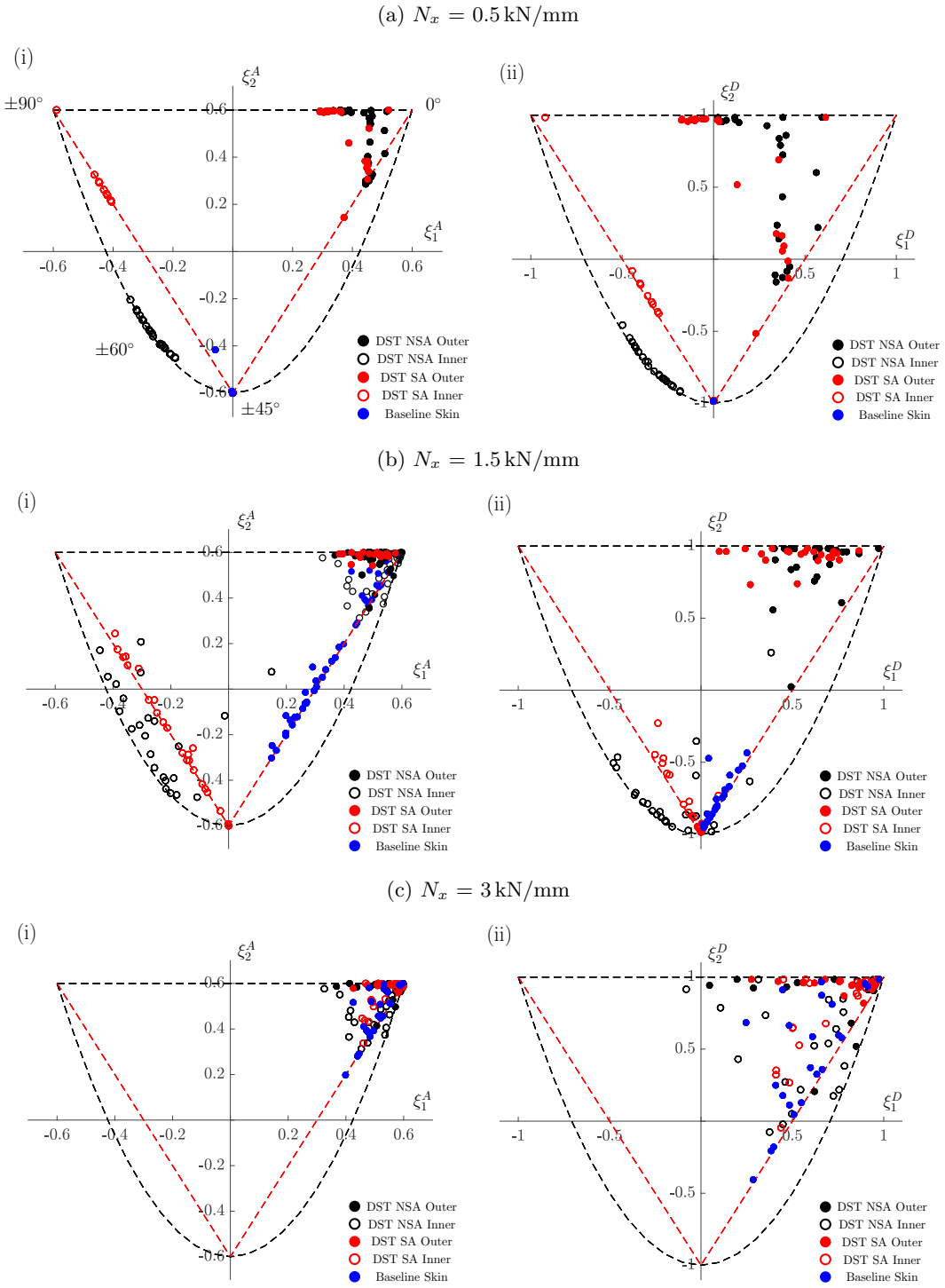

Figure 7.14: (i) In and (ii) out-of-plane lamination parameter optimum designs for DST NSA and SA, and baseline skin cases, for all design load cases.

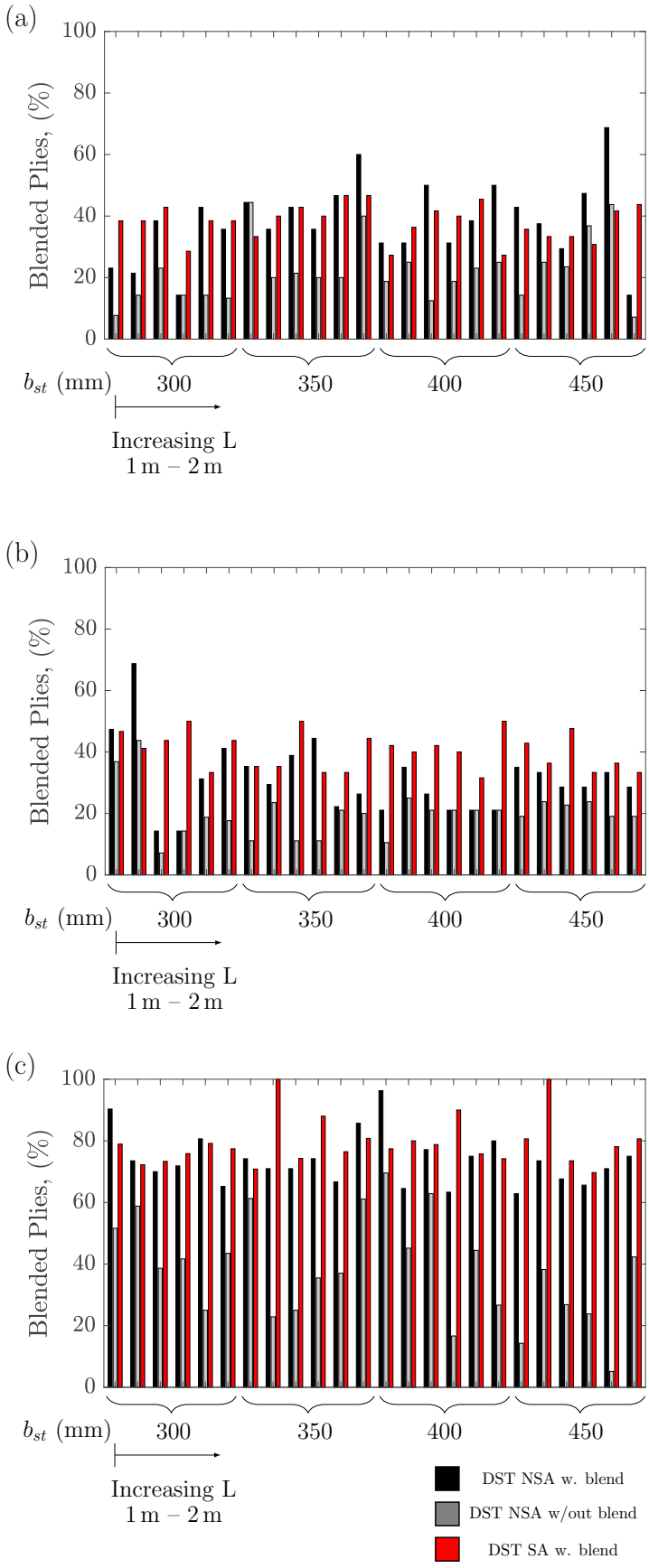

Figure 7.15: Percentage of blended plies present in the final stacking sequence solutions for all designs where (a) $N_x = 0.5$, (b) $N_x = 1.5$ and (c) $N_x = 3\,\text{kN/mm}$.

Table 7.4: Final stacking sequence solutions, panel geometries, buckling factors and strains for particular case studies.

Panel	N_x	b_{sk}	L		h_{st}	b_{fl}	b_{ext}	Mass	Buckling Factors			Strain
Type	(kN/mm)	(mm)	(m)	Stacking Sequence - No. of Plies	(mm)	(mm)	(mm)	(kg)	Global	Skin	St.	ϵ_x (µstrain)
Base	0.5	300	1	St. $[\mp 45/0/90/0/\overline{0}]_S$ - 11	29	35	-	2.86	1.003	0.987	-	2216
				Skin $[\mp 45_4/90_2/45/0/\overline{0}]_S$ - 25								
DST	0.5	300	1	St. $[\mp 45/0_3/90/\overline{0}]_S$ - 13	26	42.5	1.5	2.38	1.099	1.067	-	2888
SA				Sk_{Out} $[\pm 45/0/90/0_4/\pm 45/0/90/0]_S$ - 26				(-16.8%)				
				Sk_{In} $[\mp 45/90/0/90/\overline{90}]_S$ - 11								
DST	0.5	300	1	St. $[\mp 45/0/90/0/\overline{0}]_S$ - 11	23	39	8	2.37	1.015	1.004	-	2884
NSA				Sk_{Out} $[\mp 61/\pm 5_4/\pm 61/\pm 5]_S$ - 28				(-17.3%)				
				Sk_{In} $[\mp 61_2/61/5]_S$ - 12								
Base	0.5	300	2	St. $[\mp 45/0/90/0/\overline{0}]_S$ - 11	49	39	-	5.854	0.9718	0.9509	1.551	2391
				Skin $[\mp 45_2/45/90/\text{-}45/\pm 45/90/0_2]_S$ - 24								
DST	0.5	300	2	St. flange $[\mp 45/0_2/90/0/\overline{0}]_S$ - 13	48	44	1	5.174	0.925	0.7471	-	3094
SA				Sk_{Out} $[\mp 45/0_3/90/0_4/45/0/90/\text{-}45]_S$ - 28				(-11.6%)				
				Sk_{In} $[\mp 45/90_2/0_2/\overline{90}]_S$ - 11								
DST	0.5	300	2	St. flange $[\mp 45/0_2/90/0/\overline{0}]_S$ - 13	55	44	1	5.203	0.966	1.009	-	2988
NSA				Sk_{Out} $[\mp 60/0_4/60/0_4/\text{-}60/0/\overline{0}]_S$ - 27				(-11.1%)				
				Sk_{In} $[\mp 60/\pm 60/60/\overline{0}]_S$ - 11								
Base	3	300	2	St. $[\mp 45/0/90/0_2/45/0_2]_S$ - 18	74	35	-	13.32	0.989	1.056	0.987	1651
				Skin $[\mp 45/90/0_4/45/0/90/0_4/90/0_4/\text{-}45/0_2/\text{-}45/0_2/45/0/90/\overline{-45}]_S$ - 57								
DST	3	300	2	St. flange $[\pm 45/0/45/0_2/\mp 45/45/0_3/\text{-}45/0/90_2/0/90/0_3/90/0]_S$ - 46	51	35	25	13.22	1.049	1.378	0.987	1582
NSA				Sk_{Out} $[\pm 40/0_2/90/0_4/40/0_2/90/0_4/\text{-}40/0_2/\pm 40/90]_S$ - 46				(-1%)				
				Sk_{In} $[\pm 40/0_2/90/0_4/40/0_4/\text{-}40/0/\pm 40/\overline{40}]_S$ - 31								

7.9 Discussion

Discretely tailored stiffened panels consistently achieve greater material efficiency than traditional, standard angle, baseline optimum designs for the tip and mid-wing load cases, as observed through the comparison of plots presented in Fig. 7.13. The corresponding reduction in mass is as large as 19% for $N_x = 0.5\,\text{kN/mm}$, as illustrated in Fig. 7.13iv, but the magnitude of this reduction declines with greater in-plane load. Small local variations in the compared final masses can be attributed to the characteristics of the optimisation routine, where the final converged masses are highly dependent on the selection of initial start point, but general trends can be identified. For $N_x = 0.5\,\text{kN/mm}$, the DST case achieved consistently lower masses, and the percentage difference between the baseline and DST NSA masses generally does not significantly vary with panel length, but there is a small variation with stiffener spacing. This trend, however, is distinctly observed for $N_x = 1.5\,\text{kN/mm}$ in Fig. 7.13iv, where the difference in the final masses increases with stiffener spacing, from 7-8% for $b_{\text{sk}} = 300\,\text{mm}$, to 16-17% for $b_{\text{sk}} = 400\,\text{mm}$. Reviewing the corresponding material efficiency plots in Fig. 7.13bi-ii, it can be observed that material efficiency decreases with increased stiffener spacing for the baseline case, but discrete stiffness tailored designs are able to maintain approximately the same level of efficiency for wider stiffener bays. For example, Figure 7.13bii, it can be observed that a DST stiffened panel, of length 1.4 m with a stiffener bay width of 400 mm is equivalent in mass per unit area to n optimised panel with stiffener spacing of 300 mm. This represents the removal of 1 in 4 stiffeners across the stiffener width, constituting a significant manufacturing benefit. This trend diminishes for greater panel lengths. Negligible differences between the masses of the baseline and DST results are observed for the largest load case ($N_x = 3\,\text{kN/mm}$) considered in this study.

The overall trend, shared by both optimal baseline and non-standard angle DST stiffened panel designs, is that rate of decrease in material efficiency increased with linear variation panel length, as illustrated in Figure 7.13i - iii. As the global buckling load is inversely proportional to the square of the effective panel length, the global mode becomes critical for all longer panel length designs, as evidenced from the buckling factors in Table 7.4. The longer panels therefore require a significant increase in stiffener height to augment the second moment of area to offset the reduced global critical buckling load. The skin thicknesses remain constant between the shorter and longer panel lengths.

Standard angle DST designs, as presented in Figure 7.13iii, outwardly appear to match non-standard angle designs, (i), in terms of achievable material efficiency. However, the buckling performance of the final discrete SA designs is significantly lower than that of the non-standard angle designs, for the same final mass. Some loss in performance is expected from the conversion of continuous lamination parameters to a discrete stacking sequence solution, particularly for laminates with small numbers of plies. Using non-standard angles can be seen to limit this reduction, presumably as the lamination parameters are more precisely matched, even for thinner laminate designs. As extra plies, and therefore extra

weight, will need to be added to the standard angle designs to fulfil the buckling constraint, it can provisionally be concluded that non-standard angle designs offer an small additional weight saving when compared to traditional angle laminates.

Considering the optimum lamination parameters corresponding to panel designs supporting increasingly higher in-plane loads, presented in Figure 7.14, it can be observed that the difference between the 'Outer' and 'Inner' stiffness is greatest for the wing-tip and mid-wing loads (ai and bi), where buckling resistant, lower stiffness, plies are selected for the length between stiffeners, and stiffer plies (0°) are directed to the region attached to the stiffener. As the load increases, the 'Outer' and 'Inner' designs converge towards stiffer laminate designs, where both regions are required to support the great magnitude of in-plane load, which is redistributed to the stiffener region in the low load case. The root loading case achieves the highest material efficiency of any of the three loads considered in this study, as all the structure is utilised to support the load, whereas the active buckling constraint for most low load designs is local skin buckling, see Table 7.4. It is logical to conclude that DST would have the greatest effect for problems that would seek very disparate regional stiffnesses. The location of the transition seam between 'Outer' and 'Inner' regions, b_{ext}, for the tip and mid-wing designs generally occurs immediately post the stiffener bondline, as presented in Table 7.4. This and large and rapid variation in stiffness is facilitated by the DST methodology. For greater in-plane loads, any reduction in mass achieved due to tailoring comes as a result of thickness, and not necessary stiffness, tailoring, which was previously observed in Chapter 5 to have a limited effect on the mass reduction achieved when compared to baseline panel designs.

The in-plane lamination parameters representing the baseline optimum skin designs, vary between designs predominantly created of ±45° for resisting local skin buckling for the low load, to designs created of mainly 0° for the highest in-plane load, illustrated in Fig. 7.14a-ci. For DST designs, the load is redistributed to the stiffener regions, and mass and stiffness is reduced in the 'Inner' skin region, as previously observed in Chapter 5. However, as transverse buckling modes are included in this study, the DST designs are not solely composed of ±45° plies, as some transverse reinforcement is now required. The optimised DST NSA designs for the 'Inner' region trend towards selecting ±60° angle plies, optimised SA designs select laminate stacks that are significantly composed of ±45° and 90° plies.

For each final design presented in Table 7.4, the strain constraint is not active, which suggests that the designs are not fully optimal and are constrained by some feature of the problem formulation. Considering this, it can be assumed that the low strains are due to the selected stiffener geometry, as in this study the thicknesses of the stiffener web and stiffener flange are interdependent, where the web is double the thickness of the flange. In selecting this geometry, the industrial requirements for the web to be doubly symmetric, i.e. the flange stack is also symmetric, is met, but this causes excess mass in the panel design.

It has been established that for smaller in-plane loads, the stiffnesses of laminate skin regions are more distinct, which results in fewer continuous plies available for blending across the panel width as seen in Figure 7.15a. The average percentage of continuous blended plies is 40% for $N_x = 0.5\,\text{kN/mm}$, but this increases to 70% for $N_x = 3\,\text{kN/mm}$, as a result of both regions requiring similar stiffnesses and discrete laminate designs. When the blending constraint is not enforced, the percentages of continuous plies drop to approximately 15% and 35% for the tip and root load cases respectively. In general, standard angle ply tailored designs offer the greatest proportion of blended plies when compared to non-standard angle designs. This result could be attributed to the 10% rule, which maintains a minimum proportion of each angle ply across the laminate design and therefore acts as a surrogate blending constraint in the first stage. The feasible region for the non-standard angle was scaled to fit the traditional 10% rule bounds, but this no longer has explicit physical relevance for the proportions of plies within a given stack, and instead maintains a reasonable level of stiffness in each in-plane direction. In order to use non-standard angles within industrial applications, more research will be required to guarantee the performance of stiffness matched NSA laminates.

Due to the problem formulation, using an analytical approach combined with a permutation genetic algorithm for Stage II, the additional blending constraints do not adversely affect the solution time. The major source of increased computational expense and computational time is the increased number of wavelengths and buckling modes in Stage I.

7.10 Conclusions

In this chapter, the previously implemented optimisation methodology is amended and then employed to conduct a parametric study of minimum-mass DST panel designs for varying in-plane loads, stiffener spacing and panel length. The model used to analyse the buckling constraint is updated to have periodic boundary conditions, which better represent an aircraft wing panel. The lamination parameter feasible region is expanded to include non-standard angle designs, demonstrating the additional weight saving and greater number of blended plies that they offer.

- Discrete stiffness tailoring achieves greater material efficiency when compared to a standard angle optimum baseline design for a range of in-plane panel loads representing forces experienced at the root, mid-width and tip of a wing. Greater reduction in mass is obtained with smaller in-plane loads, where local skin buckling is the active constraint.
- Tailored stiffened panels are able to approximately maintain same level of material efficiency for wider stiffener spacings for particular load cases and geometry. As a result, fewer stiffeners may be required to support the same running load, for no additional mass.
- Non-standard angle designs offer a small reduction in mass when compared to SA

tailored designs, and preferentially select ±60° designs for resisting local longitudinal and transverse skin buckling modes, and redistribute 0° plies to beneath the stiffener bondline. The use of NSA designs more readily maintain the buckling performance of a stiffened panel design when converting between continuous lamination parameters and discrete stacking sequences.

- A blending constraint was enforced in combination with a permutation genetic algorithm, in order to obtain discretely tailored designs with significant numbers of continuous plies across the seam region. Without the constraint, for the lower load cases, only approximately 20% of plies are maintained across the width, compared to 40% with the blending constraint.

Chapter 8

Conclusions & Future Work

8.1 Conclusions

In this thesis, Discrete Stiffness Tailoring has been presented as novel concept for achieving stiffness variation across the width of a structure in order to redistribute loads, benefiting buckling performance. DST is compatible with high-deposition manufacturing techniques, and is not constrained by minimum fibre steering radii that limit curvilinear variable stiffness concepts.

In an initial proof of concept study, it was found that the simple, discrete, redistribution of stiff material across the width of a compression panel increases the critical buckling load by 16%, if all plies are tailored. The efficient strip model VICON was found to accurately assess the magnitude of the performance increase. The associated reduction in transverse strength due to the ply discontinuities was experimentally and numerically investigated, and this strength was found to be 74% lower for a full thickness tailored laminate when compared to a constant thickness QI control. However, the failure of the experimental tensile coupons was seen to initiate as a result of free-edge effects and not from failure emanating the seams. The seams in the experimental compression panels did not cause premature failure in any of the tailored designs, and did not prevent the panels from achieving the predicted increase in the buckling critical buckling stresses.

A two-stage optimisation methodology was implemented for the design of a DST stiffened panel, using a gradient-based method formulated with lamination parameters to minimise the mass of a single stiffener bay subject to buckling, strain and geometric constraints, and a genetic algorithm to return a discrete stacking sequence from the continuous lamination parameters and thicknesses. The use of lamination parameters reduces the number of variables required to describe laminate stiffnesses, and circumvents the periodic dependence of the stiffness on ply angle, creating a convex design space. The stiffened panel buckling performance was assessed using VIPASA, an earlier program upon which VICON is based. The gradient-based approach was benchmarked against a constrained Particle Swarm Optimisation, revealing the presence of local optima in the design space which are not eliminated by the use of lamination parameters. The feasible design space is presumed to be discontinuous and small, negatively impacting the performance of the PSO, which, as a stochastic optimisation technique, relies on the chance identification of a best solution within these feasible regions to guide the swarm. As the efficiency of the gradient-based

algorithm is an order of magnitude higher than the PSO, it was found to be a more suitable candidate for minimum-mass optimisation, although it will need to be re-run using multiple start points to ensure the global optimum is located.

Using the established optimisation methodology, a 14.4% reduction in mass was obtained by applying the discrete tailoring concept, simultaneously optimising stiffness and thickness across the width of the stiffened panel skin, when compared to a baseline constant stiffness and thickness design for a specific design loading. The magnitude in stiffness variation and location of the transition between regions was not constrained by minimum fibre turning radii, allowing for immediate alteration in the stiffness properties beyond the stiffener bond-line.

The critical mode for the untailored baseline panel was local skin buckling, whereas critical global and local modes occurred concurrently for the discretely stiffened design. Tailoring allowed for load redistribution to the stiffener region for global buckling resistance, whilst mass and stiffness was removed from the free length of skin in-between stiffeners, which was optimised for local skin buckling behaviour. The division of the panel skin into independently optimised regions decouples the relationship between critical modes, allowing for more efficient use of material. The effect of individually varying stiffness and thickness was explored, and a three-fold percentage decrease in mass was observed for tailoring only the stiffness when compared to tapering the laminate thickness alone.

The optimised DST panel was manufactured and experimentally tested, the first time an optimised variable-stiffness concept has been demonstrated for a representative aircraft structure. The experimentally obtained buckling load was within 4% of the VIPASA analysis, and good agreement between the experimental and analytical buckling modes was observed, validating the optimisation methodology and VIPASA model. Panel failure was as a result of material failure in the stiffener web, occurring at a load 24% greater than the skin buckling load. However as the panel length was shortened from the optimised design, the post-buckling capacity is increased. The seams within the tailored skin panel exhibited no sign of damage, despite the weak resin regions between the discontinuous plies, thus providing greater confidence in the transverse strength of a seamed region.

The optimisation routine validated by the stiffened panel experiment was subsequently used to perform a parametric study of infinitely wide stiffened panels under varying uni-axial compressive loads, representative of those experienced by commercial aircraft. Amendments to the original optimisation methodology allow for the selection of non-standard angle designs, and a blending constraint is added to maximise the arrangement of continuous plies between regions. Greater reductions in mass are obtained compared to baseline designs for panels subjected to lower in-plane loads, with an average of 17% reduction for designs located in the wing tip, opposed to 1-2% for wing root loads. Non-standard angle designs provide a small mass-saving when compared to standard angles, where designs preferentially select $\pm 60^{\circ}$ plies to resist local panel buckling.

Through the work presented in this thesis, it has been shown both analytically and experimentally that the Discrete Stiffness Tailoring concept can be used to achieve variation in stiffness benefiting buckling performance. The proposed tailoring concept has been demonstrated using both a simple compression panel and a representative aerospace structure; a T-stiffened wing skin panel. The discontinuities introduced by the discrete tailoring of plies were not found to be critical to the performance of the structure, if the seams run parallel to the applied load.

8.2 Future Work

This work has focused on the development and initial implementation of the Discrete Stiffness Tailoring concept for the design of efficient aerospace structures, with regards only to buckling performance. The failure of the experimental panel, occurring at at a load 24% higher than critical buckling load, suggests that DST can also benefit the post-buckling behaviour of a structure. Aerodynamic loads and aeroelastic performance have not been considered, but, particularly as variable-stiffness tailoring has proved to benefit the aeroelastic response of aircraft structures, research may be continued into the application of DST for aeroelastic design.

The stiffened panel geometry and loading conditions used for the demonstration of the discrete tailoring concept in this work are relatively simplistic. In particular, the selection of a T-stiffener geometry where the flange and web thicknesses are interdependent precludes comparison of the generated designs to existing datum designs. This relationship causes the stiffener to be over-engineered, and as the stiffener is found to constitute a significant proportion of the in-plane stiffness and mass of a single panel bay, which means the strain constraint is never active in the optimisation routine. Alternative stiffener configurations, such as I-stiffeners or hat-stiffeners, could be implemented alongside DST, to investigate if similar reductions in mass are achieved compared to T-stiffened panels. Aircraft wing panels are also subjected to small amount of in-plane shear loading which was excluded from the model in this study, and should be considered in future work.

The transition between adjacent regions was achieved through a fixed width seam, composed of three piecewise steps that have constant thickness and stiffness. Shear lag models indicate that a smaller seam width could be used for the transfer of load across a seam, which may benefit the performance of a laminate. Future work could focus on the optimised design of the seam region. This work has also considered the reduction in transverse strength caused by ply discontinuities as a result of discrete tailoring, and experimental results for both simple compression plates and the DST stiffened panel conclude that this weakness does not seem to be critical for seams running parallel to the load. However, as aircraft wing skins are susceptible to external impact during service, subsequent work may focus on the effect of impact damage on the integrity of the seam regions. For the commercial implementation of variable-stiffness designs, including Discrete Stiffness Tailoring, research will need to provide methods for certifying these concepts.

Appendix A: Mann-Whitney U Test

The Mann-Whitney U test is a non-parametric statistic test that is used to compare two sets of independent data, and assess if the two sets have the same distribution or are distinctly different from each other. In this instance, it is used to assess the difference between the QI and Half and Full seam compression panels. The null, H_0, and alternative, H_1, hypotheses are defined as:

H_0 : The two data sets have the same distribution.

H_1 : The two data sets do not have the same distribution, where the probability, P, of the sets being unequal is greater than a stated significance level, α

A non-parametric test is appropriate for small sample sizes, n_1 and n_2, where the subscripts 1 and 2 represent the separate data sets. The two data sets are combined, ordered from smallest to largest, and then assigned ranks based on this order. The sum of the rank positions for each set are calculated and are represented by the variables R_1 and R_2. The test statistic, U, is calculated as follows:

$$U_1 = n_1 n_2 + \frac{n_1(n_1+1)}{2} - R_1 \quad U_2 = n_1 n_2 + \frac{n_2(n_2+1)}{2} - R_2 \tag{8.1}$$

$$U = |\, U_1 - U_2 \,| \tag{8.2}$$

A critical value for U can be found in a table of critical values, based on the sample size and two-sided level of significance. In this instance, where $n_1 = n_2 = 5$ and $\alpha = 0.05$, then $U \leq 2$. For the results presented here, $U_{\text{Half}} = 3$, and $U_{\text{Full}} = 0$.

Bibliography

[1] T. J. Dodwell, R. Butler, and A. T. Rhead, "Optimum fiber steering of composite plates for buckling and manufacturability," *AIAA Journal*, vol. 54, no. 3, pp. 1139–1142, 2016.

[2] F. W. Williams, D. Kennedy, M. S. Anderson, and R. Butler, "VICONOPT - Program for exact vibration and buckling analysis or design of prismatic plate assemblies," *AIAA Journal*, vol. 29, no. 11, pp. 1927–1928, 1991.

[3] A. Jumahat, C. Soutis, F. R. Jones, and A. Hodzic, "Fracture mechanisms and failure analysis of carbon fibre/toughened epoxy composites subjected to compressive loading," *Composite Structures*, vol. 92, no. 2, pp. 295–305, 2010. [Online]. Available: http://dx.doi.org/10.1016/j.compstruct.2009.08.010

[4] A. Ataş and C. Soutis, "Strength prediction of bolted joints in CFRP composite laminates using cohesive zone elements," *Composites Part B: Engineering*, vol. 58, pp. 25–34, 2014.

[5] V. B. Hammer, M. P. Bendsøe, R. Lipton, and P. Pedersen, "Parametrization in laminate design for optimal compliance," *International Journal of Solids and Structures*, vol. 34, no. 4, pp. 415–434, 1997.

[6] S. Setoodeh, M. M. Abdalla, and Z. Gürdal, "Design of variable-stiffness laminates using lamination parameters," *Composites Part B: Engineering*, vol. 37, no. 4-5, pp. 301–309, 2006.

[7] A. J. Vizzini, "Strength of laminated composites with internal discontinuities parallel to the applied load," *AIAA Journal*, vol. 30, no. 6, pp. 1515–1520, 1992.

[8] M. W. Hyer and R. F. Charette, "Use of curvilinear fiber format in composite structure design," *AIAA Journal*, vol. 29, no. 6, pp. 1011–1015, 1991.

[9] Z. Gürdal, B. F. Tatting, and C. K. Wu, "Variable stiffness composite panels: Effects of stiffness variation on the in-plane and buckling response," *Composites Part A: Applied Science and Manufacturing*, vol. 39, no. 5, pp. 911–922, 2008.

[10] P. M. Weaver, K. D. Potter, K. Hazra, M. A. Saverymuthapulle, and M. T. Hawthorne, "Buckling of variable angle tow plates: From concept to experiment," *Collection of Technical Papers - AIAA/ASME/ASCE/AHS/ASC Structures, Structural Dynamics and Materials Conference*, no. May, pp. 1–10, 2009.

[11] S. T. IJsselmuiden, M. M. Abdalla, and Z. Gürdal, "Optimization of variable-

stiffness panels for maximum buckling load using lamination parameters," *AIAA Journal*, vol. 48, no. 1, pp. 134–143, 2010.

[12] G. Raju, Z. Wu, S. White, and P. M. Weaver, "Optimal postbuckling design of variable angle tow composite plates," *AIAA Journal*, vol. 56, no. 5, pp. 2045–2061, 2018.

[13] A. Sabido, L. Bahamonde, R. Harik, and M. J. van Tooren, "Maturity assessment of the laminate variable stiffness design process," *Composite Structures*, vol. 160, pp. 804–812, 2017.

[14] S. B. Biggers and S. Srinivasan, "Compression buckling response of tailored rectangular composite plates," *AIAA Journal*, vol. 31, no. 3, pp. 590–596, 1993.

[15] M. G. Joshi and S. B. Biggers, "Thickness optimization for maximum buckling loads in composite laminated plates," *Composites Part B: Engineering*, vol. 27, no. 2, pp. 105–114, 1996.

[16] Z. Gürdal and R. Olmedo, "In-plane response of laminates with spatially varying fiber orientations: Variable stiffness concept," *AIAA Journal*, vol. 31, no. 4, pp. 751–758, 1993.

[17] D. H. Lukaszewicz, C. Ward, and K. D. Potter, "The engineering aspects of automated prepreg layup: History, present and future," *Composites Part B: Engineering*, vol. 43, no. 3, pp. 997–1009, 2012.

[18] B. C. Kim, P. M. Weaver, and K. Potter, "Manufacturing characteristics of the continuous tow shearing method for manufacturing of variable angle tow composites," *Composites Part A: Applied Science and Manufacturing*, vol. 61, pp. 141–151, 2014.

[19] R. Butler, A. T. Rhead, and T. Dodwell, "ADAPT Project Outline," 2016.

[20] S. Tsai and J. Melo, *Composite Materials Design and Testing: Unlocking Mystery with Invariants*. Standford, CA: Composites Design Group, Department of Aeronautics & Astronautics, Stanford University, 2015.

[21] G. Duvaut, G. Terrel, F. Léné, and V. E. Verijenko, "Optimization of fiber reinforced composites," *Composite Structures*, vol. 48, no. 1-3, pp. 83–89, 2000.

[22] M. W. Hyer and R. F. Charette, "The use of curvilinear fiber format in composite structure design," in *Proceedings of the* 30^{th} *AIAA SDM Conference, Mobile, AL, USA*, 1989, pp. 1396–1403, AIAA Paper No. 89-1404.

[23] C. S. Lopes, Z. Gürdal, and P. P. Camanho, "Tailoring for strength of composite steered-fibre panels with cutouts," *Composites Part A: Applied Science and Manufacturing*, vol. 41, no. 12, pp. 1760–1767, 2010.

[24] A. Khani, M. M. Abdalla, Z. Gürdal, J. Sinke, A. Buitenhuis, and M. J. Van Tooren,

"Design, manufacturing and testing of a fibre steered panel with a large cut-out," *Composite Structures*, vol. 180, pp. 821–830, 2017.

[25] R. Olmedo and Z. Gurdal, "Buckling response of laminates with spatially varying fiber orientations," *AIAA Journal*, pp. 2261–2269, 1993.

[26] S. Nagendra, S. Kodiyalam, J. E. Davis, and N. Parthasarathy, "Optimization of tow fibre paths for composite design," in *36th AIAA/ASME/ASCE/AHS/ASC Structure, Structural Dynamics and Materials Conference*, no. 10-13 April, New Orleans, LA, 1995.

[27] B. Tatting and Z. Gurdal, "Design and manufacture of elastically tailored tow placed plates," ADOPTECH Inc. & Virginia Polytechnic Institute and State University, NASA Report. No. NASA/CR-2002-211919, 2002.

[28] C. Wu, Z. Gurdal, and J. Starnes, "Structural Response of Compression-Loaded, Tow-Placed, Variable Stiffness Panels," in *AIAA/ASME/ASCE/AHS/ASC Structures. Structural Dynamics, and Materials Conference*, no. 22-25 April, 2002.

[29] V. V. Toropov, R. Jones, T. Willment, and M. Funnell, "Weight and Manufacturability Optimization of Composite Aircraft Components Based on a Genetic Algorithm," in *Proceedings of the 6^{th} World Congresses of Structural and Multidisciplinary Optimization*, 2005.

[30] M. Sun and M. W. Hyer, "Use of material tailoring to improve buckling capacity of elliptical composite cylinders," *AIAA Journal*, vol. 46, no. 3, pp. 770–782, 2008.

[31] C. S. Lopes, Z. Gürdal, and P. P. Camanho, "Variable-stiffness composite panels: Buckling and first-ply failure improvements over straight-fibre laminates," *Computers and Structures*, vol. 86, no. 9, pp. 897–907, 2008.

[32] S. Y. Kuo and L. C. Shiau, "Buckling and vibration of composite laminated plates with variable fiber spacing," *Composite Structures*, vol. 90, no. 2, pp. 196–200, 2009.

[33] S. Setoodeh, M. M. Abdalla, S. T. IJsselmuiden, and Z. Gürdal, "Design of variable-stiffness composite panels for maximum buckling load," *Composite Structures*, vol. 87, no. 1, pp. 109–117, 2009.

[34] C. S. Lopes, P. P. Camanho, and Z. Gürdal, "Variable stiffness composite panels: Effects of stiffness variation on the in-plane and buckling response," in *Proceedings of the 7^{th} Euromech Solid Mechanics Conference*, 2009, pp. 1–13.

[35] A. W. Blom, P. B. Stickler, and Z. Gürdal, "Optimization of a composite cylinder under bending by tailoring stiffness properties in circumferential direction," *Composites Part B: Engineering*, vol. 41, no. 2, pp. 157–165, 2010.

[36] J. M. Van Campen, C. Kassapoglou, and Z. Gürdal, "Design of fiber-steered variable-stiffness laminates based on a given lamination parameters distribution," in *Proceed-*

ings of the 52nd AIAA/ASME/ASCE/AHS/ASC Structures, Structural Dynamics and Materials Conference, Denver, CO, 2011.

[37] A. Khani, M. M. Abdalla, and Z. Gürdal, "Circumferential stiffness tailoring of general cross section cylinders for maximum buckling load with strength constraints," *Composite Structures*, vol. 94, no. 9, pp. 2851–2860, 2012. [Online]. Available: http://dx.doi.org/10.1016/j.compstruct.2012.04.018

[38] M. Arian Nik, K. Fayazbakhsh, D. Pasini, and L. Lessard, "Surrogate-based multi-objective optimization of a composite laminate with curvilinear fibers," *Composite Structures*, vol. 94, no. 8, pp. 2306–2313, 2012. [Online]. Available: http://dx.doi.org/10.1016/j.compstruct.2012.03.021

[39] G. Raju, Z. Wu, B. C. Kim, and P. M. Weaver, "Prebuckling and buckling analysis of variable angle tow plates with general boundary conditions," *Composite Structures*, vol. 94, no. 9, pp. 2961–2970, 2012.

[40] K. Fayazbakhsh, M. Arian Nik, D. Pasini, and L. Lessard, "Defect layer method to capture effect of gaps and overlaps in variable stiffness laminates made by Automated Fiber Placement," *Composite Structures*, vol. 97, pp. 245–251, 2013. [Online]. Available: http://dx.doi.org/10.1016/j.compstruct.2012.10.031

[41] J. K. S. Dillinger, M. M. Abdalla, T. Klimmek, and Z. Gürdal, "Static Aeroelastic Stiffness Optimization and Investigation of Forward Swept Composite Wings," in *Proceedings of the* 10th *World Congress on Structural and Multidisciplinary Optimization*, 2013, pp. 1–10.

[42] A. P. Nagy, S. T. Ijsselmuiden, and M. M. Abdalla, "Isogeometric design of anisotropic shells: Optimal form and material distribution," *Computer Methods in Applied Mechanics and Engineering*, vol. 264, pp. 145–162, 2013. [Online]. Available: http://dx.doi.org/10.1016/j.cma.2013.05.019

[43] Z. Wu, P. M. Weaver, and G. Raju, "Postbuckling optimisation of variable angle tow composite plates," *Composite Structures*, vol. 103, pp. 34–42, 2013.

[44] S. N. Sørensen, R. Sørensen, and E. Lund, "DMTO - A method for Discrete Material and Thickness Optimization of laminated composite structures," *Structural and Multidisciplinary Optimization*, vol. 50, no. 1, pp. 25–47, 2014.

[45] M. Rouhi, H. Ghayoor, S. Hoa, and M. Hojjati, "Effect of structural parameters on design of variable-stiffness composite cylinders made by fiber steering," *Composite Structures*, vol. 118, no. 1, pp. 472–481, 2014.

[46] D. M. Peeters, S. Hesse, and M. M. Abdalla, "Stacking sequence optimisation of variable stiffness laminates with manufacturing constraints," *Composite Structures*, vol. 125, pp. 596–604, 2015.

[47] D. Peeters and M. Abdallah, "Optimisation of variable stiffness composites with ply

drops," in *Proceedings of the 56th AIAA/ASCE/AHS/ASC Structures, Structural Dynamics, and Materials Conference*, 2015, pp. 1–13.

[48] M. Jeliazkov, P. M. S. Abadi, C. S. Lopes, M. Abdalla, and D. Peeters, "Buckling and first-ply failure optimization of stiffened variable angle tow panels," in *Proceedings of the* 20^{th} *ICCM International Conferences on Composite Materials*, 2015, pp. 19–24.

[49] R. M. Groh and P. M. Weaver, "Mass optimization of variable angle tow, variable thickness panels with static failure and buckling constraints," in *Proceedings of the* 56^{th} *AIAA/ASCE/AHS/ASC Structures, Structural Dynamics, and Materials Conference*, 2015, pp. 5–9.

[50] G. Raju, Z. Wu, and P. M. Weaver, "Buckling and postbuckling of variable angle tow composite plates under in-plane shear loading," *International Journal of Solids and Structures*, vol. 58, pp. 270–287, 2015.

[51] M. J. van Tooren and A. Elham, "Optimization of variable stiffness composite plates with cut-outs subjected to compression, tension and shear using an adjoint formulation," in *Proceedings of the* 57^{th} *AIAA/ASCE/AHS/ASC Structures, Structural Dynamics, and Materials Conference*, 2016, pp. 1–15.

[52] A. Marouene, R. Boukhili, J. Chen, and A. Yousefpour, "Buckling behavior of variable-stiffness composite laminates manufactured by the tow-drop method," *Composite Structures*, vol. 139, pp. 243–253, 2016.

[53] ——, "Effects of gaps and overlaps on the buckling behavior of an optimally designed variable-stiffness composite laminates - A numerical and experimental study," *Composite Structures*, vol. 140, 2016.

[54] P. M. Weaver, Z. M. Wu, and G. Raju, "Optimisation of Variable Stiffness Plates," *Applied Mechanics and Materials*, vol. 828, pp. 27–48, 2016.

[55] M. Y. Matveev, P. J. Schubel, A. C. Long, and I. A. Jones, "Understanding the buckling behaviour of steered tows in Automated Dry Fibre Placement (ADFP)," *Composites Part A: Applied Science and Manufacturing*, vol. 90, pp. 451–456, 2016. [Online]. Available: http://dx.doi.org/10.1016/j.compositesa.2016.08.014

[56] D. M. Peeters, G. G. Lozano, and M. M. Abdalla, "Effect of steering limit constraints on the performance of variable stiffness laminates," *Computers and Structures*, vol. 196, pp. 94–111, 2018.

[57] D. C. Jegley, B. F. Tatting, and Z. Gürdal, "Optimization of elastically tailored tow-placed plates with holes," in *Proceedings of the* 4^{th} *AIAA/ASME/ASCE/AHS/ASC Structures, Structural Dynamics and Materials Conference*, 2003, pp. 205–218, AIAA Paper No. 2003-1420.

[58] D. C. Jegley, B. F. Tatting, and Z. Gürdal, "Tow-steered panels with holes subjected to compression or shear loading," in *Proceedings of the* 46^{th} *AIAA/AS-*

ME/ASCE/AHS/ASC Structures, Structural Dynamics and Materials Conference, vol. 5, 2005, pp. 3453–3466.

[59] V. S. Gomes, C. S. Lopes, F. F. Pires, Z. Gürdal, and P. P. Camanho, "Fibre steering for shear-loaded composite panels with cutouts," *Journal of Composite Materials*, vol. 48, no. 16, pp. 1917–1926, 2014.

[60] A. W. Blom, S. Setoodeh, J. M. A. M. Hol, and Z. Gu, "Design of variable-stiffness conical shells for maximum fundamental eigenfrequency," *Computers and Structures*, vol. 86, pp. 870–878, 2008.

[61] S. Güldü and A. Kayran, "Maximizing buckling load factors of fiber-placed composite cylindrical shells by particle swarm optimization," *Procedings of the 56th AIAA/ASCE/AHS/ASC Structures, Structural Dynamics, and Materials Conference*, no. January, pp. 1–25, 2015.

[62] A. Khani, M. M. Abdalla, and Z. Gürdal, "Optimum tailoring of fibre-steered longitudinally stiffened cylinders," *Composite Structures*, vol. 122, pp. 343–351, 2015.

[63] O. Stodieck, J. E. Cooper, P. M. Weaver, and P. Kealy, "Improved aeroelastic tailoring using tow-steered composites," *Composite Structures*, vol. 106, pp. 703–715, 2013. [Online]. Available: http://dx.doi.org/10.1016/j.compstruct.2013.07.023

[64] W. Raither, E. Furger, M. Zündel, A. Bergamini, and P. Ermanni, "Variable-stiffness skin concept for camber-morphing airfoils," *Journal of Intelligent Material Systems and Structures*, vol. 26, no. 13, pp. 1609–1621, 2015.

[65] T. R. Brooks, J. R. Martins, and G. J. Kennedy, "High-fidelity aerostructural optimization of tow-steered composite wings," *Journal of Fluids and Structures*, vol. 88, pp. 122–147, 2019.

[66] A. Muc, "Optimal fibre orientation for simply-supported, angle-ply plates under biaxial compression," *Composite Structures*, vol. 9, no. 2, pp. 161–172, 1988.

[67] M. C. Y. Niu, *Composite Airframe Structures: Practical Design Information and Data*. Conmilit, Hong Kong, 1992.

[68] B. H. Coburn, Z. Wu, and P. M. Weaver, "Buckling analysis of stiffened variable angle tow panels," *Composite Structures*, vol. 111, no. 1, pp. 259–270, 2014. [Online]. Available: http://dx.doi.org/10.1016/j.compstruct.2013.12.029

[69] P. Wang, X. Huang, Z. Wang, X. Geng, and Y. Wang, "Buckling and Post-Buckling Behaviors of a Variable Stiffness Composite Laminated Wing Box Structure," *Applied Composite Materials*, vol. 25, no. 2, pp. 449–467, 2018.

[70] V. Oliveri, G. Zucco, D. Peeters, G. Clancy, R. Telford, M. Rouhi, C. McHale, R. M. O'Higgins, T. M. Young, and P. M. Weaver, "Design, manufacture and test of an in-

situ consolidated thermoplastic variable-stiffness wingbox," *AIAA Journal*, vol. 57, no. 4, pp. 1671–1683, 2019.

[71] A. F. Martin and A. W. Leissa, "Application of the Ritz method to plane elasticity problems for composite sheets with variable fibre spacing," *International Journal for Numerical Methods in Engineering*, vol. 28, no. 8, pp. 1813–1825, 1989.

[72] A. W. Leissa and A. F. Martin, "Vibration and Buckling of Rectangular Composite Plates with Variable Fiber Spacing," *Composite Structures*, vol. 14, pp. 339–357, 1990.

[73] A. Alhajahmad, M. M. Abdalla, and Z. Gürdal, "Optimal design of tow-placed fuselage panels for maximum strength with buckling considerations," *Journal of Aircraft*, vol. 47, no. 3, pp. 775–782, 2010.

[74] F. X. Irisarri, D. M. Peeters, and M. M. Abdalla, "Optimisation of ply drop order in variable stiffness laminates," *Composite Structures*, vol. 152, pp. 791–799, 2016.

[75] W. R. Pogue and A. J. Vizzini, "Structural tailoring techniques to prevent delamination in composite laminates," *Journal of the American Helicopter Society*, vol. 35, no. 4, pp. 38–45, 1990.

[76] M. T. DiNardo and P. A. Lagace, "Buckling and postbuckling of laminated composite plates with ply dropoffs," *AIAA Journal*, vol. 27, no. 10, pp. 1392–1398, 1989.

[77] A. Mukherjee and B. Varughese, "Design guidelines for ply drop-off in laminated composite structures," *Composites Part B: Engineering*, vol. 32, no. 2, pp. 153–164, 2001.

[78] B. P. Kristinsdottir, Z. B. Zabinsky, M. E. Tuttle, and S. Neogi, "Optimal design of large composite panels with varying loads," *Composite Structures*, vol. 51, no. 1, pp. 93–102, 2001.

[79] W. Liu and R. Butler, "Optimum Buckling Design of Composite Wing Cover Panels with Manufacturing Constraints," in *Proceedings of the 48th AIAA/ASME/ASCE/AHS/ASC Structures, Structural Dynamics & Materials Conference*, Honolulu, HI, 2007, aIAA Paper No. 2007-2215.

[80] D. Maass, "Progress in automated ply inspection of AFP layups," *Reinforced Plastics*, vol. 59, no. 5, pp. 242–245, 2015. [Online]. Available: http://dx.doi.org/10.1016/j.repl.2015.05.002

[81] M. Molyneux, P. Murray, and B. P. Murray, "Prepreg, tape and fabric technology for advanced composites," *Composites*, vol. 14, no. 2, pp. 87–91, 1983.

[82] C. Waldhart, Z. Gürdal, and C. Ribbens, "Analysis of tow placed, parallel fiber, variable stiffness laminates," in *37th AIAA/ASME/ASCE/AHS/ASC Structure, Structural Dynamics and Materials Conference*, 1996, pp. 2210–2220.

[83] R. Mohan, H. Alshahrani, and M. Hojjati, "The effect of processing parameters on intra-ply shear property of out-of-autoclave carbon/epoxy prepreg," in *Design, Manufacturing and Applications of Composites, 10th Workshop*, 2014, pp. 231–239.

[84] G. G. Lozano, A. Tiwari, C. Turner, and S. Astwood, "A review on design for manufacture of variable stiffness composite laminates," *Proceedings of the Institution of Mechanical Engineers, Part B: Journal of Engineering Manufacture*, vol. 230, no. 6, pp. 981–992, 2016.

[85] J. M. J. F. V. Campen, C. Kassapoglou, and Z. Gürdal, "Generating realistic laminate fiber angle distributions for optimal variable stiffness laminates," *Composites Part B*, vol. 43, no. 2, pp. 354–360, 2012.

[86] Z. Wu, G. Raju, and P. M. Weaver, "Framework for the buckling optimization of variable-angle tow composite plates," *AIAA Journal*, vol. 53, no. 12, pp. 3788–3804, 2015.

[87] M. Wiehn and R. Hale, "Low cost robotic fabrication methods for tow placement," in *Proceedings of the 47th International SAMPE Symposium*, Long Beach, CA, 2002.

[88] W. M. Van Den Brink, W. J. Vankan, and R. Maas, "Buckling-optimized variable stiffness laminates for a composite fuselage window section," in *Proceedings of the 28th Congress of the International Council of the Aeronautical Sciences*, vol. 3, 2012, pp. 2315–2324.

[89] Z. Gürdal and K. Wu, "Tow-placement technology and fabrication issues for laminated composite structures," in *Proceedings of the 46nd AIAA/ASME/ASCE/AHS/ASC Structures, Structural Dynamics and Materials Conference*, Austin, Texas, 18-21 April 2005.

[90] K. Croft, L. Lessard, D. Pasini, M. Hojjati, J. Chen, and A. Yousefpour, "Experimental study of the effect of automated fiber placement induced defects on performance of composite laminates," *Composites Part A: Applied Science and Manufacturing*, vol. 42, no. 5, pp. 484–491, 2011.

[91] B. C. Kim, K. Potter, and P. M. Weaver, "Continuous tow shearing for manufacturing variable angle tow composites," *Composites Part A: Applied Science and Manufacturing*, vol. 43, no. 8, pp. 1347–1356, 2012.

[92] W. Liu and R. Butler, "Buckling optimization of variable-angle-tow panels using the infinite-strip method," *AIAA Journal*, vol. 51, pp. 1442–1449, 2013.

[93] E. Zympeloudis, K. Potter, P. Weaver, and B. Kim, "Advanced automated tape laying with fibre steering capability using continuous tow shearing mechanism," in *Proceedings of the 21st International Conference on Composite Materials*, Xi'an, China, 2017.

[94] J. Sliseris and K. Rocens, "Optimal design of composite plates with discrete variable

stiffness," *Composite Structures*, vol. 98, pp. 15–23, 2013. [Online]. Available: http://dx.doi.org/10.1016/j.compstruct.2012.11.015

[95] A. Crosky, C. Grant, D. Kelly, X. Legrand, and G. Pearce, "4 - Fibre placement processes for composites manufacture," in *Advances in Composites Manufacturing and Process Design*, P. Boisse, Ed. Woodhead Publishing, 2015, pp. 79 – 92.

[96] N. Boddeti, Y. Tang, K. Maute, D. W. Rosen, and M. L. Dunn, "Optimal design and manufacture of variable stiffness laminated continuous fiber reinforced composites," *Scientific Reports*, vol. 10, no. 1, pp. 1–15, 2020. [Online]. Available: https://doi.org/10.1038/s41598-020-73333-4

[97] H. Ghiasi, D. Pasini, and L. Lessard, "Optimum stacking sequence design of composite materials Part I: Constant stiffness design," *Composite Structures*, vol. 90, no. 1, pp. 1–11, 2009. [Online]. Available: http://dx.doi.org/10.1016/j.compstruct.2009.01.006

[98] H. Ghiasi, K. Fayazbakhsh, D. Pasini, and L. Lessard, "Optimum stacking sequence design of composite materials Part II: Variable stiffness design," *Composite Structures*, vol. 93, pp. 1–13, 2010.

[99] L. Schmit and B. Farshi, "Optimum design of laminated composites," *International Journal for Numerical Methods in Engineering*, vol. 11, pp. 623–640, 1977.

[100] B. G. Falzon and G. P. Steven, "Buckling mode transition in hat-stiffened composite panels loaded in uniaxial compression," *Composite Structures*, vol. 37, no. 2, pp. 253–267, 1997.

[101] J. Enrique Herencia, P. M. Weavers, and M. I. Friswell, "Optimization of long anisotropic laminated fiber composite panels with T-shaped stiffeners," *AIAA Journal*, vol. 45, no. 10, pp. 2497–2509, 2007.

[102] R. Vescovini and C. Bisagni, "Buckling analysis and optimization of stiffened composite flat and curved panels," *AIAA Journal*, vol. 50, no. 4, pp. 904–915, 2012.

[103] W. Stroud and M. S. Anderson, "PASCO: Structural Panel Analysis and Sizing Code, Capability and Analytical Foundations," NASA, Langley Research Center, Virginia, NASA Technical Memorandum NASA-TM-80181, 1980.

[104] S. Nagendra, Z. Gürdal, R. T. Haftka, and J. H. Starnes, "Buckling and failure characteristics of compression-loaded stiffened composite panels with a hole," *Composite Structures*, vol. 28, no. 1, pp. 1–17, 1994.

[105] W. Liu, R. Butler, A. R. Mileham, and A. J. Green, "Bilevel optimization and postbuckling of highly strained composite stiffened panels," *AIAA Journal*, vol. 44, no. 11, pp. 2562–2570, 2006.

[106] Y. Hirano, "Optimum design of laminated plates under axial compression," *AIAA Journal*, vol. 17, no. 9, pp. 1017–1019, 1979.

[107] R. T. Haftka and J. L. Walsh, "Stacking-sequence optimization for buckling of laminated plates by integer programming," *AIAA Journal*, vol. 30, no. 3, pp. 814–819, 1992.

[108] P. M. Zadeh, M. Fakoor, and M. Mohagheghi, "Bi-level optimization of laminated composite structures using particle swarm optimization algorithm," *Journal of Mechanical Science and Technology*, vol. 32, no. 4, pp. 1643–1652, 2018.

[109] R. Le Riche and R. T. Haftka, "Optimization of laminate stacking sequence for buckling load maximization by genetic algorithm," *AIAA Journal*, vol. 31, no. 5, pp. 951–956, 1993.

[110] S. Nagendra, D. Jestin, Z. Gürdal, R. T. Haftka, and L. T. Watson, "Improved genetic algorithm for the design of stiffened composite panels," *Computers and Structures*, vol. 58, no. 3, pp. 543–555, 1996.

[111] B. Liu, R. T. Haftka, M. A. Akgün, and A. Todoroki, "Permutation genetic algorithm for stacking sequence design of composite laminates," *Computer Methods in Applied Mechanics and Engineering*, vol. 186, no. 2-4, pp. 357–372, 2000.

[112] G. Soremekun, Z. Gürdal, C. Kassapoglou, and D. Toni, "Stacking sequence blending of multiple composite laminates using genetic algorithms," 2001.

[113] W. Tsai, Stephen and H. T. Hahn, *Introduction to Composite Materials*. CRC Press, 1980.

[114] S. Tsai and N. Pagano, "Invariant properties of composite materials," in *Composite Materials Workshop*, S. Tsai, H. J.C., and N. Pagano, Eds. Stamfort Connecticut: Technomic Publishing Co., 1968, pp. 233–253.

[115] J. Grenestedt and P. Gudmundson, "Layup optimization of composite material structures," in *Optimal Design with Advanced Materials*, P. Pedersen, Ed. Amsterdam: Elsevier Science Publishers, 1993, pp. 311–336.

[116] J. Foldager, J. S. Hansen, and N. Olhoff, "A general approach forcing convexity of ply angle optimization in composite laminates," *Structural Optimization*, vol. 16, no. 2-3, pp. 201–211, 1998.

[117] C. G. Diaconu and H. Sekine, "Layup optimization for buckling of laminated composite shells with restricted layer angles," *AIAA Journal*, vol. 42, no. 10, pp. 2153–2163, 2004.

[118] M. W. Bloomfield, C. G. Diaconu, and P. M. Weaver, "On feasible regions of lamination parameters for lay-up optimization of laminated composites," *Proceedings of*

the Royal Society A: Mathematical, Physical and Engineering Sciences, vol. 465, no. 2104, pp. 1123–1143, 2009.

[119] S. Setoodeh, M. M. Abdalla, and Z. Gürdal, "Approximate feasible regions for lamination parameters," in *Collection of Technical Papers - 11th AIAA/ISSMO Multidisciplinary Analysis and Optimization Conference*, vol. 2, no. September, 2006, pp. 814–822.

[120] H. Fukunaga and G. N. Vanderplaats, "Stiffness optimization of orthotropic laminated composites using lamination parameters," *AIAA Journal*, vol. 29, no. 4, pp. 641–646, 1991.

[121] M. Miki and Y. Sugiyama, "Optimum design of laminated composite plates using lamination parameters," *AIAA Journal*, vol. 31, no. 5, pp. 921–922, 1993.

[122] J. E. Herencia, P. M. Weaver, and M. I. Friswell, "Initial sizing optimisation of anisotropic composite panels with T-shaped stiffeners," *Thin-Walled Structures*, vol. 46, no. 4, pp. 399–412, 2008.

[123] M. W. Bloomfield, J. E. Herencia, and P. M. Weaver, "Enhanced two-level optimization of anisotropic laminated composite plates with strength and buckling constraints," *Thin-Walled Structures*, vol. 47, no. 11, pp. 1161–1167, 2009. [Online]. Available: http://dx.doi.org/10.1016/j.tws.2009.04.008

[124] D. Liu, V. V. Toropov, O. M. Querin, and D. C. Barton, "Bilevel optimization of blended composite wing panels," *Journal of Aircraft*, vol. 48, no. 1, pp. 107–118, 2011.

[125] S. T. Ijsselmuiden, M. M. Abdalla, and Z. Gürdal, "Implementation of strength-based failure criteria in the lamination parameter design space," *AIAA Journal*, vol. 46, no. 7, pp. 1826–1834, 2008.

[126] M. M. Abdalla, C. Kassapoglou, and Z. Gürdal, "Formulation of composite laminate robustness constraint in lamination parameters space," in *Proceedings of the 50th AIAA/ASME/ASCE/AHS/ASC Structures, Structural Dynamics and Materials Conference*, 2009, pp. 1–15, aIAA 2009-2478.

[127] T. A. Dutra and S. F. M. de Almeida, "Composite plate stiffness multicriteria optimization using lamination parameters," *Composite Structures*, vol. 133, pp. 166–177, 2015.

[128] M. Autio, "Determining the real lay-up of a laminate corresponding to optimal lamination parameters by genetic search," *Structural and Multidisciplinary Optimization*, vol. 20, no. 4, pp. 301–310, 2000.

[129] K. Yamazaki, "Two-level optimization technique of composite laminate panels by genetic algorithms," in *Proceedings of the 37th AIAA/ASME/ASCE/AHS/ASC Struc-*

ture, Structural Dynamics and Materials Conference, 1996, pp. 1882–1887, AIAA Paper No. 96-1539.

[130] S. T. IJsselmuiden, M. M. Abdalla, O. Seresta, and Z. Gürdal, "Multi-step blended stacking sequence design of panel assemblies with buckling constraints," *Composites Part B: Engineering*, vol. 40, no. 4, pp. 329–336, 2009.

[131] T. Macquart, N. Werter, and R. De Breuker, "Aeroelastic design of blended composite structures using lamination parameters," *Journal of Aircraft*, vol. 54, no. 2, pp. 561–571, 2017.

[132] L. Parnas, S. Oral, and Ü. Ceyhan, "Optimum design of composite structures with curved fiber courses," *Composites Science and Technology*, vol. 63, no. 7, pp. 1071–1082, 2003.

[133] Z. Wu, P. M. Weaver, G. Raju, and B. Chul Kim, "Buckling analysis and optimisation of variable angle tow composite plates," *Thin-Walled Structures*, vol. 60, pp. 163–172, 2012.

[134] B. Liu and R. T. Hafkta, "Composite wing structural design optimization with continuity constraints," in *AIAA/ASME/ASCE/AHS/ASC Structures. Structural Dynamics, and Materials Conference*, Seattle, WA, 2001.

[135] J. Stegmann and E. Lund, "Discrete material optimization of general composite shell structures," *International Journal for Numerical Methods in Engineering*, vol. 62, no. 14, pp. 2009–2027, 2005.

[136] E. Lund, "Buckling topology optimization of laminated multi-material composite shell structures," *Composite Structures*, vol. 91, no. 2, pp. 158–167, 2009. [Online]. Available: http://dx.doi.org/10.1016/j.compstruct.2009.04.046

[137] M. M. Abdalla, S. Setoodeh, and Z. Gürdal, "Design of variable stiffness composite panels for maximum fundamental frequency using lamination parameters," *Composite Structures*, vol. 81, no. 2, pp. 283–291, 2007.

[138] K. Svanberg, "A Class of Globally Convergent Optimization Methods Based on Conservative Convex Separable Approximations," *SIAM Journal on Optimization*, vol. 12, no. 2, pp. 555—-573, 2002.

[139] P. Hao, X. Yuan, C. Liu, B. Wang, H. Liu, G. Li, and F. Niu, "An integrated framework of exact modeling, isogeometric analysis and optimization for variable-stiffness composite panels," *Computer Methods in Applied Mechanics and Engineering*, vol. 339, pp. 205–238, 2018.

[140] P. Hao, D. Liu, Y. Wang, X. Liu, B. Wang, G. Li, and S. Feng, "Design of manufacturable fiber path for variable-stiffness panels based on lamination parameters," *Composite Structures*, vol. 219, no. January, pp. 158–169, 2019. [Online]. Available: https://doi.org/10.1016/j.compstruct.2019.03.075

[141] G. Serhat and I. Basdogan, "Lamination parameter interpolation method for design of manufacturable variable-stiffness composite panels," *AIAA Journal*, vol. 57, no. 7, pp. 3052–3065, 2019.

[142] M. A. Albazzan, R. Harik, B. F. Tatting, and Z. Gürdal, "Efficient design optimization of nonconventional laminated composites using lamination parameters: A state of the art," *Composite Structures*, vol. 209, pp. 362–374, 2019. [Online]. Available: https://doi.org/10.1016/j.compstruct.2018.10.095

[143] D. B. Adams, L. T. Watson, Z. Gürdal, and C. M. Anderson-Cook, "Genetic algorithm optimization and blending of composite laminates by locally reducing laminate thickness," *Advances in Engineering Software*, vol. 35, no. 1, pp. 35–43, 2004.

[144] F. X. Irisarri, A. Lasseigne, F. H. Leroy, and R. Le Riche, "Optimal design of laminated composite structures with ply drops using stacking sequence tables," *Composite Structures*, vol. 107, pp. 559–569, 2014. [Online]. Available: http://dx.doi.org/10.1016/j.compstruct.2013.08.030

[145] T. Macquart, M. T. Bordogna, P. Lancelot, and R. De Breuker, "Derivation and application of blending constraints in lamination parameter space for composite optimisation," *Composite Structures*, vol. 135, pp. 224–235, 2016. [Online]. Available: http://dx.doi.org/10.1016/j.compstruct.2015.09.016

[146] S. Tsai, "Weight and cost reduction by using unbalanced and unsymmetric laminates." in *Proceedings of the 18^{t}h International Conference on Composite Materials*, Jeju, Korea, 2011.

[147] K. J. Johnson, R. Butler, E. G. Loukaides, C. Scarth, and A. T. Rhead, "Stacking sequence selection for defect-free forming of uni-directional ply laminates," *Composites Science and Technology*, vol. 171, no. November 2018, pp. 34–43, 2019. [Online]. Available: https://doi.org/10.1016/j.compscitech.2018.11.048

[148] M. W. Bloomfield, J. Enrique Herencia, and P. M. Weaver, "Optimization of anisotropic laminated composite plates incorporating non-conventional ply orientations," *Collection of Technical Papers - AIAA/ASME/ASCE/AHS/ASC Structures, Structural Dynamics and Materials Conference*, no. April, pp. 1–15, 2008.

[149] D. Peeters and M. Abdalla, "Design guidelines in nonconventional composite laminate optimization," *Journal of Aircraft*, vol. 54, no. 4, pp. 1454–1464, 2017.

[150] R. Butler, *Polymer Composites in the Aerospace Industry.* Elsevier Ltd, 2015, ch. Chapter 4: Buckling and compressive strength of laminates with optimized fibre-steering and layer-stacking for aerospace applications.

[151] L. Culliford, R. Choudhry, R. Butler, and A. Rhead, "Buckling and strength analysis of panels with discrete stiffness tailoring," *Composite Structures*, vol. 234, 2020.

[152] M. I. Darby, J. M. Richards, and B. Yates, "Effect of discontinuous plies on the

tensile strength of CFRP laminates," *Journal of Materials Science Letters*, vol. 4, no. 2, pp. 203–206, 1985.

[153] W. H. Wittrick and F. W. Williams, "Buckling and vibration of anisotropic or isotropic plate assemblies under combined loadings," *International Journal of Mechanical Sciences*, vol. 16, no. 4, pp. 209–239, 1974.

[154] M. S. Anderson, F. W. Williams, and C. J. Wright, "Buckling and vibration of any prismatic assembly of shear and compression loaded anisotropic plates with an arbitrary supporting structure," *International Journal of Mechanical Sciences*, vol. 25, no. 8, pp. 585–596, 1983.

[155] W. H. Wittrick and F. W. Williams, "An Algorithm for Computing Critical Buckling Loads of Elastic Structures," *Journal of Structural Mechanics*, vol. 1, no. 4, pp. 497–518, 1973.

[156] *ABAQUS^{TM} Theory Manual,.*

[157] E. Barbero, *Finite Element Analysis of Composite Materials Using ABAQUS^{TM}*. CRC Press, 2013, ch. Chapter 4: Buckling.

[158] E. Riks, "An incremental approach to the solution of snapping and buckling problems," *International Journal of Solids and Structures*, vol. 15, no. 7, pp. 529–551, 1979. [Online]. Available: http://dx.doi.org/10.1016/0020-7683(79)90081-7

[159] R. S. Choudhry, S. F. Hassan, S. Li, and R. Day, "Damage in single lap joints of woven fabric reinforced polymeric composites subjected to transverse impact loading," *International Journal of Impact Engineering*, vol. 80, pp. 76–93, 2015.

[160] M. Benzeggagh and M. Kenane, "Measurement of mixed-mode delamination fracture toughness of unidirectional glass/epoxy composites with mixed-mode bending apparatus," *Composites Science and Technology*, vol. 56, pp. 439–449, 1996.

[161] J. Dizy, R. Palacios, and S. T. Pinho, "Homogenisation of slender periodic composite structures," *International Journal of Solids and Structures*, vol. 50, no. 9, pp. 1473–1481, 2013. [Online]. Available: http://dx.doi.org/10.1016/j.ijsolstr.2013.01.017

[162] *ABAQUS^{TM} Theory Manual, Section 32.5, Modelling with cohesive elements.*

[163] "American Society for Testing and Materials International. Standard test for compressive residual strength properties of damaged polymer matrix composite plates. ASTM D7137/D7137M-07."

[164] HBM, "catman Data Acquisition Software."

[165] Correlated Solutions, "VIC-3D System."

[166] M. H. Datoo, *Mechanics of Fibrous Composites.* Elsevier Science Publishers, 1991, ch. Chapter 9: Interlaminar stresses - Free edge effects.

[167] G. Czél, M. Jalalvand, and M. R. Wisnom, "Demonstration of pseudo-ductility in unidirectional hybrid composites made of discontinuous carbon/epoxy and continuous glass/epoxy plies," *Composites Part A: Applied Science and Manufacturing*, vol. 72, pp. 75–84, 2015.

[168] J. Kennedy and R. Eberhart, "Particle Swarm Optimization," in *Proceedings of ICNN'95 - International Conference on Neural Networks*, vol. 15, Perth, Australia, 1995, pp. 45–82.

[169] C. Yoo and S. Lee, *Stability of Structures: Principles and Applications*. Elsevier, 2011, ch. Chapter 1 - Buckling of Columns, pp. 1–73.

[170] W. Liu, "Analysis and Testing of Composite Stiffened Compression Panels for Integrated Design and Manufacture," 2005.

[171] W. H. Wittrick, "General sinusoidal stiffness matrices for buckling and vibration analyses of thin flat-walled structures," *International Journal of Mechanical Sciences*, vol. 10, no. 12, pp. 949–966, 1968.

[172] W. Wittrick and F. Williams, "A general algorithm for computing natural frequencies of elastic structures," *The Quarterly Journal of Mechanics and Applied Mathematics*, vol. 24, no. 3, pp. 263–284, 1971.

[173] B. Liu, R. T. Haftka, and P. Trompette, "Maximization of buckling loads of composite panels using flexural lamination parameters," *Structural and Multidisciplinary Optimization*, vol. 26, no. 1-2, pp. 28–36, 2004.

[174] K. He, S. V. Hoa, and R. Ganesan, "The study of tapered laminated composite structures: A review," *Composites Science and Technology*, vol. 60, no. 14, pp. 2643–2657, 2000.

[175] Z. Michalewicz and M. Schoenauer, "Evolutionary Algorithms for Constrained Parameter Optimization Problems," *Evolutionary Computation*, vol. 4, no. 1, pp. 1–32, 1996.

[176] T. Hatanaka, T. Korenaga, N. Kondo, and K. Uosaki, *Particle Swarm Optimization*. IntechOpen, 2009, no. January, ch. Search Performance Improvement for PSO in High Dimensional Space.

[177] G. T. Pulido and C. A. Coello Coello, "A constraint-handling mechanism for particle swarm optimization," in *Proceedings of the 2004 Congress on Evolutionary Computation, CEC2004*, vol. 2, no. 4, 2004, pp. 1396–1403.

[178] N. A. A. Aziz, M. Y. Alias, A. W. Mohemmed, and K. A. Aziz, "Particle Swarm Optimization for Constrained and Multiobjective Problems: A Brief Review," in *2011 International Conference on Management and Artificial Intelligence*, vol. 6, Bali, Indonesia, 2011, pp. 146–150.

[179] Z. Michalewicz and G. Sazhiyath, "Genocop 111: A co-evolutionary algorithm for numerical optimization problems with nonlinear constraints." in *Proceedings of the Second IEEE International Conference on Evolutionary Computation*, Piscataway, New Jersey, 1995, pp. 647 – 651.

[180] X. Hu and R. Eberhart, "Solving constrained nonlinear optimisation problems with particle swarm optimisation," in *Proceedings of the Sixth World Multiconference on Systemics, Cybernetics and Informatics*, Orlando, USA, 2002.

[181] S. Helwig, J. Branke, and S. Mostaghim, "Experimental analysis of bound handling techniques in particle swarm optimization," *IEEE Transactions on Evolutionary Computation*, vol. 17, no. 2, pp. 259–271, 2013.

[182] O. Falcó, J. A. Mayugo, C. S. Lopes, N. Gascons, A. Turon, and J. Costa, "Variable-stiffness composite panels: As-manufactured modeling and its influence on the failure behavior," *Composites Part B: Engineering*, vol. 56, pp. 660–669, 2014.

[183] A. T. Rhead, R. Butler, and G. W. Hunt, "Enhanced compressive fatigue model for impact damaged laminates," in *Proceedings of the 16th ICCM International Conference on Composite Materials*, Kyoto, Japan, 2007.

[184] A. P. Piotrowski, J. J. Napiorkowski, and A. E. Piotrowska, "Population size in Particle Swarm Optimization," *Swarm and Evolutionary Computation*, vol. 58, no. April, p. 100718, 2020.

[185] L. Culliford, C. Scarth, T. Maierhofer, R. Jagpal, A. Rhead, and R. Butler, "Discrete Stiffness Tailoring: Optimised design and testing of minimum mass stiffened panels," *Composites Part B: Engineering*, vol. 221, no. 109026, 2021. [Online]. Available: https://doi.org/10.1016/j.compositesb.2021.109026

[186] Z. Sápi, R. Butler, and A. Rhead, "High fidelity analysis to predict failure in T-joints," *Composite Structures*, vol. 225, no. February, pp. 111 – 143, 2019.

[187] S. Tsai, J. Melo, S. Sihn, A. Arteiro, and R. Rainsberger. Stanford Aeronautics and Astronautics, 2017.

[188] Z. Zabinsky, M. Tuttle, and C. Khompatraporn, *Global optimization: Scientific and engineering case studies*. Springer, 2006, ch. Chapter 21: A case study: composite structure design optimization.

[189] G. Soremekun, Z. Gürdal, C. Kassapoglou, and D. Toni, "Stacking sequence blending of multiple composite laminates using genetic algorithms," *Composite Structures*, vol. 56, no. 1, pp. 53–62, 2002.

[190] S. Zein, P. Basso, and S. Grihon, "A constraint satisfaction programming approach for computing manufacturable stacking sequences," *Computers and Structures*, vol. 136, pp. 56–63, 2014. [Online]. Available: http://dx.doi.org/10.1016/j.compstruc.2014.01.016

[191] X. Liu, C. A. Featherston, and D. Kennedy, "Buckling optimization of blended composite structures using lamination parameters," *Thin-Walled Structures*, vol. 154, no. April, p. 106861, 2020. [Online]. Available: https://doi.org/10.1016/j.tws.2020.106861

[192] D. Liu, V. V. Toropov, D. C. Barton, and O. M. Querin, "Weight and mechanical performance optimization of blended composite wing panels using lamination parameters," *Structural and Multidisciplinary Optimization*, vol. 52, no. 3, pp. 549–562, 2015.

[193] D. Goldberg and R. Lingle, "Alleles, loci and the traveling salesman problem," in *Proceedings of the 1st International Conference on Genetic Algorithms*, 1985, pp. 154 – 159.

[194] D. B. Adams, L. T. Watson, and Z. Gürdal, "Optimization and blending of composite laminates using genetic algorithms with migration," *Mechanics of Advanced Materials and Structures*, vol. 10, no. 3, pp. 183–203, 2003.